



National Library
of Canada

Acquisitions and
Bibliographic Services Branch

395 Wellington Street
Ottawa, Ontario
K1A 0N4

Bibliothèque nationale
du Canada

Direction des acquisitions et
des services bibliographiques

395, rue Wellington
Ottawa (Ontario)
K1A 0N4

Your file - Votre référence

Our file - Notre référence

NOTICE

The quality of this microform is heavily dependent upon the quality of the original thesis submitted for microfilming. Every effort has been made to ensure the highest quality of reproduction possible.

If pages are missing, contact the university which granted the degree.

Some pages may have indistinct print especially if the original pages were typed with a poor typewriter ribbon or if the university sent us an inferior photocopy.

Reproduction in full or in part of this microform is governed by the Canadian Copyright Act, R.S.C. 1970, c. C-30, and subsequent amendments.

AVIS

La qualité de cette microforme dépend grandement de la qualité de la thèse soumise au microfilmage. Nous avons tout fait pour assurer une qualité supérieure de reproduction.

S'il manque des pages, veuillez communiquer avec l'université qui a conféré le grade.

La qualité d'impression de certaines pages peut laisser à désirer, surtout si les pages originales ont été dactylographiées à l'aide d'un ruban usé ou si l'université nous a fait parvenir une photocopie de qualité inférieure.

La reproduction, même partielle, de cette microforme est soumise à la Loi canadienne sur le droit d'auteur, SRC 1970, c. C-30, et ses amendements subséquents.

UNIVERSITY OF ALBERTA

EFFECT OF SIZE ON FLEXURAL
BEHAVIOUR OF HIGH-STRENGTH CONCRETE BEAMS

BY

NEDIM ALCA



A THESIS

SUBMITTED TO THE FACULTY OF GRADUATE STUDIES AND RESEARCH
IN PARTIAL FULFILLMENT OF THE REQUIREMENTS FOR THE
DEGREE OF MASTER OF SCIENCE

DEPARTMENT OF CIVIL ENGINEERING

EDMONTON, ALBERTA

SPRING, 1993



National Library
of Canada

Acquisitions and
Bibliographic Services Branch

395 Wellington Street
Ottawa, Ontario
K1A 0N4

Bibliothèque nationale
du Canada

Direction des acquisitions et
des services bibliographiques

395, rue Wellington
Ottawa (Ontario)
K1A 0N4

Your file / Votre référence

Our file / Notre référence

The author has granted an irrevocable non-exclusive licence allowing the National Library of Canada to reproduce, loan, distribute or sell copies of his/her thesis by any means and in any form or format, making this thesis available to interested persons.

L'auteur a accordé une licence irrévocable et non exclusive permettant à la Bibliothèque nationale du Canada de reproduire, prêter, distribuer ou vendre des copies de sa thèse de quelque manière et sous quelque forme que ce soit pour mettre des exemplaires de cette thèse à la disposition des personnes intéressées.

The author retains ownership of the copyright in his/her thesis. Neither the thesis nor substantial extracts from it may be printed or otherwise reproduced without his/her permission.

L'auteur conserve la propriété du droit d'auteur qui protège sa thèse. Ni la thèse ni des extraits substantiels de celle-ci ne doivent être imprimés ou autrement reproduits sans son autorisation.

ISBN 0-315-82051-9

Canada

UNIVERSITY OF ALBERTA

RELEASE FORM

NAME OF AUTHOR: NEDIM ALCA
TITLE OF THESIS: EFFECT OF SIZE ON FLEXURAL BEHAVIOUR OF
HIGH-STRENGTH CONCRETE BEAMS
DEGREE: MASTER OF SCIENCE
YEAR THIS DEGREE GRANTED: SPRING, 1993

Permission is hereby granted to the University of Alberta to reproduce single copies of this thesis and to lend or sell such copies for private, scholarly or scientific research purposes only.

The author reserves all other publication and other rights in association with the copyright in the thesis, and except as hereinbefore provided neither the thesis nor any substantial portion thereof may be printed or otherwise reproduced in any material form whatever without the author's prior written permission.



Plevne Bul. 12/7
Alsancak/Izmir
35220
Turkey

Date: April 14, 1993

UNIVERSITY OF ALBERTA
FACULTY OF GRADUATE STUDIES AND RESEARCH

The undersigned certify that they have read, and recommend to the Faculty of Graduate Studies and Research for acceptance, a thesis entitled EFFECT OF SIZE ON FLEXURAL BEHAVIOUR OF HIGH-STRENGTH CONCRETE BEAMS submitted by NEDIM ALCA in partial fulfillment of the requirements for the degree of Master of Science.



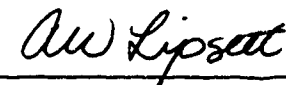
Dr. J.G. MacGregor, Supervisor



Dr. D.J.L. Kennedy



Dr. S.H. Simmonds



Dr. A.W. Lipsett

Date: April 14, 1993

Abstract

Corley, in 1966, reported that the effect of size on the rotational capacity of plastic hinges is not significant. In 1988, Hillerborg used a somewhat different approach, and by using Corley's beam tests, concluded that the rotational capacity of a reinforced concrete hinging section is inversely proportional to the effective depth of the member.

To investigate the effect of size on the behaviour of flexural members an experimental program was conducted. Twelve simply supported, under-reinforced, high-strength concrete beams were tested. The design of the tests was based on three different effective depths and two different concrete strengths. The beams were subjected to two point loading.

Effect of size on deformation capacity of the beams tested and the development of failure are discussed. There was no apparent effect of size on flexural strength or rotational capacity.

Using a method based on a least squares fit of a polynomial expression to the experimental data from the beam tests, stress-strain curves for concrete in the compression zone of the beams were obtained. Two different methods were used to calculate the concrete stress block parameters.

Acknowledgements

This research was conducted under the supervision of Professor James G. MacGregor. The privilege of working with him has been a source of inspiration for me. His helpful guidance and invaluable support are greatly appreciated.

I would like to thank Dr. S.D.B. Alexander for his innovative ideas and for his assistance throughout the experimental program.

The technical assistance of L. Burden, R. Helfrich and D. Erikssen, of the L.F. Morrison Laboratory, in the fabrication and testing of the specimens was of great help. I would like to thank my colleagues: H. Ibrahim, S.T. Undershute, J. Xie, M. Bartlett, S. Iravani and summer student C. Jordan, who also assisted in the fabrication and testing of the specimens.

The discussions and suggestions by H. Ibrahim, M. Bartlett and Dr. M. Ghoneim are greatly appreciated with respect to the analysis of the test results and preparation of the thesis.

Special thanks to S.T. Undershute for his support and understanding on issues related to daily life, and the struggle and fun it brings.

Financial assistance received from the Network of Centres of Excellence on High-Performance Concrete is gratefully acknowledged.

Table of Contents

1 Introduction	1
1.1 Statement of Problem	1
1.2 Objectives and Scope	1
1.3 Organization of Thesis	2
2 Literature Review	3
2.1 Introduction	3
2.2 Rotational Capacity of Reinforced Concrete Sections and Members	3
2.3 Effect of Size on the Behaviour of Concrete Members	4
2.4 Size Effect on Rotational Capacity of Reinforced Concrete Sections	6
2.5 Objectives of Testing	11
3 Experimental Program	16
3.1 Introduction	16
3.2 Test Specimens	16
3.2.1 Proportioning of Specimens	16
3.2.2 Details of Specimens	17
3.2.3 Beam Designations	18
3.3 Materials	18
3.3.1 Concrete	18
3.3.2 Reinforcement	22
3.4 Testing	23
3.4.1 Test Set-up and Instrumentation	23
3.4.2 Test Procedure	25
4 Test Results and Observations	38
4.1 Introduction	38
4.2 Definitions	38
4.3 Load-Deformation Relationships	38
4.3.1 Load-Centerline Deflection	38

4.3.2 Moment Carryin Capacity	39
4.3.3 Curvature and Rotation Measurements	40
4.4 Extreme Compression Fiber Strain Measurements	41
4.5 Neutral Axis Depth-Centerline Deflection Relationships	43
4.6 Development of Failure	43
5 Effect of Size on Deformation Capacity of Beams	65
5.1 Introduction	65
5.2 Effect of Size on Extreme Compression Fiber Strain	65
5.3 Effect of Size on Rotational Capacity	66
5.4 Discussion	67
6 Concrete Stress Block Behaviour in Beams	70
6.1 Introduction	70
6.2 Obtaining Concrete Stress-strain Curves	70
6.2.1 Methods of Analysis	70
6.2.2 Comparison of Methods and Results	72
6.2.3 Discussion	74
6.3 Concrete Stress Block Parameters	74
6.3.1 Methods of Analysis	74
6.3.2 Comparison of Methods and Results	76
6.3.3 Discussion	76
6.4 Overall Discussion and Recommendations	77
7 Summary and Conclusions	87
7.1 Summary	87
7.2 Conclusions	87
References	89

List of Tables

Table 3.1	Specimen Descriptions	26
Table 3.2	Stirrup and Corbel Reinforcement Details	26
Table 3.3	Concrete Mix Designs	27
Table 3.4	Some Properties of Cements Used	28
Table 3.5	Concrete Strength Test Data	28
Table 3.6	Reinforcement Coupon Test Results	29
Table 4.1	Centerline Deflections	46
Table 4.2	Parts of Ultimate Moment	47
Table 4.3	Moments	48
Table 4.4	Total Angle Change in the Test Regions	49
Table 4.5	Average Extreme Compression Fiber Strains	50
Table 4.6	Neutral Axis Depths	51
Table 6.1	Concrete Stress-strain Curve Fitting Data	79
Table 6.2	Concrete Stress Block Parameters	80

List of Figures

Figure 2.1	Size Effect on Uniaxial Compression, van Mier (1986)	12
Figure 2.2	Idealization for Stress-strain Curve, Hillerborg (1988a)	12
Figure 2.3	Strain and Stress Distribution at Ultimate Moment Capacity	13
Figure 2.4	Normalized Rotation vs l/d	13
Figure 2.5	Normalized Rotation vs Stirrup Ratio	14
Figure 2.6	Stirrup Ratio vs l/d	14
Figure 2.7	Extreme Compression Fiber Strain vs l/c	15
Figure 2.8	Extreme Compression Fiber Strain vs l/d	15
Figure 3.1	Typical Beam Geometry	30
Figure 3.2	Beams in Scale	31
Figure 3.3	Formwork and Reinforcement for a Large Beam	32
Figure 3.4	Stress-strain Curve for Concrete from Cylinder Tests	32
Figure 3.5	Concrete Notched Beam Tests	33
Figure 3.6	Typical Coupon Tests of Reinforcing Bars	33
Figure 3.7	Test Set-up	34
Figure 3.8	Support Conditions	35
Figure 3.9	Rotation Meter Arrangement for a Small Beam	36
Figure 3.10	LVDT Arrangement for a Large Beam	36
Figure 3.11	Overall View of the Test Set-up for a Large Beam	37
Figure 4.1	Definitions	52
Figure 4.2	Load vs Centerline Deflection, Beam MH1	53
Figure 4.3	Ductility Index vs ρ/ρ_b	53
Figure 4.4	Comparison of Rotation Meters, Beam LL1	54
Figure 4.5	Comparison of Curvature Measurements, Worst Case	55
Figure 4.6	Comparison of Curvature Measurements, Best Case	55
Figure 4.7	Moment vs Total Angle Change	56
Figure 4.8	Normalized Moment vs Total Angle Change	56
Figure 4.9	Demec Gauge Strains, Lower Concrete Strength Beams	57

Figure 4.10	Demec Gauge Strains, Higher Concrete Strength Beams	58
Figure 4.11	Regression of Average 2" Demec Gauge Strains, Beam SH1	59
Figure 4.12	Comparison of Strain Measurements, Worst Case	60
Figure 4.13	Comparison of Strain Measurements, Best Case	60
Figure 4.14	Comparison of Neutral Axis Depth Measurements, Worst Case	61
Figure 4.15	Comparison of Neutral Axis Depth Measurements, Best Case	61
Figure 4.16	Typical Small Lower Concrete Strength Beam After Failure	62
Figure 4.17	Typical Medium Lower Concrete Strength Beam After Failure	62
Figure 4.18	Typical Large Lower Concrete Strength Beam After Failure	63
Figure 4.19	Typical Small Higher Concrete Strength Beam After Failure	63
Figure 4.20	Typical Medium Higher Concrete Strength Beam After Failure	64
Figure 4.21	Typical Large Higher Concrete Strength Beam After Failure	64
Figure 5.1	Extreme Compression Fiber Strain vs $1/c$, U of A Tests	68
Figure 5.2	Extreme Compression Fiber Strain vs $1/c$	68
Figure 5.3	Normalized Rotation vs $1/d$, U of A Tests	69
Figure 5.4	Normalized Rotation vs $1/d$	69
Figure 6.1	Comparison of Methods of Obtaining Stress-strain Curves	81
Figure 6.2	Normalized Moment vs Extreme Compression Fiber Strain	81
Figure 6.3	Effect of Degree of Polynomial on Stress-strain Curves	82
Figure 6.4	Concrete Stress-strain Curves, LSC Beams	82
Figure 6.5	Concrete Stress-strain Curves, HSC Beams	83
Figure 6.6	Concrete Stress-strain Curves, All Beams	83
Figure 6.7	Conditions at Ultimate Load	84
Figure 6.8	k_1 from Stress-strain Curves vs Concrete Cylinder Strength	84
Figure 6.9	k_2 vs Concrete Cylinder Strength	85
Figure 6.10	k_3 from Stress-strain Curves vs Concrete Cylinder Strength	85
Figure 6.11	k_1, k_2 vs Concrete Cylinder Strength	86
Figure 6.12	$k_2/k_1, k_3$ vs Concrete Cylinder Strength	86

Notation

- a = depth of the equivalent rectangular stress block.
- l = shear span
- s_{min} = minimum spacing of flexural cracks.
- A_e = effective area of concrete in tension.
- A_s = area of tension reinforcement.
- A_s' = area of compression reinforcement.
- A_v = area of shear reinforcement within a distance s .
- b = beam width.
- c = neutral axis depth.
- c_f = neutral axis depth at failure.
- c_{Mu} = neutral axis depth at ultimate moment.
- c_y = neutral axis depth at yield.
- $c_{\theta u}$ = neutral axis depth at ultimate rotation.
- C = total compression force in concrete.
- d = effective depth = distance from extreme compression fiber to centroid of tension reinforcement.
- f_c = concrete cylinder strength.
- f_c = concrete stress at extreme compression fiber.
- f_o = average concrete stress in concrete compression zone.
- f_s = stress in tension reinforcement at ultimate moment.
- f_s' = stress in compression reinforcement at ultimate moment.
- f_t = tensile strength of concrete.
- G_F = fracture energy.
- h = overall depth of beam.
- h = height of prism.
- k = a multiple of d where $kd = l$.
- k_1 = ratio of average stress to maximum stress.

- k_2 = ratio of the distance between the extreme compression fiber and the resultant of the compressive force to the neutral axis depth.
- k_3 = ratio of maximum stress in compression zone to cylinder strength.
- l = length over which curvature is measured.
- L = length of beam.
- m_o = a modified moment term.
- M = moment.
- M' = moment due to the compression force in concrete alone about the neutral axis.
- M_f = moment at failure.
- M_{pr} = moment predicted using concrete stress-strain curve.
- M_t = moment from test.
- M_u = ultimate moment.
- M_y = moment at yield.
- $M_{\theta u}$ = moment at ultimate rotation.
- n = a multiple of d where $nd = c$.
- o = perimeter of bar.
- $P_{c,v}$ = average load.
- s = spacing of shear reinforcement.
- T = total tension force in reinforcement.
- u = average bond stress.
- w = deformation from stress-deformation curve.
- β_1 = ratio of depth of rectangular stress block, a , to neutral axis depth, c .
- δ_f = centerline deflection at failure.
- δ_{Mu} = centerline deflection at ultimate moment.
- δ_y = centerline deflection at yield.
- $\delta_{\theta u}$ = centerline deflection at ultimate rotation.
- ϵ = strain.
- ϵ_c = strain in concrete.
- ϵ_{cf} = extreme compression fiber strain at failure.
- ϵ_{cMu} = extreme compression fiber strain at ultimate moment.

- ϵ_{cu} = strain in extreme compression fiber at ultimate.
 ϵ_{cy} = extreme compression fiber strain at yield.
 $\epsilon_{c\theta u}$ = extreme compression fiber strain at ultimate rotation.
 ϵ_s = strain in steel.
 μ_f = deflection ductility index = δ_f/δ_y .
 θ_{cr} = critical rotation.
 θ_f = rotation at failure.
 θ_{Mu} = rotation at ultimate moment.
 θ_{in} = total inelastic rotation at ultimate, occurring between the section of maximum moment and adjacent section of zero moment.
 θ_u = ultimate rotation.
 θ_y = rotation at yield.
 ρ = ratio of tension reinforcement = A_s/bd .
 ρ_b = reinforcement ratio corresponding to balanced strain conditions.
 σ = stress.
 σ_{max} = maximum stress.
 ϕ = bar diameter.
 ψ = curvature.
 ψ_u = curvature at ultimate.
 ω = mechanical tension reinforcement ratio at ultimate moment = $A_s f_s / f_c b d$.
 ω' = mechanical compression reinforcement ratio at ultimate moment = $A_s' f_s' / f_c b d$.

1 Introduction

1.1 Statement of Problem

In the design of reinforced concrete structures, it is customary to assume that redistribution of moments takes place between the members. In order to have moment redistribution, plastic hinging regions should have adequate deformation capacity. The stability of a ductile reinforced concrete frame subjected to an earthquake depends on the deformation capacity of the plastic hinges forming in the beams. For the safety of structures it is essential to know the behaviour of these plastic hinging regions.

A hinging region in a beam consists of plastically deforming sections. The deformation capacity of a hinging section is strongly affected by the deformation capacity of the concrete in the compression zone of the beam.

There are many variables affecting the behaviour of these hinging regions and the concrete in their compression zones. One of them may be the size of the beam.

1.2 Objectives and Scope

Hillerborg (1988a, 1988b, 1989, 1990) suggested that the deformation behaviour of concrete in the compression zone of a reinforced concrete hinging beam section is size dependent. He concluded that the rotational capacity of a hinging beam section is hence size dependent. The primary objective of the research presented in this thesis is to investigate the effect of size on the rotational capacity of reinforced high-strength concrete hinging sections subjected to flexure.

To achieve this objective, 12 simply supported, under-reinforced high-strength concrete beams were tested. The variables were the effective depth and the concrete strength. The beams were geometrically scaled relative to the bar diameter. The beams were subjected to two point loading producing a constant moment test region which formed the hinging region.

To better understand the behaviour, an attempt was made to obtain the stress-strain curves and the stress block parameters for the concrete in the compression zones of the beams.

1.3 Organization of Thesis

A literature review is presented in Chapter 2. This outlines some of the research done on the rotational capacity and on the effect of size on various concrete members. The experimental program is presented in Chapter 3. Details about the test specimens, test set-up and the materials used are given in Chapter 3. Information about how the data from the beam tests were analyzed is given in Chapter 4. Development of failure in the beams is presented in Chapter 4 as well. The effect of size on the deformation capacity of the test specimens is discussed in Chapter 5. The concrete stress-strain curves and concrete stress block parameters for the beams tested are presented in Chapter 6. Finally, a summary and conclusions are presented in Chapter 7.

2 Literature Review

2.1 Introduction

Different types of members under various loading conditions may behave differently depending on their size. It is particularly important to know the effect of size on the rotational capacity of a hinging section. In this chapter, the importance of rotational capacity for the overall behaviour of a structure is discussed. Previous research on the effect of size on the behaviour of concrete members, ideas prompting the test program and the effect of various variables on rotational capacity are discussed. Finally, the objectives of the research are presented.

2.2 Rotational Capacity of Reinforced Concrete Sections and Members

The rotational capacity is a measure of the ability of a hinging region in a structure to undergo inelastic deformations without significant loss of strength. Two rotational capacities can be defined, rotational capacity of a section and rotational capacity of a member. Rotational capacity of a section can be predicted with the principles of equilibrium of forces and compatibility of deformations. Rotational capacity of a member is more difficult to predict. It is related to the spread of plasticity and it is affected by many variables.

In 1950s and 1960s plastic design was widely used to design steel structures. Similarly, so called "limit design" of structural concrete was proposed by several researchers (Sawyer, 1955; Ernst, 1956; Baker, 1956; Macchi, 1960). Both methods ensure formation of sufficient number of plastic hinges to transform all or part of a structure into a mechanism and hence cause its collapse. As concrete is much less deformable than steel, the strain capacity of a reinforced concrete hinging section can be exhausted well before full redistribution of bending moments is achieved in the structure as a whole. Therefore, it is essential to limit the rotations in the hinging regions to safe values. Extensive research has been done to obtain these safe values and to predict the rotational capacities (Chan, 1962; Baker & Amarakone, 1964; Roy & Sozen 1964; Mattock, 1965; Corley, 1966).

As plastic design is not suitable for designing complex structures, it was soon downplayed. The results from these tests led to the clauses in modern concrete codes limiting the ultimate concrete strain, the amount of flexural reinforcement, the allowable moment redistribution, and to clauses defining the detailing of hinging regions.

2.3 Effect of Size on the Behaviour of Concrete Members

Bazant and Cedolin (1991) showed analytically that there is size effect on strength and post-peak deformation of a concrete structure. They used the term structure in a broad sense but in some cases failed to define clearly the type of structure and loading condition referred to. Using fracture mechanics concepts, they analyzed the effect of size on the strength of members where behaviour of concrete in tension is important. To explain size effect on deformation of concrete cylinders and softening hinges, a stability approach was used. These concepts will be summarized in the following paragraphs.

Using fracture mechanics, it was shown analytically that, release of stored fracture energy causes a size effect on plain concrete subjected to uniaxial tension. The theory is based on the hypothesis that the fracture front dissipates the same amount of energy per unit area of fracture surface regardless of the member size. The larger the member, the greater is the volume from which the energy is released. As a result, larger specimens would fail at lower stresses. To prove this theory, Bazant and Cedolin reported tests of diagonal shear failure of beams, punching shear failure of slabs, torsional failure of beams, and pull-out failure of bars. It is important to mention that most of these tests were conducted on very small specimens using less than full size aggregates. More convincing results were obtained by Bosco et al. (1990a, 1990b) from tests of real size beams. Bosco et al. concluded that the minimum steel percentage is inversely proportional to the beam depth for high-strength concrete beams. They also observed that the brittleness was increased by increasing the beam size and/or decreasing the steel area. Kani (1967) suggested that size is important for the load carrying capacity of beams without stirrups failing in shear. Currently, a test program at the University of Toronto is underway to investigate the effect of size on the shear capacity of beams having longitudinal reinforcement alone. Note that in all these cases the behaviour of concrete in tension is important in the overall behaviour of the members.

Bazant and Cedolin, define damage due to compression as continuously distributed (smeared) fractures. Theoretically, damage localizes into a zone of the minimum possible size permitted by the continuum model. Damage is considered as a source of structural instability. When the stress-strain curve of a material is descending due to damage, instabilities and bifurcations can arise. In a uniaxial compression test, damage is assumed to start at peak stress. It is shown theoretically that, after bifurcation, the slope of the descending branch is size dependent. To prove this, they used concrete prism test data reported by van Mier (1986). This approach for material behaviour may be particularly important for constitutive modelling.

van Mier (1986) reported results of uniaxial compression tests on plain concrete prisms with varying heights and constant cross-section. These tests showed that, the shorter the specimen, the flatter was the descending branch of the concrete stress-strain curve as shown in Figure 2.1(a). When deformations, instead of strains, were plotted beyond peak stress, almost identical descending branches were obtained regardless of the height of the specimen as illustrated in Figure 2.1(b). It was reported that localized fractures were observed in some of the specimens. Additionally, it was reported that size did not have any effect on strength. These tests were performed using brush platens. When rigid steel platens are used, different behaviour may be observed. van Mier concludes from the surface measurements of the prism tests that: "*... the experimentally observed strain-softening branch reflects the response of the structure formed by the specimen and the complete loading system, and cannot be considered as a material property.*"

Koike et al. (1987) reported results of uniaxial compression tests on plain concrete prisms having scaled sizes in all three dimensions. They concluded that, as the prisms get larger, the compressive strength increases and the descending branch gets steeper.

Hillerborg (1988a, 1988b, 1989, 1990) analyzed the van Mier data using an approach similar to Bazant and Cedolin. Hillerborg proposed a model for concrete under uniaxial compression which assumes a stress-strain curve for the ascending branch and a stress-deformation curve for the descending branch. As shown in Figure 2.2, the basis of the model is that, after the peak stress, damage localizes in a band and while all the shortening takes place in this band, the rest of the specimen is unloading and hence is elongating. Thus, the strain is defined as,

$$\epsilon' = \epsilon + \frac{w}{h} \quad (2.1)$$

where ϵ is the strain in the unloading portion of the specimen, w is the deformation from the stress-deformation curve, h is the height of the specimen. Note that, w is equal to zero at peak stress, is constant at failure and it is independent of the height. Thus, as the height increases ϵ' decreases and the descending branch of the stress-strain curve becomes as shown in Figure 2.1(a).

2.4 Size Effect on Rotational Capacity of Reinforced Concrete Sections

The strain and stress distribution for a reinforced concrete beam section at ultimate moment capacity are shown in Figure 2.3. A rectangular stress block has been used for convenience. The curvature at ultimate moment, ψ_u , is defined as

$$\psi_u = \frac{\epsilon_{cu}}{c} \quad \text{where} \quad c = \frac{a}{\beta_1} \quad \text{and} \quad a = \frac{A_s f_s}{0.85 f_c b} \quad (2.2)$$

Rearranging,

$$\psi_u = \frac{0.85 f_c b \beta_1 \epsilon_{cu}}{A_s f_s} \quad (2.3)$$

In Equations (2.2) and (2.3), ϵ_{cu} is the extreme compression fiber strain at ultimate moment capacity, c is the neutral axis depth, a is the depth of the rectangular stress block, β_1 is the ratio a/c , A_s is the area of steel, f_s is the stress in the steel, b is the width.

The rotation at ultimate, θ_u , is defined as,

$$\theta_u = \psi_u l \quad \text{and} \quad l = kd \quad (2.4)$$

where k is a constant, l is the length over which the rotation is measured, d is the effective depth.

Substituting Equation (2.3) into Equation (2.4),

$$\theta_u = \frac{0.85 f_c b \beta_1 \epsilon_{cu}}{A_s f_s} kd \quad (2.5)$$

The mechanical reinforcement ratio, ω , is defined as,

$$\omega = \frac{A_s f_s}{f_c b d} \quad (2.6)$$

Rearranging,

$$\theta_u = \frac{0.85 \beta_1 \epsilon_{cu}}{\omega} k \quad (2.7)$$

and,

$$\theta_u \omega = 0.85 \beta_1 \epsilon_{cu} k \quad (2.8)$$

In the conventional code approach, ϵ_{cu} is assumed to be constant and β_1 is a function of concrete strength. Thus, Equation (2.7) suggests that hinging sections having the same ω and concrete strength will have the same rotation at ultimate. Equation (2.8) suggests that normalized rotation at ultimate, $\theta_u \omega$, is constant for any hinging section having the same concrete strength.

Hillerborg (1988a, 1988b, 1989, 1990), extends the stress-strain model discussed in Section 2.3 to a beam under flexure by assuming that the compression block in a beam behaves similarly to a uniaxially compressed prism. Assuming that the length h in Equation (2.1) is proportional to the neutral axis depth for a beam and assuming that w/h dominates the right hand side of Equation (2.1), the model leads to the conclusion that the extreme compression fiber strain in a beam at ultimate is approximately inversely proportional to its effective depth;

$$\epsilon_{cu} \approx \frac{\text{constant}}{d} \quad (2.9)$$

Substituting Equation (2.9) into Equation (2.8),

$$\theta_u \omega = \frac{\text{constant}}{d} \quad (2.10)$$

Equation (2.10) suggests that the normalized rotation of a reinforced concrete hinging section is inversely proportional to its effective depth. As a result, Hillerborg concludes that the limiting extreme compression fiber strain should be size dependent.

Hillerborg, used the numerical version of the stress-strain curve given in Figure 2.2 in a moment-curvature analysis. He concluded that the rotational capacity of under-reinforced concrete sections and the ultimate strength of over-reinforced concrete sections are both inversely proportional to the effective depth. Hillerborg further suggested that the size effect could be particularly important for high-strength concrete hinging sections as steeper descending branches are obtained from high-strength concrete cylinder tests.

To prove his theory, Hillerborg used the beam tests reported by Corley (1966), and plotted $\theta_u(\omega - \omega')$ against $1/d$ where ω' is the mechanical compression reinforcement ratio, see Figure 2.4. Equation (2.10) predicts the data should fall along a radial line similar to the dashed line while Equation (2.8) predicts a horizontal line. In Figure 2.4, the data reported by Mattock (1965) is also included. Mattock (1965) and Corley (1966) reported results from reinforced concrete beams subjected to midpoint loading. In the four papers published by Hillerborg on the topic, two different definitions for θ_u were used. Both of these definitions were based on θ_{pu} , a plastic rotation calculated from measured deflections, which is a measure

of member rotational capacity rather than sectional rotational capacity. Because the tests reported in this thesis studied sectional rotational capacity, a different definition of θ_u presented in the next paragraph has been used to plot Figure 2.4.

Both Mattock and Corley reported ψ_u , the curvature at ultimate, measured in a gauge length equal to the effective depth, d . The values of θ_u used in Figure 2.4 were calculated using the relationship $\theta_u = \psi_u d$ which gives a better measure of the sectional rotational capacity. In a midpoint bending test, it is not possible to measure the exact value for the sectional rotational capacity due to moment gradient and spread of plasticity. The values of ω and ω' used to plot Figure 2.4 were obtained as follows. Using the reported curvatures and extreme compression fiber strains, the neutral axis depths and the average strains in the tension and compression reinforcement were calculated. The stress-strain curves for the tension reinforcement were reported by Mattock and Corley in terms of points defining a tri-linear diagram. The ultimate tensile strength was not reported. Using the reported parameters idealizing the reinforcement stress-strain curves, the force in the tension reinforcement at ultimate was calculated. It was observed that, in some of the beams, this calculation gave steel stresses up to 2.5 times the yield stress, in those cases the steel stresses were taken as 1.5 times the yield stress. These calculated tension steel stresses were used to calculate ω . For the compression reinforcement, only the yield strength of steel was given. In all the beams the strain in the compression steel was above yield strain and lower than the strain at the onset of strain hardening which was assumed to be 10,000 microstrain. Thus, ω' was based on yield force in the compression reinforcement.

Corley reported that nine of the beams developed noticeable inclined cracking at the ultimate load or near the end of the test. Mattock also reported results from seven beams subjected to two point loading. These sixteen beams were excluded in the analyses presented here.

In Figure 2.4, the dashed line shows the trend suggested by Hillerborg. Hillerborg's theory suggests that the dashed line should pass through zero and the slope is a material property of concrete. Hillerborg assumed that the constant in Equation (2.10) is a multiple of w , the deformation from the stress-deformation curve. As he assumed that the w at ultimate is constant for concrete, it is valid to treat the slope of the dashed line as a material property. The slope of this trend line depends on the definitions and assumption made in calculating the $\theta_u(\omega - \omega')$ values. As Hillerborg defined θ_u differently in his four papers, the slope had two different values in those four papers. The slope of the dashed line in Figure 2.4 is shown as an example and is different from either of Hillerborg's definitions.

Mattock defined the test variables as: the concrete strength, the reinforcement yield strength, the effective depth, the span and the amount of tension reinforcement. Corley defined the test variables as: the width, the effective depth, the span, the amount of tension reinforcement and the amount of stirrups. From the test results, Corley concluded that extreme compression fiber strain at ultimate moment, ϵ_{cu} , is a function of the amount of stirrups inside the test region and the width to shear span ratio. One of the primary objectives of Corley's tests was to investigate the effect of size on the rotational capacity of hinging regions. Using specimens having similar width to shear span ratios and similar amounts of stirrups, Corley concluded that the direct effect of size on extreme compression fiber strain was not significant.

When the normalized rotation, $\theta_u(\omega - \omega')$, is used as a measure of rotational capacity, the variables listed above theoretically reduce to: the effective depth, the width, the span and the amount of stirrups. To better understand the effect of these variables on rotational capacity new variables were defined as: the stirrup ratio, A_v/sb ; the width to effective depth ratio, b/d ; the width to span ratio, b/L ; and the effective depth to span ratio; d/L . It was observed that $\theta_u(\omega - \omega')$ was mostly strongly affected by A_v/sb as illustrated in Figure 2.5. This suggests that the stirrups acted to confine the compression zone, allowing larger strains and hence larger θ_u . It is important to note that the smallest specimens had the highest A_v/sb as well, as shown in Figure 2.6. There was slight increase in $\theta_u(\omega - \omega')$ with increasing b/L . The effects of A_v/sb and b/L on $\theta_u(\omega - \omega')$ is expected as $\theta_u(\omega - \omega')$ is directly proportional to ϵ_{cu} . There were no apparent effects of b/d and d/L on $\theta_u(\omega - \omega')$ in the Mattock and Corley data. Although the effect of reinforcement is considered to be taken into account by normalizing the rotation, plotting $\theta_u(\omega - \omega')$ vs $(\omega - \omega')$ showed that $\theta_u(\omega - \omega')$ had slightly decreasing trend with increasing $(\omega - \omega')$. There were no specimens having the same A_v/sb , b/d , b/L or d/L but different l/d , suggesting that the test series were not designed properly to investigate the size effect. It is believed that scaled specimens having a constant mechanical reinforcement ratio should be tested to find the effect of size on the rotational capacity.

In Figure 2.7, ϵ_{cu} vs $1/c$ is plotted for Mattock and Corley tests to check Hillerborg's theory that the extreme compression fiber strain is inversely proportional to the depth of the compression block. Figure 2.7 does not support this idea. Very large strains would be attributed to the confinement caused by the compression reinforcement, the stirrups and the loading plate.

The relationship between ϵ_{cu} and $1/d$ for Mattock and Corley tests is shown in Figure 2.8. The trend observed in Figure 2.8 is similar to that in Figure 2.4. The trend in Figure 2.4 is not surprising considering Figure 2.8. All the variables affecting ϵ_{cu} and/or $\theta_u(\omega - \omega')$ seem to combine their effects when the horizontal axis is $1/d$.

Bazant and Cedolin use the stability approach discussed in Section 2.3 for a softening hinge. A hinge is said to be softening when moment is decreasing as the rotation increases. Such behaviour was observed in beams carrying large axial loads and in over-reinforced beams. It is analytically shown that the hinge rotation at the stability limit, θ_{cr} , which is equal to θ_u , is inversely proportional to the beam depth. The discussion of Hillerborg theory by the writers is: "... the assumption that the compression zone behaves as a uniaxially compressed beam seems to be an oversimplification. So does a uniaxial treatment of the compression fracture at bending, since this type of fracture is inherently a three-dimensional phenomenon".

Koike et al. (1987) reported results from over-reinforced scaled beam tests under two point loading. The study was combined with the scaled prism tests mentioned in Section 2.3. They concluded that the size of the specimens affected the moment-rotation curves due to the size effect of the concrete in compression zone. The moment-rotation curves given in the paper seem to be very close to each other regardless of the size of the beam.

Koike et al. (1989) reported results from 75 scaled beam tests under midpoint loading. Some of the beams were under-reinforced and some were over-reinforced. They concluded that moment-rotation curves became more brittle with increasing size. The curves given in this paper do not seem to show any significant size effect on rotational capacity. It was interesting to note that, for highly reinforced beams, the normalized ultimate moment, M_u/bd^2 , seemed to decrease with increasing size.

Kotsovos (1982) reported results from beam tests under third point loading. Using the lateral strains and axial strains measured from beam tests together with those from uniaxial compressive cylinder tests, Kotsovos concludes that the rotational capacity in a beam is due to the triaxial state of stress in the compression zone rather than the descending branch behaviour observed in a cylinder. This conclusion suggests that concrete in the compression zone of a beam and concrete in a uniaxially loaded specimen do not behave the same way.

2.5 Objectives of Testing

As discussed in previous sections, the effect of size on the behaviour of a concrete member is not clear. The reason for different conclusions on size effect on the strength of uniaxial compression is believed to be due to the various loading and reinforcing arrangements used in the tests. Regardless of the testing conditions, all the reports seem to agree on the effect of size on the descending branch behaviour of a uniaxially loaded specimen. There is evidence to suggest that, for tension critical cases, the size of a member is important on its strength and deformation. In the case of rotational capacity of hinging sections, there is no clear evidence whether size has a significant effect on the behaviour or not.

The primary question is, "Is size effect a material property for concrete?". If size effect is a material property then what kind of test is appropriate to determine this property? It seems that the behaviour of concrete in different size members under various type of loading conditions is member dependent.

Rather than trying to find whether size effect is a material property, it may be more useful to know the type of members and loading conditions affected by the member size. The main objective of the test program presented in this thesis is to investigate the effect of size on the behaviour of concrete in the compression zone of a section under flexure. The rotational capacity of a hinging reinforced concrete section may give the required information for this purpose. As rotational capacity is important for the reasons discussed in Section 2.2, knowledge of the effects of size on the rotational capacity of hinging sections is essential for the safety of concrete structures. In addition, an attempt will be made to obtain the stress-strain curves and the stress block parameters for the concrete in the compression zone of the beams.

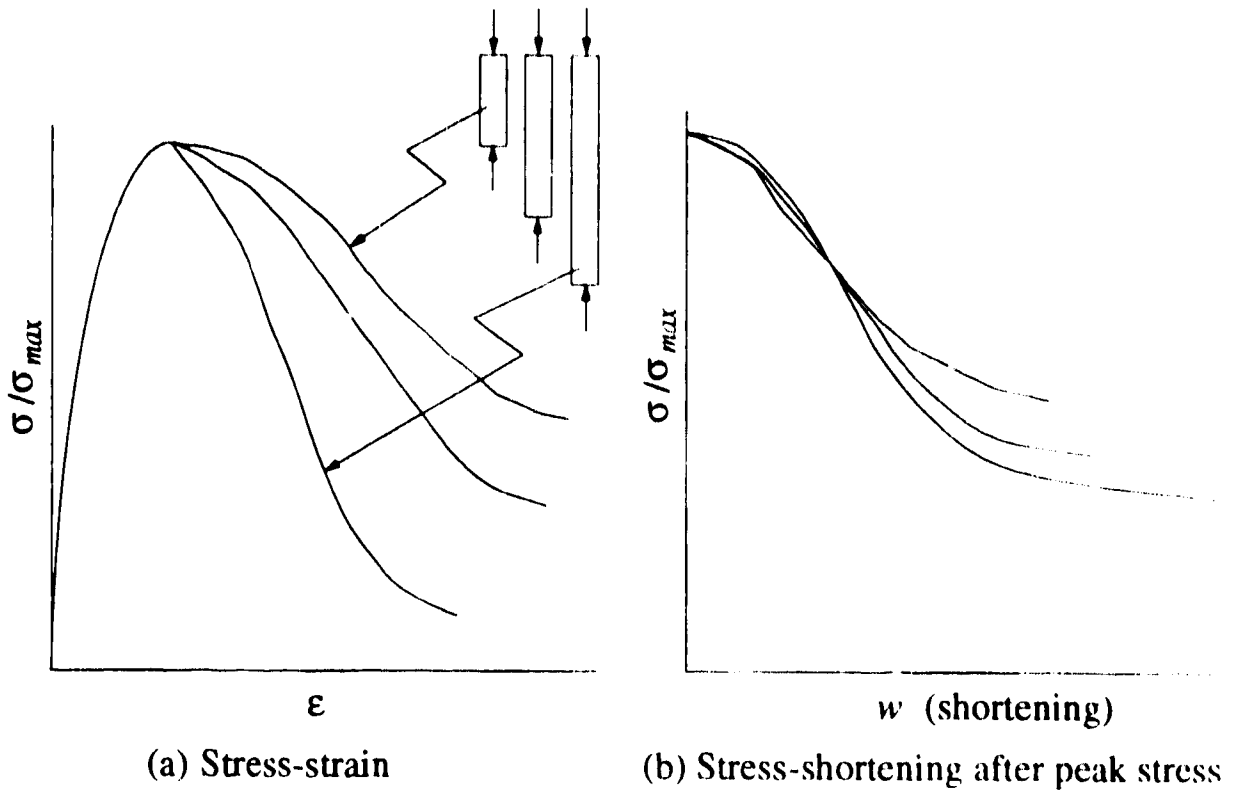


Figure 2.1 Size Effect on Uniaxial Compression, van Mier (1986)

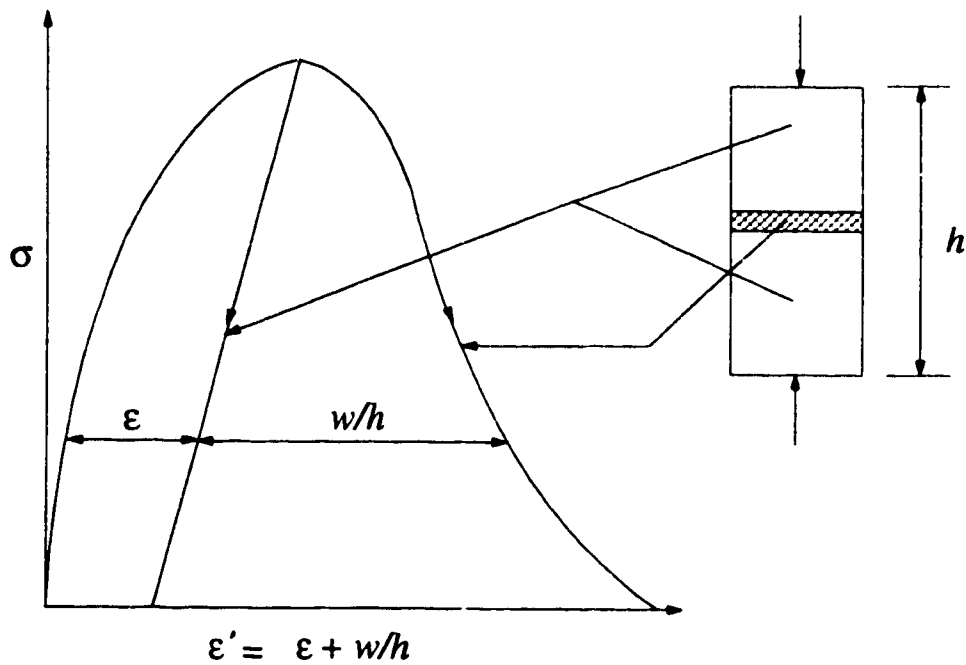


Figure 2.2 Idealization for Stress-strain Curve, Hillerborg (1988a)

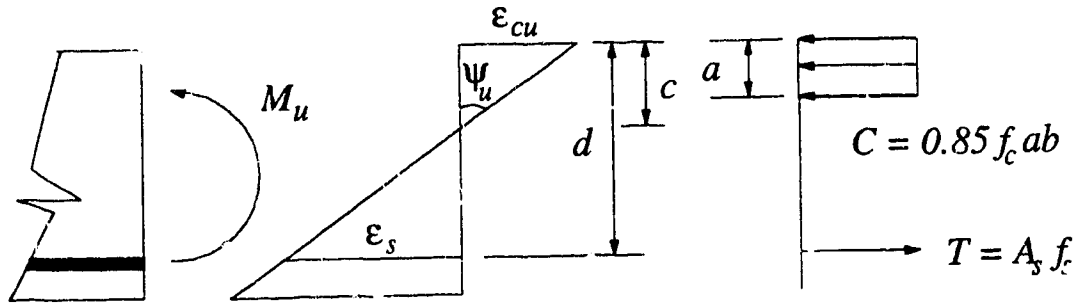


Figure 2.3 Strain and Stress Distribution at Ultimate Moment Capacity

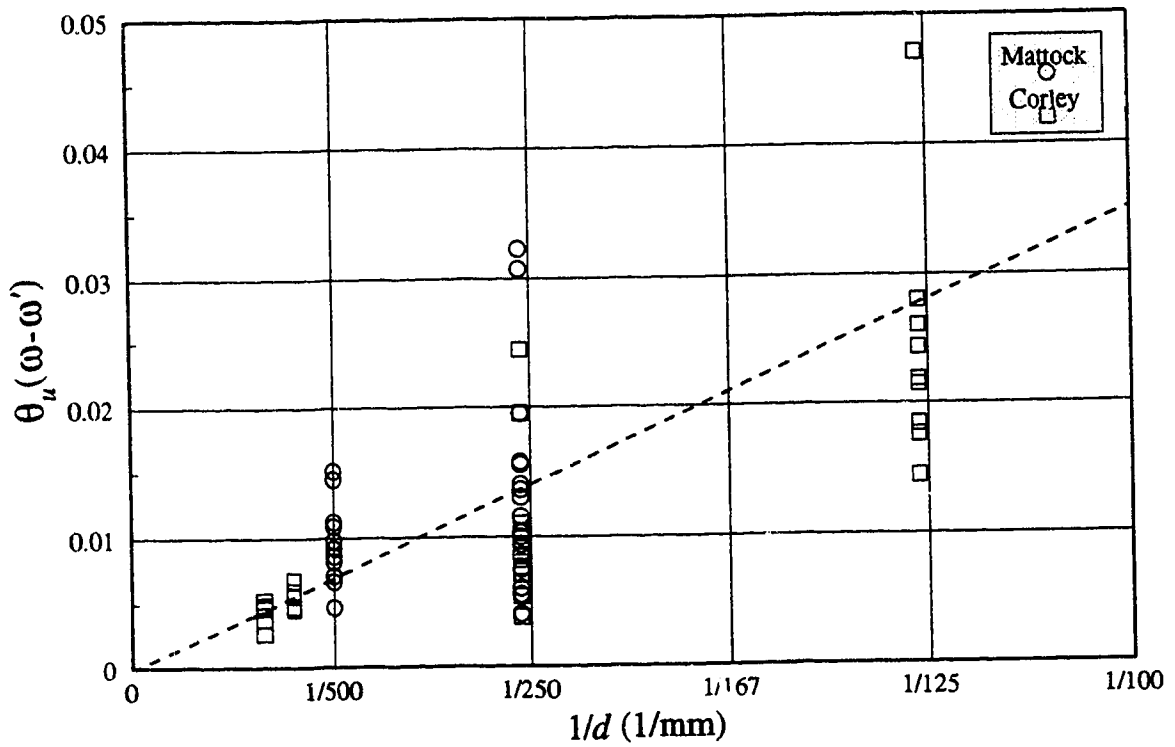


Figure 2.4 Normalized Rotation vs $1/d$

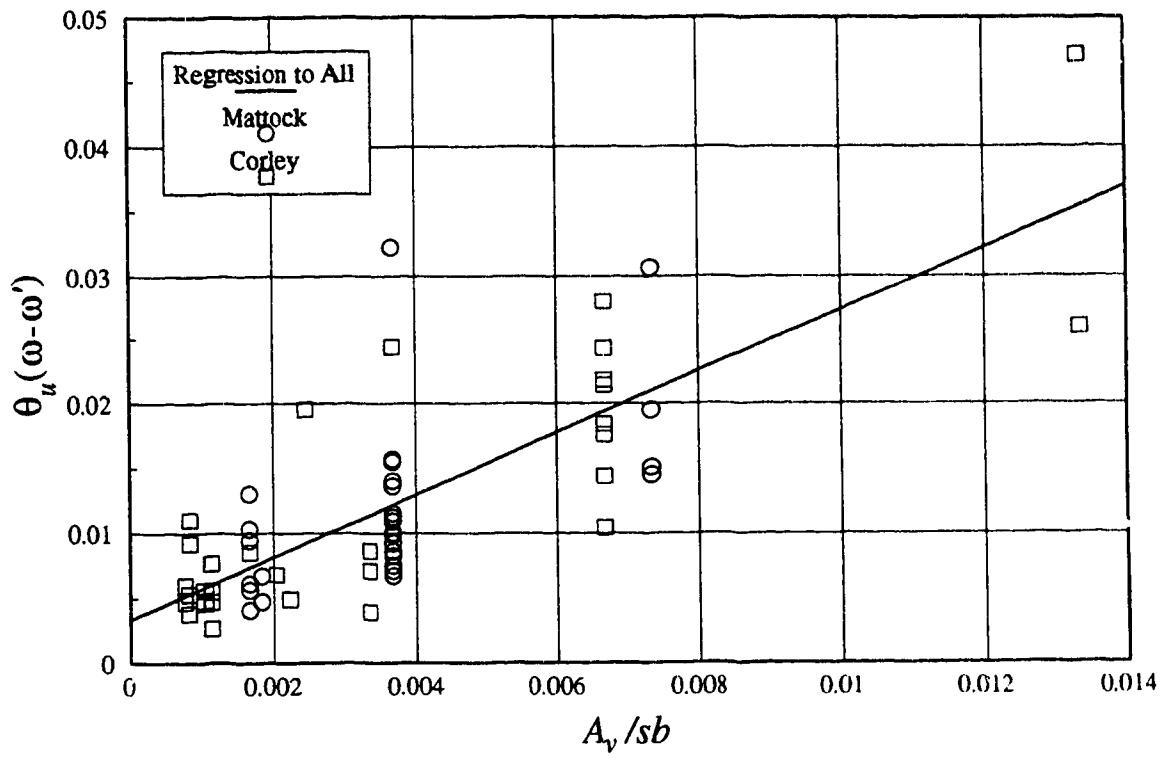


Figure 2.5 Normalized Rotation vs Stirrup Ratio

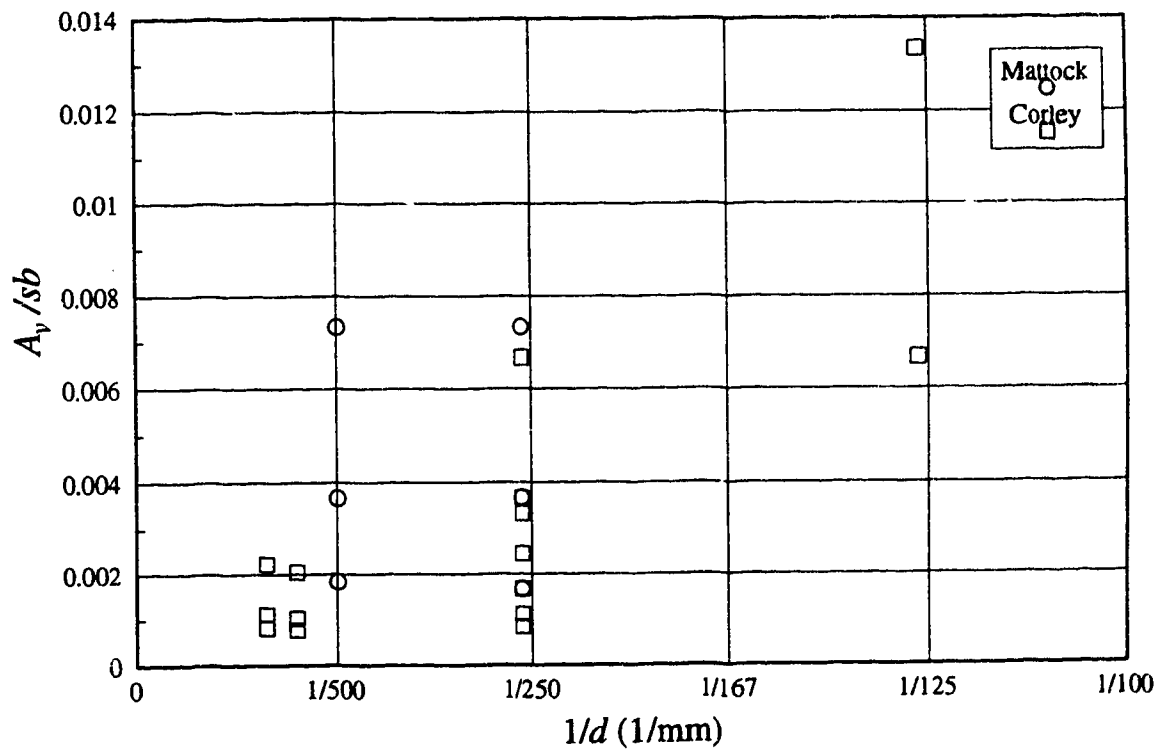


Figure 2.6 Stirrup Ratio vs $1/d$

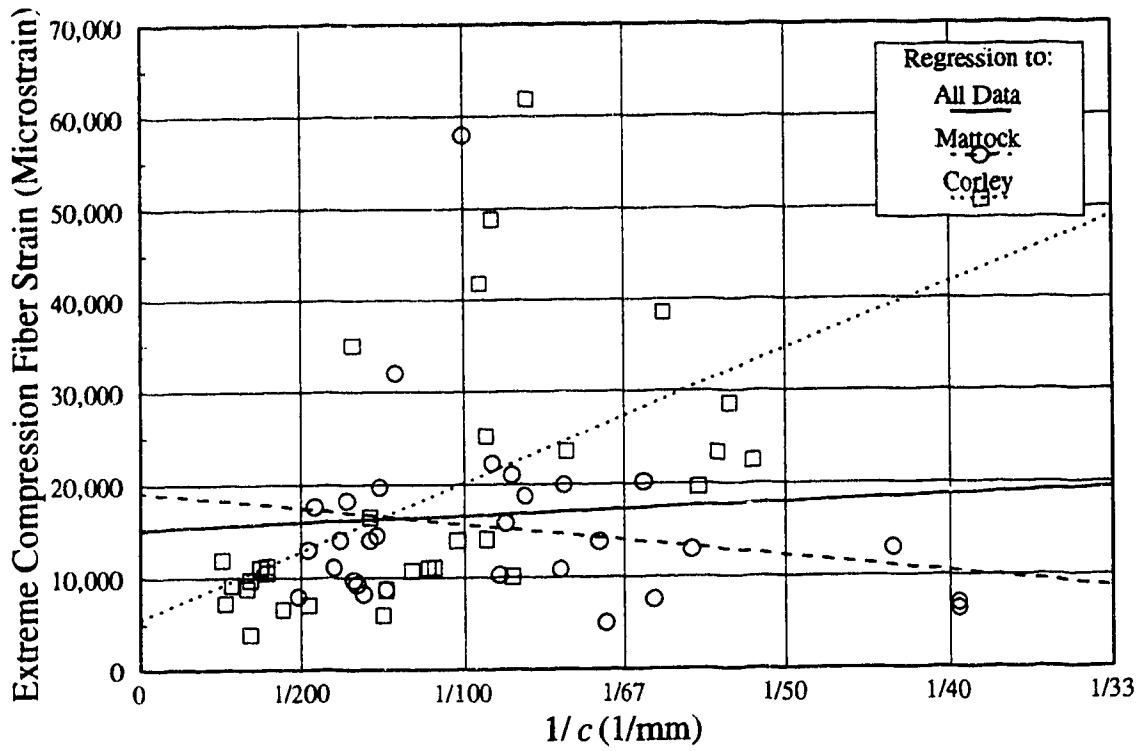


Figure 2.7 Extreme Compression Fiber Strain vs $1/c$

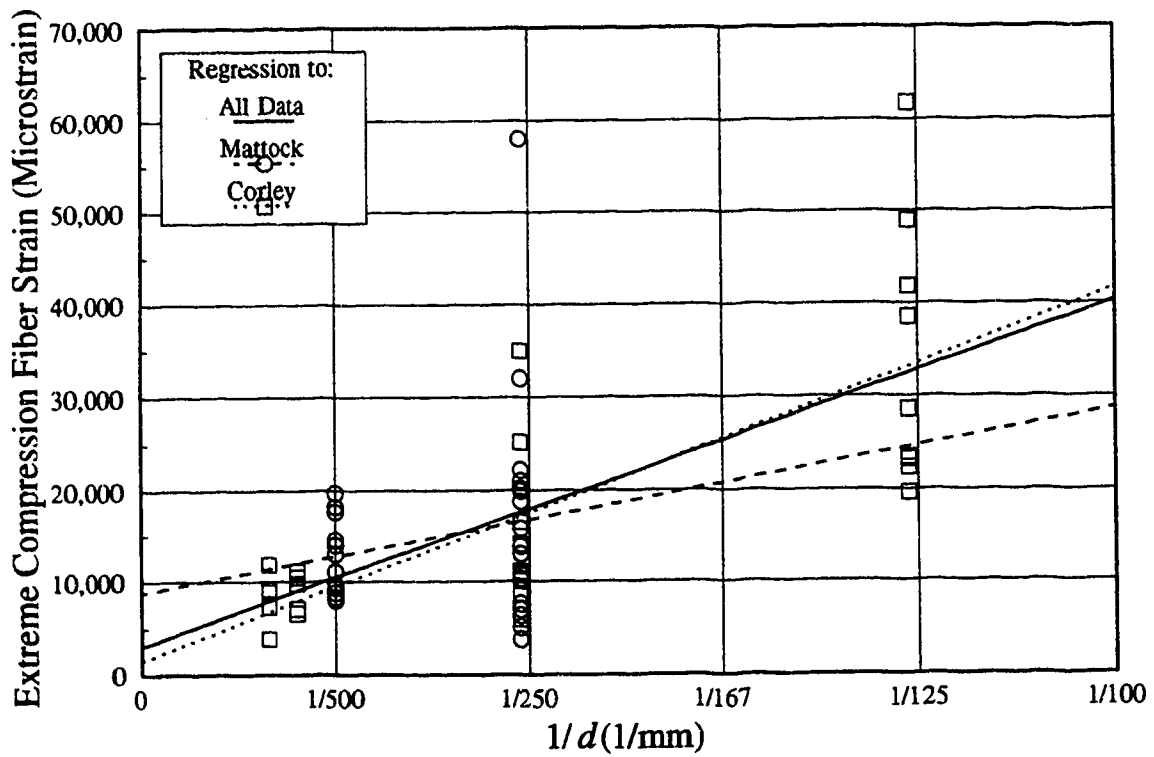


Figure 2.8 Extreme Compression Fiber Strain vs $1/d$

3 Experimental Program

3.1 Introduction

The experimental program consisted of tests of 12 simply supported, under-reinforced, high-strength concrete beams and related material tests. The beams were tested under two point loading. The variables involved were the effective depth and the concrete strength. Three different effective depths and two different concrete strengths were planned to be used. In order to have a feel for the scatter of the data, the combinations were duplicated.

3.2 Test Specimens

3.2.1 Proportioning of Specimens

As discussed in Section 2.4, many variables may affect the rotational capacity of a reinforced concrete beam. These include: the effective depth, d ; the stirrup ratio, A_v/sb ; the width to effective depth ratio, b/d ; the effective depth to length ratio, b/L ; and the mechanical reinforcement ratio, ω . To isolate the effect of d on the rotational capacity, all the variables other than d should be kept constant. Because the size effect is assumed to come from the behaviour of concrete in compression, the compression contribution to the overall behaviour should be maximized. Thus, heavily reinforced, but still under-reinforced, specimens should be tested.

Three different sizes of specimens, namely: small, medium and large, were tested. To obtain the sectional rotational capacity beams were subjected to two point loading. This also allowed A_v/sb to be set equal to zero. The mechanical reinforcement index, ω , was intended to be kept constant. After some preliminary calculations, for the small beams, it was decided to use 4#15 bars in one layer and 8#15 bars in two layers for target concrete strengths of 50 MPa and 100 Mpa, respectively. The beam width for the small beams was determined as 150 mm by the bar spacing requirements. In order to isolate the effects of the descending branch of the concrete stress strain curve on the behaviour, d was chosen in such a way that failure would take place while the steel is still at its yield plateau. Assuming a linear distribution of strains and choosing ϵ_s/ϵ_c at ultimate moment equal to 2, the corresponding d can be calculated as 230 mm for the small beams. At this stage, the bar diameter to effective depth ratio, ϕ/d , and the width to effective depth ratio, b/d , are known and the

section dimensions for the medium and large beams can be scaled up for #25 bars and #35 bars, respectively. This was done using the theoretical bar diameters rather than the nominal diameters implied by the bar size numbers.

The typical beam configuration is shown on Figure 3.1. Selecting a shear span to effective depth ratio, $a/d = 4$, with adequate stirrups ensures flexural failure and provides adequate development length for the longitudinal steel. To have a long test region, the distance between the load points was chosen to be equal to $6d$. The longitudinal reinforcement should be extended beyond the zero moment section to anchor the hooks adequately. Choosing d for the hook development length and supplying additional stirrups at the hook locations satisfy all the requirements given in the ACI code (1989). Standard 180° hooks were provided at the ends of the longitudinal reinforcement in the lower concrete strength beams. In the higher concrete strength beams, the bottom layer of reinforcement had 90° hooks and the upper layer of reinforcement had 180° hooks. The total length of the beams was $L = 16d + 4\phi$. The resulting specimen dimensions together with the abbreviation descriptions are given in Table 3.1. The clear cover to the longitudinal reinforcement in the beams were scaled; 44, 70, and 97 millimeters for small, medium, and large beams, respectively. All the spacings between the bundles of bars were also scaled. Figure 3.2 shows the sections and the side view of the beams in scale. It is important to mention that the geometry of the beams were scaled without scaling the size of the aggregates used.

3.2.2 Details of Specimens

Many previous tests were affected by the strain concentrations caused by the loading plates on top of the specimens. These strain concentrations lead to premature failures close to the loading points. To avoid this, the beams were loaded through the corbels shown in Figure 3.1. The length of the corbels in the direction of longitudinal axis of the beams was equal to twice the beam width. The corbels were designed by a simple strut-and-tie model. Threaded rods extending through the corbels were used to attach lifting lugs to handle the specimens.

The shear spans were reinforced for shear ignoring the contribution of the concrete to the shear carrying capacity. For placing convenience, U-shaped stirrups with standard 135° hooks were used. The stirrups in the corbel regions were designed to lift the entire corbel load to the top of the beams as the beams are effectively loaded from their bottoms. Details of the shear span and corbel reinforcement are given in Table 3.2.

Forms were made out of plywood and wood. Battens were provided on the sides of the forms to prevent bulging. All the beams were cast upside down. Casting upside down has a number of advantages. Threaded rods at appropriate locations at the top of the forms were used both to support the steel cage at the correct location and to keep the top of the forms at the desired width. In this way there was good control on the location of the longitudinal reinforcement and on the width of the beams throughout their lengths. Another advantage of casting the beams upside down is that the uniformity and quality of the concrete in the compression side of the beams was not affected by bleed water. Figure 3.3 shows the formwork and the reinforcement for a large higher concrete strength beam.

3.2.3 Beam Designations

Each beam was referred to using two letters and a number. The first letter was S, M or L for small, medium or large. The second letter was L or H for lower strength (50 MPa) or higher strength (100 MPa) concrete. The number 1 or 2 referred to which of the two duplicate beams the beam was. See Table 3.1.

3.3 Materials

3.3.1 Concrete

There were basically two different mix designs; one for the lower strength concrete (target strength of 50 MPa at 56 days) and one for the higher strength concrete (target strength of 100 MPa at 56 days). In designing the mixes the procedures given by P-C. Aitcin and the proposed ACI 211.4R-XX report "*Guide for Selecting Proportions for High Strength Concrete*" were followed. The target for the lower strength concrete was reached without difficulty. The trial batching experience showed that the highest possible concrete strength using local aggregates and no silica fume is around 90 MPa in 56 days. After casting the small and medium specimens, some minor changes were made in the higher strength concrete mix design. All the mix designs are given in Table 3.3.

Bagged Type 10, Normal Portland Cement, was used to cast the specimens. Cement supplied by Lafarge Canada Inc. was used to cast the small and medium beams. Inland Cement supplied the cement for casting the large beams. Information about both cements is given in Table 3.4.

Local sands and coarse aggregates were used to cast the beams. The results of the petrographic analysis of sand indicated that it was composed of 21.7% orthoquartzite, 63.0% quartzite, 4.9% sandstone, 1.5% trap (basalt), 1.9% granite. These "good" rock types formed 93% of the total sand. Similarly, the coarse aggregate was composed of 62.6% orthoquartzite, 14.1% quartzite, 10.6% hard sandstone, 5.6% trap (basalt), 4.0% rhyolite, 0.1% granite. These "good" rock types formed 97% of the total coarse aggregate.

The laboratory mixer could produce a maximum 0.2 cubic meter batch. Using the laboratory mixer required 2 batches for the small beams, 5 batches for the medium beams and 13 batches for the large beams.

All the beams except ML2 and MH2 were cast using concrete batched in the laboratory. Because the large beams required a large quantity of concrete it would have been much easier to cast them using ready-mix concrete. In order to experiment whether local suppliers could produce ready-mix high-strength concrete, beams ML2 and MH2 were cast using concrete batched by transit mix. Bulk Type 10 Inland Cement was used in both mixes.

The laboratory batching experience showed that more uniform mixes can be obtained by the following batching scheme. First put all the sand, cement, water and the superplasticizer into the mixer and mix until a slurry is obtained. The mix will look dry at the beginning but after mixing couple of minutes, if there is enough superplasticizer and water, the mix will suddenly turn into a semi-liquid. Then, add the coarse aggregate and mix for another three to four minutes. Slump for these mixes is not a good measure of workability. The workability of the mix can be checked rather qualitatively inside the mixer. Check the concrete by running it through fingers or stopping the mixer and pressing on the surface of concrete inside the mixer. If it feels like a waterbed the mix is workable and ready to place. Retempering mixes at this stage gives successful results. For mixes having high superplasticizer amounts, using water or superplasticizer to retemper the mix does not seem to make a difference. If the total amount of water and/or superplasticizer is added at the beginning, a more workable mix is obtained.

The beams were cast in layers and segments. Casting started usually at the north end of the beam. For example; dividing the large beams into three segments, the two shear spans and the test region, gave almost equal segments. First three batches were placed in the north shear span and flow of concrete into the test region was prevented by putting wooden blocks supported by one of the stirrups inside the corbel region. Next three batches were placed in the test region again flow of concrete to the next segment was prevented. Then the remaining part of the north shear span was filled. Next three batches were placed in the

south shear span and then the remaining part of the test region and the south shear span were filled. The large beams were cast in two to two and a half hours. No cold joints were formed during casting as the time between casting two layers or two segments was no longer than half an hour. The concrete was vibrated for short periods during casting of each layer and was vibrated for longer from one end to the other after the form was filled up completely. Moisture contents of the aggregates were measured every three batches and the corresponding corrections were made for the next batch using a spreadsheet program. Similar procedures were followed to cast small and medium size beams. Cores drilled from the ends of the medium and large beams for another research project showed slight variation on concrete strength through the length and depth of the beams. The details about the core data are given in two papers by Bartlett and MacGregor (1993a, 1993b).

The concrete in ML2 was supplied by a local ready mix company. The mix design for ML2 was used by the supplier for another job. The target strength for this mix was 42 MPa at 56 days. ML2 cylinder strength reached 52.0 MPa at 28 days and as a result beam ML2 was tested much earlier than anticipated.

The mix design for MH2 was similar to that for MH1. After three unsuccessful trials, the fourth mix was used to cast beam MH2. The first three batches were from a wet batching plant and the fourth one was from a dry batching plant. In a wet batching plant all the ingredients are mixed in a mixer at the plant and the concrete is transferred to a truck. In a dry batching plant, all the ingredients are loaded to the drum of the truck where the mixing takes place. The first three mixes had serious segregation of the coarse aggregate. While the concrete at the bottom of the bucket was hardening almost immediately, a lot of water was collecting on the top. As the time between batching and casting would be about half an hour some retarder was used in the first trial. All the superplasticizer was added at the batching plant as well. In the second trial no retarder was used, again all the superplasticizer was added to the mix at the batching plant. In the third trial all the superplasticizer was added to the truck in the laboratory. But as there was water inside the drum left over from the washing of the previous mix, again the result was unsuccessful. In the fourth trial the dry batching plant was used thinking that amount of water inside the mix would be controlled much better. All the excess water in the drum was emptied. Five liters of superplasticizer, which is one quarter of the total amount that was anticipated, was added at the batching plant. When the concrete arrived to the laboratory 2.5 liters of superplasticizer was added to the truck. In total 37% of the superplasticizer anticipated based on laboratory batching

was added to the mix. Trial batching in the laboratory with the cement used in these mixes showed that this amount of superplasticizer would give a mix that was impossible to work with.

The quality control of the ready-mix concrete supplied for this job was very poor. There are many sources of error. As there is very little water in high-strength concrete mixes, errors in weighing water and errors in moisture content of aggregates influence the outcome considerably. Taking moisture contents of aggregates from the bottom of the bins and using larger volume mixes would lead to more successful results.

Along with each beam, ten 100 mm by 200 mm cylinders for uniaxial compression tests, three 6" by 12" cylinders for split tensile strength tests and three 100 mm by 100 mm by 840 mm beams for notched beam tests were cast. These specimens were cast using part of the batch filling the test region. In cases where more than one batch of concrete was used to cast compression zone of the test region, concrete from each of these batches were used to cast the specimens. When casting was complete, the beams and the specimens for material property tests were wrapped in polyethylene sheets. The beam and the specimens were stripped after 24 hours. The beam was then wrapped with polyethylene sheets for one week. The other specimens were placed in a curing tank in lime saturated water at laboratory temperature (about 20°C) until one or two weeks before the beams were tested. They were tested after letting them dry for at least 7 days. The cylinder tests were carried out on the day of testing of the accompanying beam. The split cylinder tests and the notched beam tests were carried out whenever the scheduling in the laboratory allowed. The results from these tests are given in Table 3.5. The specimens are grouped into three groups relative to their cylinder strengths.

Typical stress-strain curves from cylinder tests for lower and higher concrete strengths are shown in Figure 3.4. The ends of the specimens were lapped. The tests were carried out by a system where a computer program written under Labview 2 creates a differential signal between the load signal and the displacement signal giving a control parameter for loading. This allowed the negative slope of the descending branch of the high-strength concrete stress-strain curve to be recorded. The rate of loading was around 12 microstrain per second. The strains were measured by the LVDT inside the testing machine. The deformations of the loading system itself were calibrated by loading a steel cylinder with strain gauges attached. The deformations given by the LVDT minus the deformation in the loading system gave the shortening of the concrete cylinders.

Typical curves obtained from notched beam tests are shown in Figure 3.5. To obtain the fracture energy, G_F , of concrete the RILEM Draft Recommendation (1986) was followed. The beams were sawn with a stiff diamond saw under wet conditions. The depth of the notches were equal to half the beam depth. The thickness of the notches was 3 mm. The specimens were tested under three-point bending. Some details are shown in Figure 3.5.

Regardless of whether it was a uniaxial compression test, a split cylinder test, or a notched beam test, distinctly different failure surfaces were observed for lower and higher concrete strength specimens. The lower concrete strength specimens developed irregular failure surfaces including a large amount of bond failures between the mortar and the aggregates. The failure planes in higher concrete strength specimens were nearly plane and passed through the aggregate and the mortar.

3.3.2 Reinforcement

Longitudinal tensile reinforcing bars ranging from #15 to #35 in size were used in the beams. To support the stirrups in the shear span #15 bars were used regardless of the size of the beam. Only coupons from the longitudinal tensile reinforcement were tested. Typical coupon tests are shown in Figure 3.6. As steel strains in excess of 15,000 microstrain were not expected in the beam tests, some of the coupons were not tested further to protect the tension grips of the testing machine. Because the #15 bars used in the small specimens were cut and bent in the laboratory it was possible to test coupons for every individual beam. The coupon tests of #15 bars showed that all the steel used in the small beams came from the same lot. Thus, average yield bar force values were used for analysis purposes.

Coupons from #25 and #35 bars used in the medium and large specimens were cut by the supplier at the time the bars were bent. The supplier grouped the coupons in three groups. One group for lower concrete strength beams, two groups for higher concrete strength beams; one for upper layer and one for lower layer of reinforcement. As the coupon tests for #25 bars gave unreasonable results, judging from the observed behaviour of the medium beams, coupons were cut from all the longitudinal bars at one end of the beams and tested. All the #35 coupons cut by the supplier and the coupons extracted from one end of beam LH2 were tested. The coupon tests for the #35 bars showed that there were two lots of steel, see Figure 3.6. The average static yield bar force per bar as well as the average bar force per bar at the strain corresponding to the ultimate moment, which is used for analysis purposes, are given

in Table 3.6. The average bar force per bar at the strain corresponding to ultimate moment was computed as the total force based on the measured strains in the beam tests divided by the number of bars.

The values of the mechanical reinforcement ratio, ω , the ratio of tension reinforcement, ρ and the ratio of actual to balanced steel ratio ρ/ρ_b (calculated using the ACI code approach) values are given in Table 3.6. For reinforced concrete beams ρ by itself is not too meaningful. The mechanical reinforcement index, ω , is a better measure of the reinforcement in a section. The higher concrete strength beams had larger ω values as concrete strengths around 90 MPa were achieved instead of 100 MPa. The medium beams had larger ρ values due to rounding off the scaled effective depth and width of these specimens.

3.4 Testing

3.4.1 Test Set-up and Instrumentation

The beams were tested in the loading frame shown in Figure 3.7. In the small and medium beam tests the north reaction was a roller support and south reaction was a restricted roller support, effectively a hinge support. In the large beam tests, both reactions were roller supports with stops provided at both ends. Figure 3.8 shows these support conditions. Depending on the size of the beam, different spreader beam arrangements were used to load the beams through the corbels. The specimens were loaded by two 1780 kN capacity hydraulic jacks which were pressurized by an "air on oil" system. Flow of oil to each jack was controlled separately to maintain equal loads. For the sake of safety, lateral bracing not touching the specimens were provided as there is always a chance of rigid body rotation of the specimen if it is not aligned properly.

All the loads and reactions were measured using various load cells. It was interesting to note that Kyota type load cells were very sensitive to alignment. As the statics were not satisfied in testing of beam SL1, these load cells were calibrated again after the test. Putting a shim of thickness equal to 0.13 mm under one side of the load cell caused about 10% error in the readings. These load cells were replaced by Strainsert flat type load cells and this type of load cells were used for all the other tests.

Centerline deflections were measured by a cable transducer attached to the bottom of the beams.

The total angle change in the test region was measured by a pair of rotation meters attached to 1/2" embedded threaded rods on the east face of the beams. These threaded rods were located above the neutral axis at $0.26d$ from the top surface. The rotation meters were located $d/2$ away from the corbels which put them $3.7d$ apart. A rotation meter consisted of two arms and an LVDT. The bottom arm is fixed to the specimen. The arm at the top pivots at one end and at the other end there is an adjusting screw and an LVDT attached. Before every reading, the upper arms of the rotation meters were leveled by using the spirit level attached. This way the LVDT would read the change in the vertical distance from which the angle change could be computed. Figure 3.9 shows the rotation meter arrangement for a small beam.

In the small and medium beams, the south reaction was a pin support and the change in shear span was measured by measuring the movement of the south load point relative to a fixed reference. For this purpose an LVDT was used. In large beams, change in the shear span was measured by two cable transducers one of which measured the increase in the distance between the two reactions and the other measured the decrease in the distance between the two load points. In either method symmetry of deformations is assumed. The shear spans increased by 1 to 2.5 percent of the initial shear span length, $4d$, during the test. The increased length was used to compute the moments in the beams. See Section 4.3.2 for typical contribution of the moment due to increase in the shear span to the total ultimate moment.

On the west face of the beams, three to five pairs of LVDTs were used to measure the curvatures and the neutral axis depths at different sections along the test regions. At the bottom of the beams these were attached to the embedded threaded rods carrying the steel cage during casting. On top of the beams, threaded rods were embedded during casting above the neutral axis at a distance of $0.175d$ below the top surface of the beams. In the small beam tests, instead of the top LVDTs a 5" Demec gauge was used. The side LVDT arrangement for a large beam is shown in Figure 3.10. The gauge length for the LVDTs was around 300 mm. Actual gauge lengths, measured from the beams before testing, were used in the analysis of the test data. The LVDTs could read to the nearest 0.01 mm allowing strain to be measured to the nearest 30 microstrain.

Strains in the longitudinal reinforcement were measured by 5 mm foil strain gauges attached on top and bottom of every bar. It was observed that upon yielding of the reinforcement the strain gauges started to give unreasonable values.

Strains on the top surface of the beams were measured by a 2" Demec gauge. The Demec targets were attached by sealing wax or hot glue. Regardless of the size of the beam, the Demec targets were located 1" apart. Every reading was assumed to give average strain at a location at the middle of the gauge length. The 2" Demec gauge had an accuracy of 25 microstrain. The total number of readings taken at each set were 39, 59, and 89 for small, medium, and large beams, respectively.

Figure 3.11 shows the overall view of the test set-up for a large beam.

3.4.2 Test Procedure

The specimens were aligned and plastered to the reaction point knife edges. The spreader beams were also aligned and plastered to the corbels. Special care was taken to make sure that the loads and the reactions were all on the same line and shear spans had equal lengths. The geometry of the test regions were measured at five or six different sections. The actual dimensions of the test regions were within one to two millimeters of that was intended. All the instrumentation was attached to the beams after they were aligned in the test frame. Thus, the measurements do not include the effects of the dead load.

At every load step the data other than the Demec gauge readings were recorded by the data acquisition system. The data were recorded within two to three minutes after the loading had been stopped. The Demec gauge readings were recorded on a spreadsheet program using the computer. Additional electronic data readings were taken after every Demec gauge reading set and after other long pauses. At every second or third load step cracks were marked.

The load steps were adjusted such that yielding would occur in 10 to 15 load steps. Loading speed before yielding was adjusted such that every load step would take about 15 minutes. Two to three sets of Demec gauge readings were taken before yielding. The total time until yielding was about 3 to 4 hours.

After yielding the speed of loading was slower. Depending on the size of the beam a loading rate of 2 to 5 mm of centerline deflection per 15 minutes was used. The loading rate was even slower towards the end of the tests. Depending on the deformation capacity of the beam, testing took between 8 to 12 hours to reach failure. It is believed that the loading rate was slow enough that there was no dynamic effect. In total, in the entire test, five to seventeen Demec gauge reading sets were taken.

Table 3.1
Specimen Descriptions

Specimen	Bar size (mm)	Size	Concrete Strength	<i>b</i> (mm)	<i>d</i> (mm)	<i>h</i> (mm)	<i>L</i> (mm)
SL1, SL2	16.0	S mall	L ower	150	230	282	3740
SH1, SH2	16.0	S mall	H igher	150	230	302	3740
ML1, ML2	25.2	M edium	L ower	235	360	443	5860
MH1, MH2	25.2	M edium	H igher	235	360	475	5860
LL1, LL2	35.7	L arge	L ower	335	515	630	8380
LH1, LH2	35.7	L arge	H igher	335	515	678	8380

Table 3.2
Stirrup and Corbel Reinforcement Details

Specimen	Stirrups Shear Spans	Corbel Reinforcement Transverse, Stirrups
SL1, SL2	#10 @ 115 mm	2 #10, 2 #10
SH1, SH2	#10 @ 115 mm	2 #15, 3 #10
ML1, ML2	#10 @ 160 mm	3 #10, 4 #10
MH1, MH2	#15 @ 160 mm	3 #15, 4 #15
LL1, LL2	#15 @ 230 mm	4 #15, 4 #15
LH1, LH2	#15 @ 115 mm	5 #20, 8 #15

Table 3.3
Concrete Mix Designs

	SPECIMEN(S)			
	SL1, SL2, ML1 LL1, LL2	ML2	SH1, SH2 MH1	MH2 LH1, LH2
Water/Cementitious	0.483	0.315	0.27	0.27
Cement (kg/m ³) (Type 10)	410	355	550	550
Fly Ash (kg/m ³)	-	90	-	-
Water (l/m ³) ¹	198	140	150	148.5
Coarse Agg (kg/m ³) Min-max size (mm)	1088 5-19 uncrushed	1040 5-14 crushed	1100 5-14 crushed	1100 5-14 crushed
Fine Agg (kg/m ³) Fineness modules	669 2.3	640 -	667 2.7	595 2.7
SPN (l/m ³) ²	-	-	21.2	16.2
WRDA (l/m ³) ³	-	2.1	-	-
DARAVAIR (l/m ³) ⁴	-	0.2	-	-
DARACEM (l/m ³) ⁵	-	1.6	-	-
Air (assumed)	1%	5%	2%	2%

1 Water content includes water in the admixtures.

2 A poly-naphthaline sulfate based superplasticizer produced by CONCHEM. Contains 70% water by volume.

3 Water reducing admixture produced by W.R. Grace & Co. of Canada Ltd.. A non-chloride, aqueous solution of highly purified metallic salts of lignin sulfonic acids.

4 Air-entraining admixture produced by Grace. An aqueous solution of completely neutralized vinsol resin.

5 A high-range water reducing admixture produced by Grace. Blend of sodium and potassium salts, lignosulfonate and polymerized naphthalene sulfonic acid.

Table 3.4
Some Properties of Cements Used

Cement	C ₃ S (%)	C ₂ S (%)	C ₃ A (%)	C ₄ AF (%)	Fineness (cm ² /g)
Lafarge Type 10	55.1	18.2	6.4	8.7	4180
Inland Type 10	49.0	22.0	8.6	8.9	4161

Table 3.5
Concrete Strength Test Data

Specimen	f_c (MPa) ⁶	f_t (MPa) ⁷	G_F (N/m) ⁸
SL1	51.1 @ 56 days	4.6 @ 90 days	178.5 @ 138 days
SL2	51.1 @ 56 days	4.0 @ 83 days	182.7 @ 131 days
ML1	52.7 @ 56 days	4.3 @ 106 days	193.0 @ 104 days
ML2	54.1 @ 37 days	3.7 @ 99 days	233.5 @ 97 days
LL1	54.2 @ 52 days	4.2 @ 85 days	219.2 @ 160 days
LL2	43.8 @ 44 days	3.8 @ 70 days	218.4 @ 145 days
MH2	73.4 @ 73 days	4.6 @ 78 days	211.9 @ 76 days
SH1	90.1 @ 56 days	6.5 @ 76 days	216.5 @ 124 days
SH2	85.6 @ 56 days	5.5 @ 69 days	193.9 @ 117 days
MH1	90.3 @ 56 days	6.2 @ 92 days	255.7 @ 90 days
LH1	90.3 @ 46 days	5.6 @ 62 days	224.2 @ 137 days
LH2	87.7 @ 47 days	5.2 @ 55 days	233.4 @ 130 days

6 Average of 6 to 8 cylinder tests.

7 Average of 2 to 3 split cylinder tests.

8 Average of 2 to 3 notched beam tests.

Table 3.6
Reinforcement Coupon Test Results

Specimen	ω^9	ρ	ρ/ρ_b	Average Static Yield Bar Force per Bar (kN)	Average Bar Force per Bar at Ultimate Moment (kN)
SL1	0.186	0.0232	0.54	81.98	81.98
SL2	0.186	0.0232	0.54	81.98	81.98
ML1	0.184	0.0236	0.55	204.74	204.74
ML2	0.177	0.0236	0.53	202.00	202.00
LL1	0.183	0.0232	0.53	408.80	428.00
LL2	0.217	0.0232	0.58	408.80	409.50
MH2	0.259	0.0473	0.78	200.81	200.81
SH1	0.211	0.0464	0.64	81.98	81.98
SH2	0.222	0.0464	0.68	81.98	81.98
MH1	0.210	0.0473	0.64	200.81	200.81
LH1	0.219	0.0464	0.63	406.10	426.00
LH2	0.229	0.0464	0.67	412.20	432.40

⁹ Calculated using the average bar force per bar at ultimate moment.

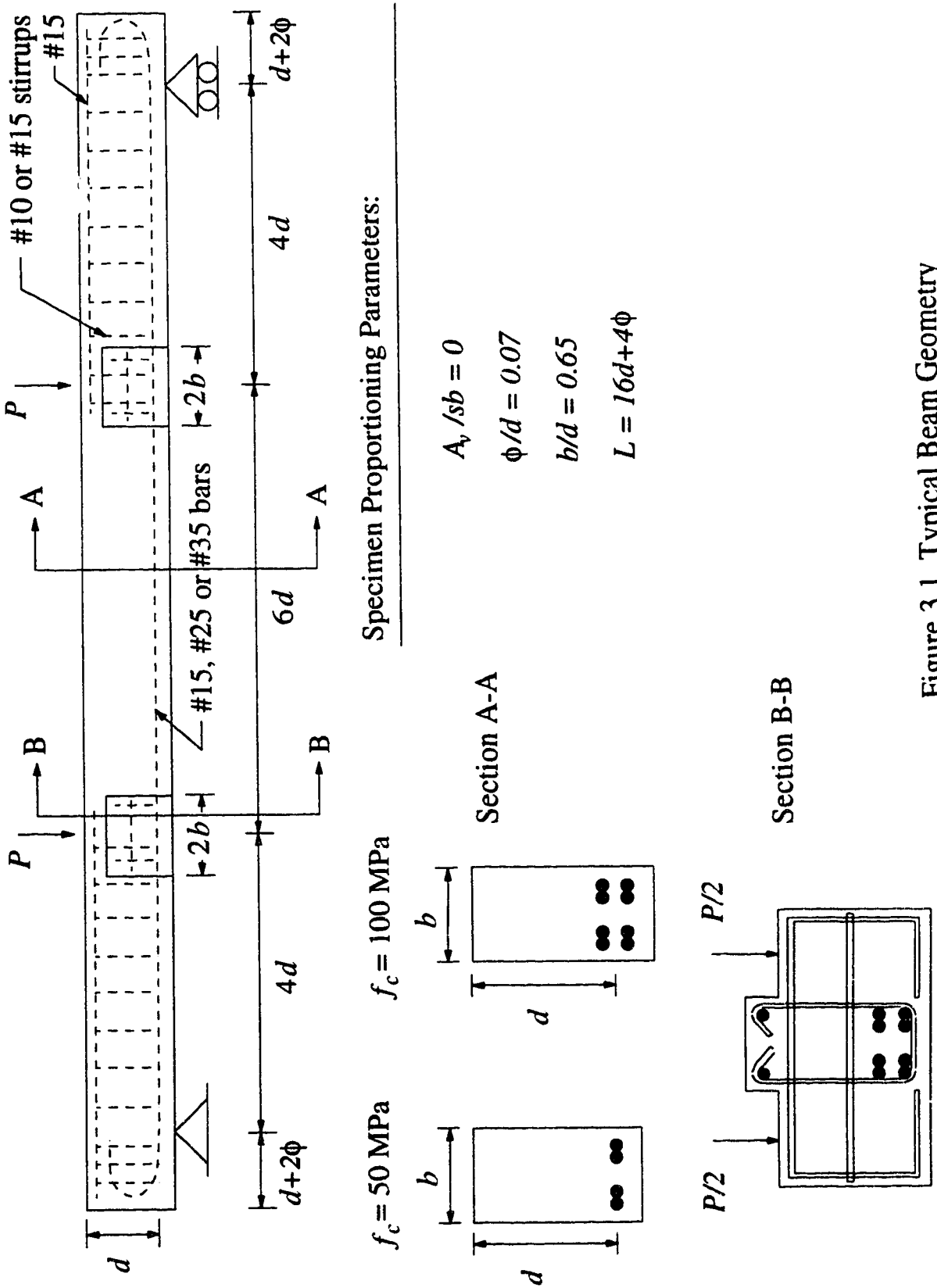


Figure 3.1 Typical Beam Geometry

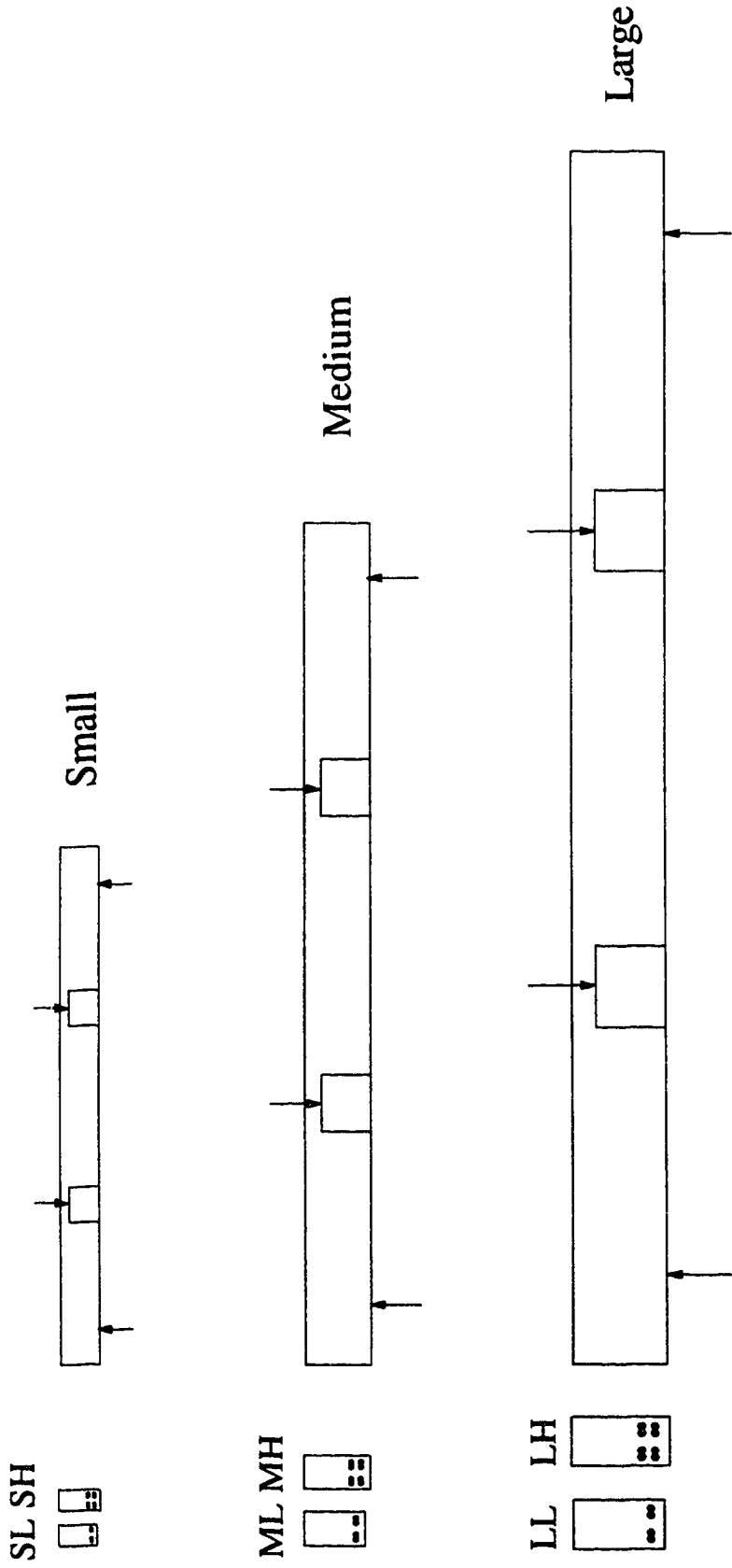


Figure 3.2 Beams in Scale



Figure 3.3 Formwork and Reinforcement for a Large Beam

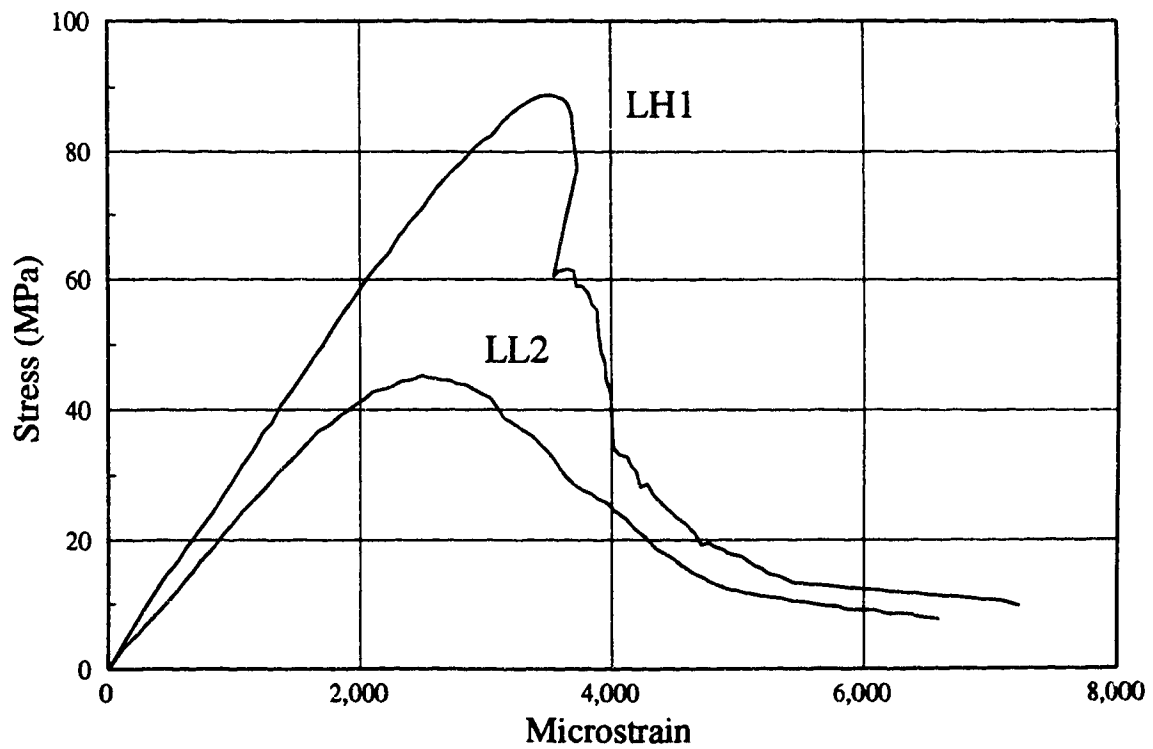


Figure 3.4 Stress-Strain Curve for Concrete from Cylinder Tests

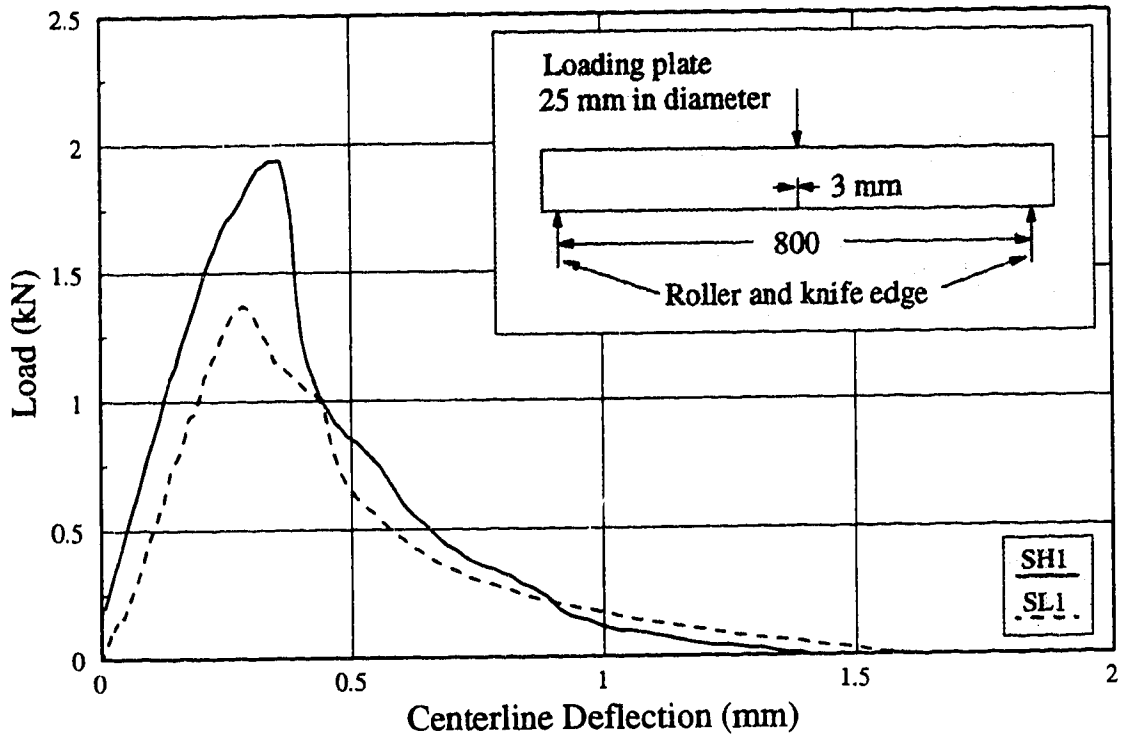


Figure 3.5 Concrete Notched Bearing Tests

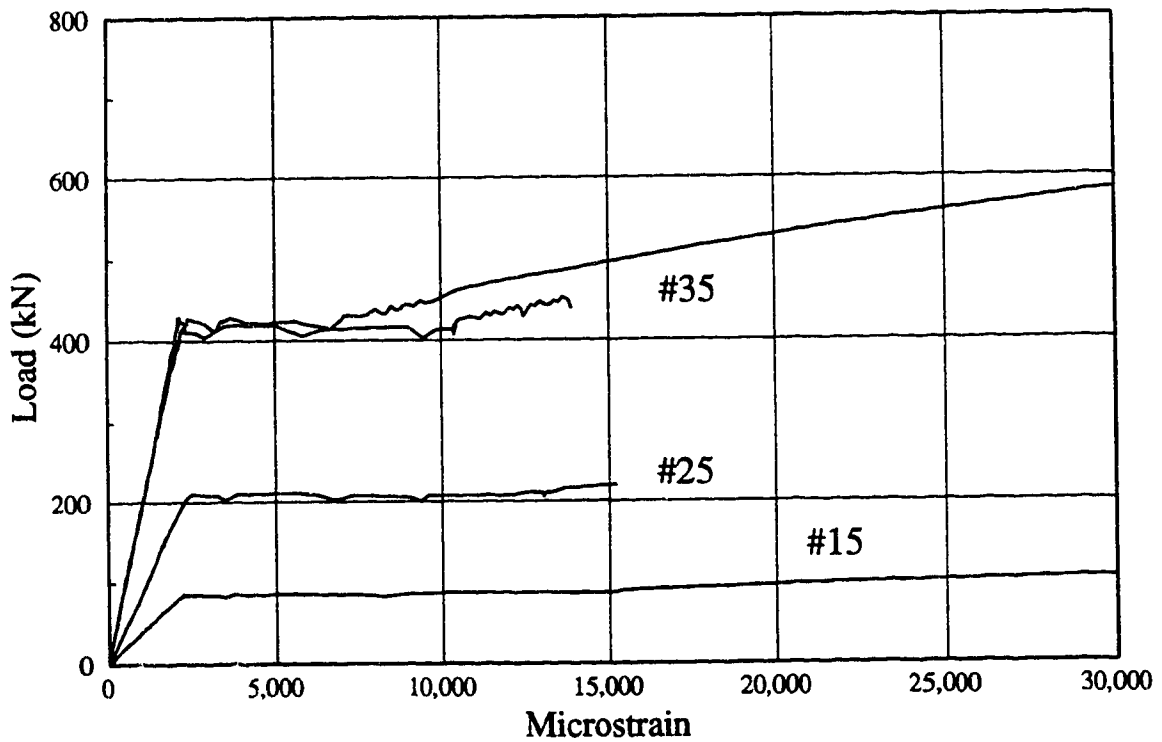


Figure 3.6 Typical Coupon Tests of Reinforcing Bars

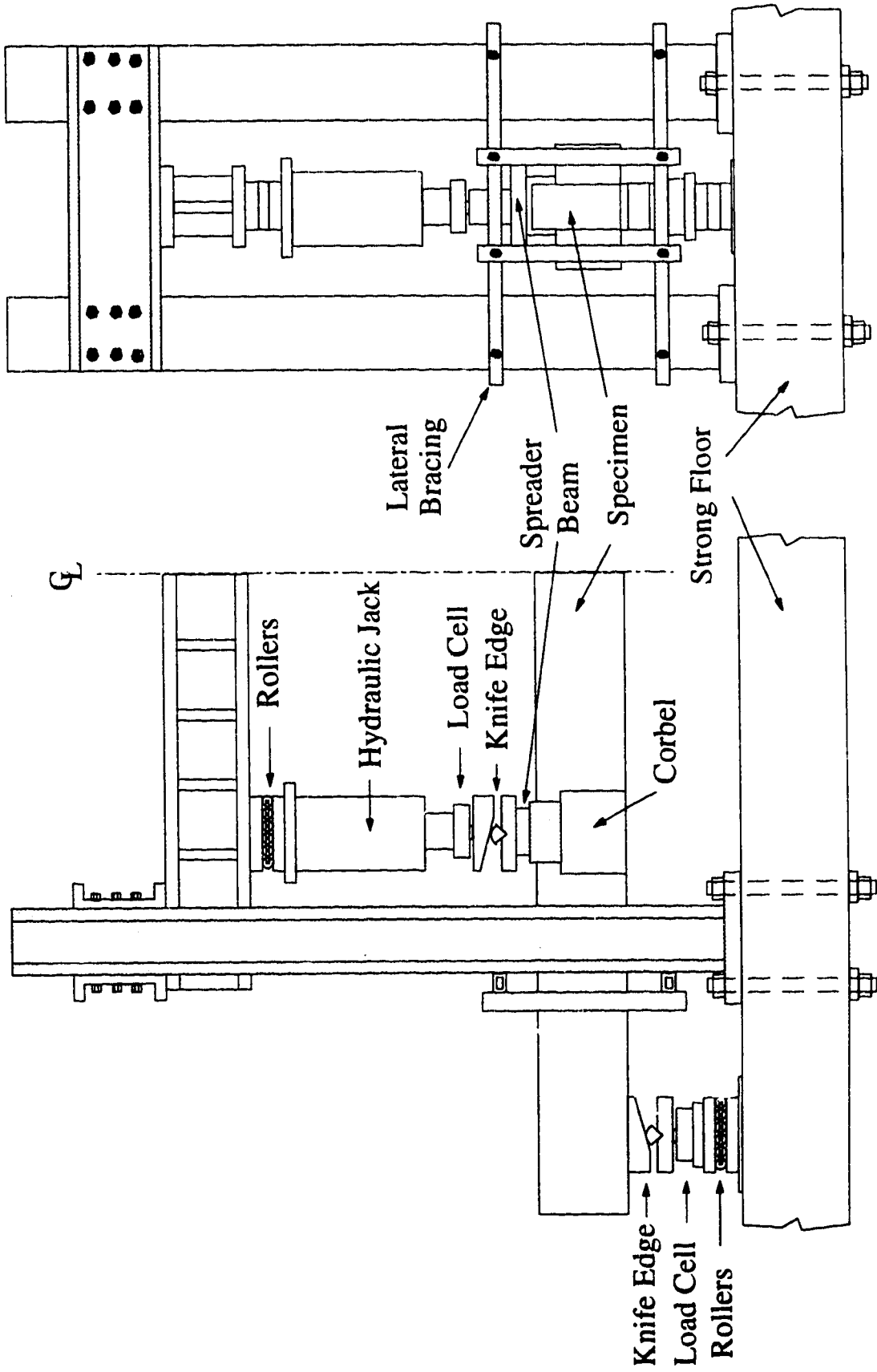
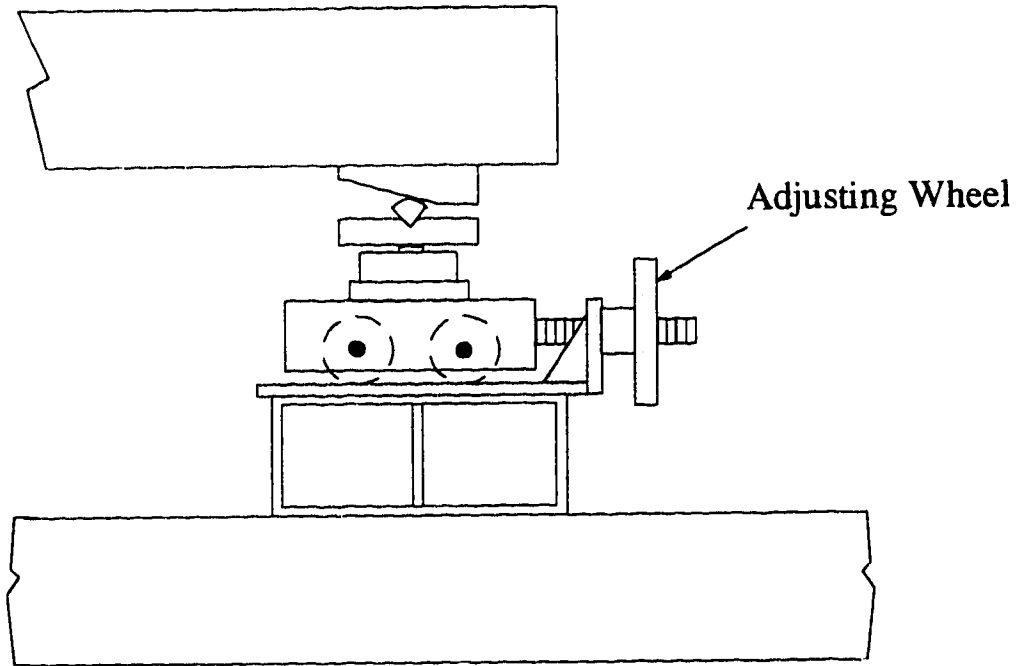
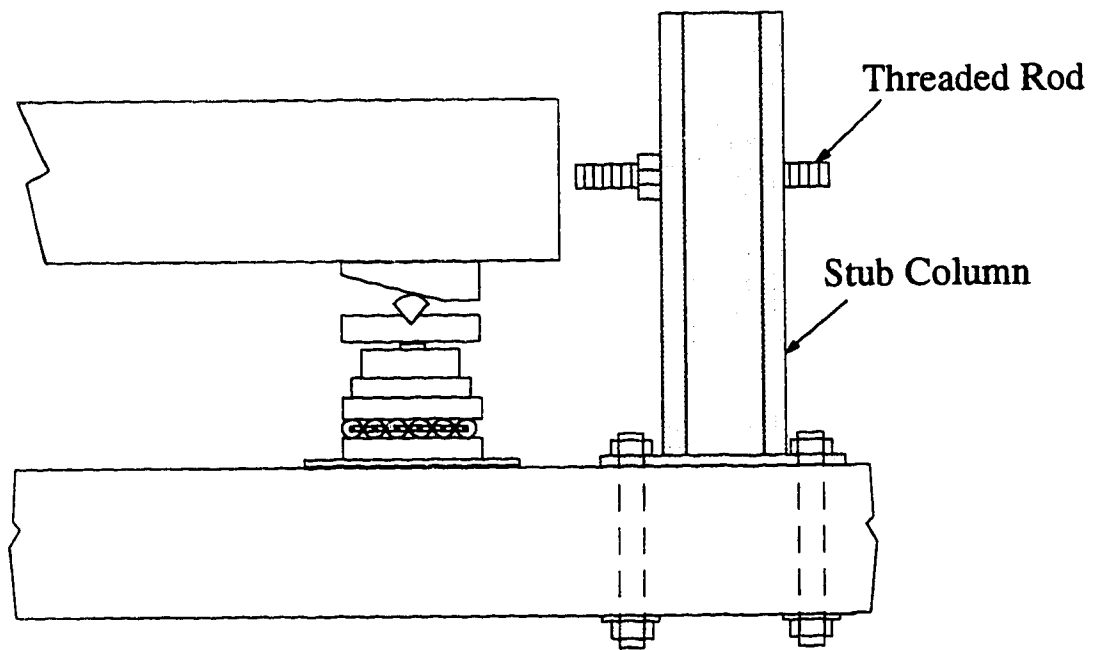


Figure 3.7 Test Set-up



South Support Configuration for Small and Medium Beams



North and South Support Configuration for Large Beams

Figure 3.8 Support Conditions

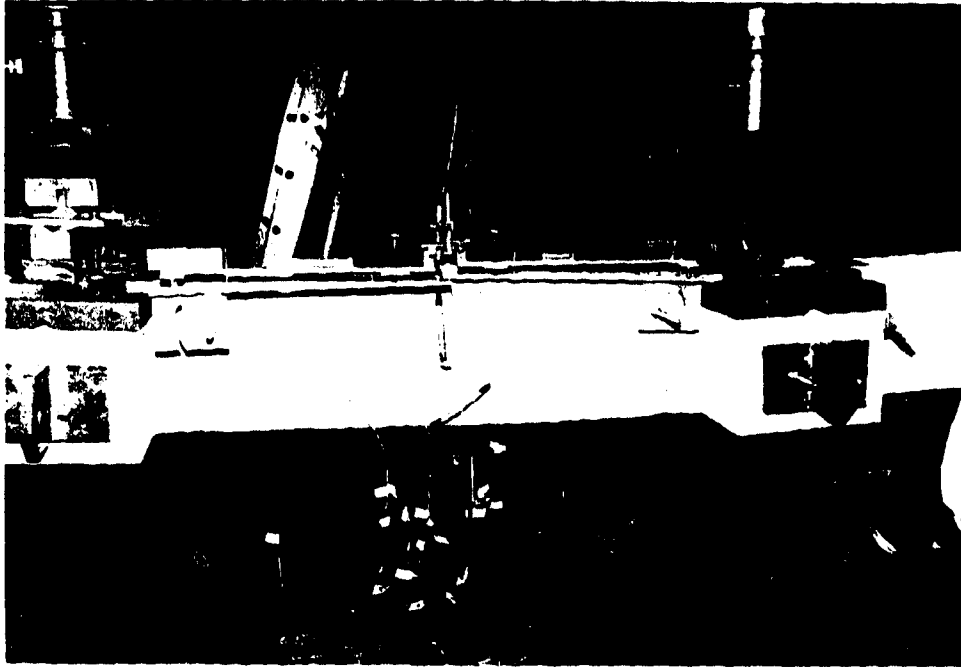


Figure 3.9 Rotation Meter Arrangement for a Small Beam

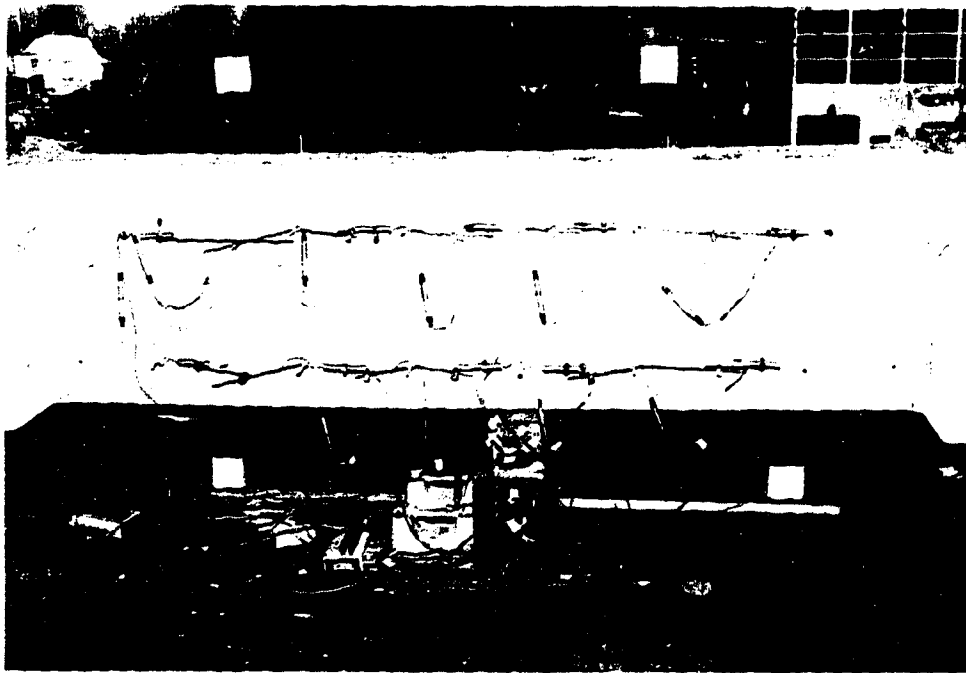


Figure 3.10 LVDT Arrangement for a Large Beam

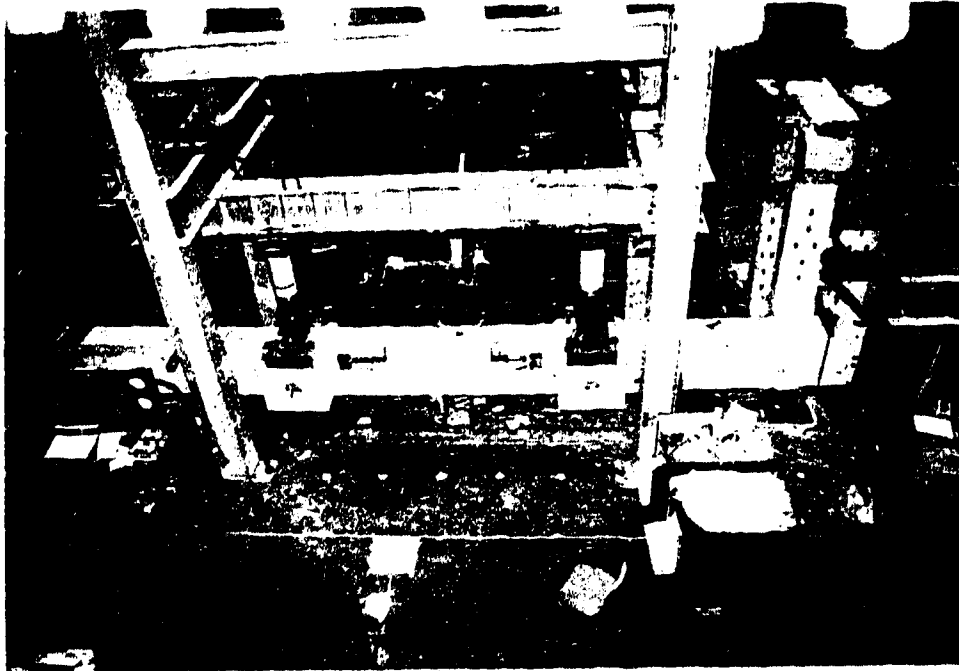


Figure 3.11 Overall View of the Test Set-up for a Large Beam

4 Test Results and Observations

4.1 Introduction

The material presented in this chapter gives information about how the data from the beam tests were analyzed and prepares the basis for further analyses done in Chapter 5 and Chapter 6. The behaviour of the beams and the development of failure are explained.

4.2 Definitions

While investigating the flexural behaviour of a reinforced concrete section, it is important to define certain points on the load deformation relationship. These points are those corresponding to yield, ultimate moment, ultimate rotation and failure. The definitions used are illustrated for moment-rotation relationship in Figure 4.1. The stress-strain curves for all the reinforcement used had definite yield points. Thus, the moment-rotation diagrams for the lower concrete strength beams, which had one layer of reinforcement, had definite yield points. For the higher concrete strength beams the yielding occurred gradually as there were two layers of reinforcement. The yield load for these beams is defined as the load at which both layers of reinforcement had yielded. The yield deformation is calculated by averaging the deformations corresponding to the yielding of the first and the second layers. This yield load and deformation would be obtained if all the steel was in one layer instead of two layers. The ultimate moment is the peak load carrying capacity reached by the beam. After the peak of the load deformation curve the beams generally had some capacity to deform without significant reduction in load. Recognizing this, the ultimate deformation is defined as the deformation at which the load starts to drop significantly. The failure point is the last data recorded before total loss of load carrying capacity.

4.3 Load-Deformation Relationships

4.3.1 Load-Centerline Deflection

Typical load-centerline deflection curves using the load and reaction point load cells are given in Figure 4.2. Load-centerline deflection curves were important for monitoring and controlling the tests. A simple moment-curvature spreadsheet program was developed and used to predict the load-centerline deflection behaviour of the beams. For symmetry of the tests and to maintain zero shear in the test region, special attention was paid to make

sure that the loads and reactions were equal during testing. The centerline deflections at yield, δ_y , at ultimate moment, δ_{Mu} , at ultimate rotation, $\delta_{\theta u}$, and at failure, δ_f , are given in Table 4.1.

The deflection ductility index, $\mu_f = \delta_f/\delta_y$, for high-strength concrete beams has been reported to be much lower than that for normal strength concrete beams (Leslie et al. 1976). In light of this conclusion, Leslie et al. have suggested that the maximum allowable amount of reinforcement for a beam, given in the ACI code as 75% of the balanced reinforcement, should be reduced to 35% of the balanced reinforcement for high-strength concrete beams. The deflection ductility indices for the beams tested are given in Table 4.1. The μ_f values are compared with the beam tests reported by Leslie et al. (1976) and Shin et al. (1989) in Figure 4.3. Both test series consisted of simply supported beam tests under two point loading. The pure bending regions in the Leslie et al. beams had only tension reinforcement with concrete strengths between 64 MPa and 81 MPa. The pure bending regions in the Shin et al. beams were reinforced as columns; equal reinforcement at four corners with closely spaced stirrups (76 mm or 152 mm spacing) and had concrete strengths between 28 MPa and 103 MPa. In their paper, Shin et al. concluded that reducing the stirrup spacing from 152 mm to 76 mm did not improve performance. The University of Alberta tests did not show any significant difference between the ductilities of the 50 MPa concrete beams ($\rho/\rho_b < 0.6$) and the 90 MPa concrete beams ($\rho/\rho_b > 0.6$) other than that expected due to change in ρ/ρ_b .

In order to have moment redistribution a minimum deflection ductility index of 4 is required. It is believed that a high-strength concrete section having compression steel and at least a minimum amount of stirrups would satisfy the required ductility criteria.

4.3.2 Moment Carrying Capacity

The total moment carried by the beams could be divided into three parts. The first part is the moment due to the dead weight of the beam. The dead weight of the beams were not measured. The moment due to the dead load was calculated from the geometry of the beams and assuming a unit weight of 24 kN/m³. The second part is the moment calculated by multiplying the average of the loads and/or reactions by the initial shear span which is equal to four times the effective depth, $4d$. The third part is the moment due to the increase in the shear span. The contribution of each part forming the total ultimate moment is given

in Table 4.2. The dead load moment was 1 to 5 percent of the total ultimate moment and the contribution of the moment due to change in shear span was 1 to 2 percent of the total ultimate moment.

The ratio of test to ACI code values for ultimate moment, M_u , are given in Table 4.2. In calculating code values, the average bar force at ultimate moment, f_s , given in Table 3.6 and the concrete cylinder strengths, f_c , given in Table 3.5 were used in Equation (4.1).

$$M_u = A_s f_s \left(d - \frac{a}{2} \right) = A_s f_s \left(d - \frac{A_s f_s}{1.7 f_c b} \right) \quad (4.1)$$

In Equation (4.1), A_s is the area of steel, d is the effective depth, b is the width, a is the depth of the rectangular stress block. The steel stress has been taken as f_s rather than f_y in Equation (4.1) since in some cases the steel had strain hardened. The average test to code ratios for ultimate moment and the standard deviations for all beams, for lower concrete strength beams and for higher concrete strength beams are given in Table 4.2. The value for beam MH2 is not included in either group because its concrete strength fell between the lower and higher strengths. The average test to code value for the lower concrete strength beams is slightly lower than that of the higher concrete strength beams. The standard deviation for higher concrete strength beams is remarkably low. The ACI code predicts the ultimate moment carrying capacity of the beams tested quite well.

The moment values at yield, M_y , at ultimate moment, M_u , at ultimate rotation, M_{θ_u} , and at failure, M_f , are given in Table 4.3. Up to 10% increase in moment was observed after yielding. The moment at ultimate rotation was within 1.2% of the ultimate moment.

4.3.3 Curvature and Rotation Measurements

The curvatures and rotations in the beams were measured in two different ways; using the rotation meters and using the side LVDT arrangements.

The two rotation meters measured the angle changes occurring at the two ends of the test region. Adding the angle changes at the two ends gave the total angle change taking place in the test region. Dividing the total angle change by the distance between the rotation meters, $3.7d$, gave the average curvature along the test region. Due to the symmetry of the test, equal rotations would be expected at the two points where the rotations were measured. Figure 4.4 shows typical rotation vs centerline deflection plots using the two rotation meters. In all the tests the two rotation meters measured about the same rotations at the two ends of the test regions. The curves could be defined by two straight lines; one from zero to yield

and another from yield to failure. Towards the end of the tests the rotation meters were detached for protection. The data were extrapolated using the centerline deflections and the last 5 to 10 rotation readings prior to removing the rotation meters.

Using the LVDTs on the side, curvatures at different segments along the test region were measured. These curvatures were affected by their gauge lengths, number of cracks inside the gauge lengths and variation in the crack openings. Towards the end of the tests the LVDTs were detached and data was not further extrapolated.

The curvature measurements using these two methods are compared in Figure 4.5 and Figure 4.6. These plots show the best and worst cases selected from all the beam tests. There are two conclusions from these figures. The first conclusion is that the rotation meters gave good average values for curvature. The measurements from the rotation meters were either very close or slightly higher than the average of the curvatures measured by the side LVDTs. Secondly, curvatures were not always uniform along the test region. As a result, curvature measurements from the rotation meters were used in further analysis of data whenever an average behaviour was needed, see Chapter 5 and Chapter 6. Additionally, it was observed that lower concrete strength beams tend to have more variation in curvature along the test region compared to the higher concrete strength beams.

If all the beams were scaled perfectly and if they all had the same concrete strength and mechanical reinforcement ratio, ω , then according to the conventional approach all the beams would have the same rotational behaviour, see Section 2.4. Also, they would all yield at the same rotation and fail at the same rotation. When ω is almost constant, the effect of concrete strength alone is not significant, see Equation (2.7). Figure 4.7 shows the moment vs rotation curves and Figure 4.8 shows the normalized moment vs rotation curves for all 12 beams tested. The dead load moments are not included in either figure and the rotations are those measured by the rotation meters. Recognizing that the beams had different but similar ω values, observed rotational behaviours are comparable. The beam having the lowest rotation at failure was MH2. This beam had the highest ω value.

The total angle change measured by the rotation meters at yield, θ_y , at ultimate moment, θ_{Mu} , at ultimate rotation, θ_u , and at failure, θ_f , are given in Table 4.4.

4.4 Extreme Compression Fiber Strain Measurements

The extreme compression fiber strains were measured in two different ways; using the 2" Demec gauge and using the side LVDT arrangements.

Typical strain distributions measured on top surface of the beams by the 2" Demec gauge are presented in Figure 4.9 and Figure 4.10 for lower concrete strength beams and for higher concrete strength beams, respectively. The average of each set of reading is also plotted in the same figures. The arrows in the figures show the load points. It was observed that before yielding of the tension reinforcement, the strain distributions did not have significant variation from the mean throughout the length of the test region regardless of concrete strength and size of the beam. After yielding, the higher concrete strength beams followed the same trend as before yielding. In the lower concrete strength beams, the strain distribution became more and more non-uniform as failure was approached. With increasing deformation, the strains started to increase considerably at one section or part of the beam while the strains at other sections either remained constant or increased slightly. In general, higher compressive strains were measured above the location of cracks.

Figure 4.11 shows the typical average extreme compression fiber strains from 2" Demec gauge readings vs centerline deflection relationship. A regression line from zero to yield and another regression line from yield to failure are also plotted in Figure 4.11. The regression lines allowed the average extreme compression fiber strain, ϵ_c , at any centerline deflection to be calculated.

The extreme compression fiber strains calculated using the side LVDT arrangements and using the regression lines obtained from 2" Demec gauge measurements are compared in Figure 4.12 and Figure 4.13. These two plots show the best and worst cases. The side LVDTs and the 5" Demec gauge measured the strain at a certain distance below the top surface. The extreme compression fiber strains from these measurements are calculated by assuming a linear distribution of strains along the depth of the beams. The regression lines from 2" Demec gauge readings were not consistently above or below the average of the side measurements. Confidence on the 2" Demec gauge measurements is higher as the strains were measured directly on top of the beams over the entire length of the test region. The strain values calculated using the regression lines for the average 2" Demec gauge strains were used in the analyses presented in Chapter 5 and Chapter 6.

The average extreme compression fiber strains at yield, ϵ_{cy} , at ultimate moment, ϵ_{cMu} , at ultimate rotation, $\epsilon_{c\theta u}$, and at failure, ϵ_{cf} , calculated using the regression lines explained above are given in Table 4.5. The mean extreme compression fiber strains at ultimate rotation were 4501 microstrain for the lower concrete strength beams and 4979 microstrain for the higher concrete strength beams excluding beam MH2. It should be noted that the beams took 8 to 12 hours to test and these values may include some creep strains.

4.5 Neutral Axis Depth-Centerline Deflection Relationships

The neutral axis depth along the test region was measured in two different ways; using the rotation meters together with the 2" Demec gauge readings, and using the side LVDT arrangements.

Knowing the curvature, ψ , and the average extreme compression fiber strain, ϵ_c , the neutral axis depth, c , is calculated using the relationship $c = \epsilon_c / \psi$. The average curvature from rotation meters together with the ϵ_c from the regression lines of the 2" Demec gauge strains gave the average neutral axis depth along the test region.

As the strains at the top and at the bottom of the test region were measured, the side LVDT arrangements gave the neutral axis depth in a direct way. Assuming linear distribution of strains is essential in this method.

The two methods are compared in Figure 4.14 and 4.15 for the worst and the best cases, respectively. As the entire test region was treated as the critical section, average measurements are desirable to explain the behaviour. Similar to the curvature and extreme compression fiber strain measurements explained above, the neutral axis depths calculated using the rotation meters and the 2" Demec gauge strains were not consistently above or below the average of the depths measured by the side LVDT arrangements. Thus, for the analyses presented in Chapter 5 and Chapter 6 the neutral axis depth values calculated from the rotation meters and the average 2" Demec gauge strains were used.

The average neutral axis depths at yield, c_y , at ultimate moment, c_{Mu} , at ultimate rotation, c_{θ_u} , and at failure, c_f , calculated using the rotation meters and the 2" Demec gauge strains are given in Table 4.6.

4.6 Development of Failure

Since all the beams tested were under-reinforced, the failure occurred by the failure of concrete in compression zone after the tension reinforcement had yielded. Primary flexural cracks were first visible at 5% to 10% of the ultimate load. These flexural cracks extended towards the compression zone quite rapidly during the first few load steps and their progress slowed down later. Close to the yield load new flexural cracks started to appear and these secondary cracks extended to about the same level as the primary cracks in a few load steps. After yield the cracks widened and some horizontal cracking was observed at the level of longitudinal reinforcement.

Depending on the concrete strength of the beam, different crack propagation and failure patterns were observed. These patterns will be explained in the following paragraphs.

In the lower concrete strength beams, the primary cracks started to split into two or more branches that propagated at an angle away from the primary cracks. The secondary cracks extended vertically to the same level as the tips of the branches of the primary cracks. The failure took place at a section where a primary crack existed. It was often possible to predict the location of the failure from the distress of the concrete at the top of the beam and from the real time plot of 2" Demec gauge strains. The strain patterns recorded from the 2" Demec gauge readings increased consistently at a section or at a part of the test region, and usually allowed detection of the failure section before any distress was visual. The first sign of distress was spalling of the corners at the top of the beam, later, cracks propagating across the width of the top surface were visible. At this stage, the average extreme compression fiber strains were between 3,000 and 3,800 microstrain with local strains as high as 5,300 microstrain and the centerline deflections were between 65% and 75% of the failure deflections. The failure was localized at a single section for the small and large beams. A somewhat different failure was observed for the medium beams. In both of the medium beams, the branches of the adjacent primary cracks connected to form a failure plane together with crushing at a section. In all the lower concrete strength beams the failure surfaces were irregular and included a large amount of bond failure between mortar and aggregates, similar to that observed in the material tests. The failures were not explosive. Typical lower concrete strength beams after failure are shown in Figure 4.16, Figure 4.17 and Figure 4.18 for small, medium and large beams, respectively.

In the higher concrete strength beams, very few of the primary cracks branched. All the cracks propagated to a height about the same distance below the top surface. It was not possible to predict where the failure would take place. The 2" Demec gauge strains were quite uniform, see Figure 4.10. When the first distress of the top surface corners was visible, the average extreme compression fiber strains were between 3,400 and 4,100 microstrain with local strains as high as 4,600 microstrain at centerline deflections between 60% and 80% of the failure deflections. When failure occurred it was sudden and explosive. The failure surfaces passed through both mortar and aggregates. In general, the failure surface was V-shaped, the bottom of the V being at the middle of the test region and below the neutral axis. After failure it was observed that there was crushing at a section of the test region as well. Typical higher concrete strength beams after failure are shown in Figure

4.19, Figure 4.20 and Figure 4.21 for small, medium and large beams, respectively. The dislodged pieces of concrete in these photographs had not been moved since the failure occurred when the pictures were taken.

The number of cracks in the test region of the higher concrete strength beams was about 1.5 times that in the lower concrete strength beams. The reason for this is believed to be the larger area of the longitudinal reinforcement. This conclusion was reached by using the theoretical equation suggested by Hognestad (1962) for predicting the minimum spacing of cracks, a_{min} , as $a_{min} = (A_e f_t) / (u \sum o)$. In this equation, A_e is the effective area of concrete in tension, f_t is the tensile strength of concrete, u is the average bond stress, and $\sum o$ is the sum of the perimeters of the bars. Assuming the same tensile concrete strength and bond stress, this equation predicts that the cracks would be 1.4 times closer in the case where there are two layers of reinforcement.

Two factors affecting the failure of the beams are related to the strain energy balance of the system consisting of the load frame and the specimen itself. One of these is the release of strain energy stored in the testing frame. As the beam is deformed past the ultimate load carrying capacity and the load drops, there is a continuous release of strain energy from the test frame to the specimen. Another factor affecting the failure is the strain energy released from the shear spans of the beam as the load drops. As the curvature is increasing only in the test region, all the released strain energy should be stored at this part of the beam. When the test region is unable to store all the released energy, failure occurs. It is believed that these two factors always worked together and they were indistinguishable.

During testing beam SL1, about midway between yield and failure, there was a sudden flow of oil to one of the hydraulic jacks due to opening the control valve too much. This created a shear of 10 kN inside the test region while the beam was carrying about 65 kN. Some cracking was heard at the same time. It is believed that due to this mistake beam SL1 failed earlier than it otherwise would have. This may explain why δ_f/δ_y was lower for SL1 than SL2.

Table 4.1
Centerline Deflections

Specimen	ρ/ρ_b	δ_y (mm)	δ_{Mu} (mm)	$\delta_{\theta u}$ (mm)	δ_f (mm)	δ_f/δ_y
SL1	0.54	23.2	40.0	51.0	51.0	2.2
SL2	0.54	22.3	60.5	63.0	63.9	2.9
ML1	0.55	36.8	75.2	79.3	81.8	2.2
ML2	0.53	36.4	112.1	112.1	114.2	3.1
LL1	0.53	53.0	130.8	130.8	133.0	2.5
LL2	0.58	54.8	97.7	100.1	100.3	1.8
MH2	0.78	44.2	59.0	61.0	61.5	1.4
SH1	0.64	26.3	55.1	57.0	57.0	2.2
SH2	0.68	26.9	54.6	54.6	54.6	2.0
MH1	0.64	40.2	86.3	87.8	88.3	2.2
LH1	0.63	59.5	132.2	132.2	134.0	2.3
LH2	0.67	59.5	136.8	136.8	137.1	2.3

Table 4.2
Parts of Ultimate Moment

Specimen	Dead Load Moment (kN-m)	$P_{av} * 4d$ (kN-m)	Increase in Shear Span (mm)	Moment due to Increase in Shear Span (kN-m)	Total Moment (kN-m)	M_u test/code	
SL1	1.74	66.17	12.8	0.92	68.83	1.025	
SL2	1.74	66.21	20.4	1.47	69.42	1.034	
ML1	9.92	243.03	19.1	3.22	256.17	0.974	
ML2	9.92	258.88	35.1	6.31	275.11	1.055	
LL1	38.44	723.17	35.2	12.35	773.96	0.984	
LL2	38.44	699.90	27.2	9.22	747.56	1.016	
MH2	10.65	460.59	15.1	4.82	476.06	0.971	
SH1	1.88	131.84	19.3	2.76	136.48	1.033	
SH2	1.88	129.61	18.9	2.67	134.16	1.023	
MH1	10.65	502.60	24.5	8.56	521.81	1.030	
LH1	41.38	1476.51	38.8	27.81	1545.70	1.011	
LH2	41.38	1496.55	38.4	27.89	1565.82	1.016	
(Excluding MH2)						Average all	1.014
						Std Dev all	0.026
						Average LSC	1.015
						Std Dev LSC	0.031
						Average HSC	1.022
						Std Dev HSC	0.008

Table 4.3
Moments

Specimen	M_y (kN-m)	M_u (kN-m)	M_{eu} (kN-m)	M_f (kN-m)
SL1	65.33	68.83	68.66	67.50
SL2	64.86	69.42	69.01	68.26
ML1	248.19	256.17	255.50	252.22
ML2	250.55	275.11	275.11	273.64
LL1	722.03	773.96	773.96	766.71
LL2	720.22	747.56	739.37	734.83
MH2	475.50	476.06	474.48	467.11
SH1	128.24	136.48	134.81	134.81
SH2	128.75	134.16	134.16	134.16
MH1	493.76	521.80	519.79	518.13
LH1	1431.93	1545.70	1545.70	1540.01
LH2	1439.97	1565.82	1565.82	1564.52

Table 4.4
Total Angle Change in the Test Regions

Specimen	θ_y (radians)	θ_{Mu} (radians)	θ_v (radians)	θ_f (radians)
SL1	0.0161	0.0335	0.0448	0.0451
SL2	0.0158	0.0574	0.0604	0.0620
ML1	0.0155	0.0415	0.0444	0.0458
ML2	0.0155	0.0707	0.0707	0.0724
LL1	0.0159	0.0517	0.0517	0.0527
LL2	0.0165	0.0373	0.0384	0.0385
MH2	0.0201	0.0286	0.0299	0.0302
SH1	0.0191	0.0491	0.0518	0.0518
SH2	0.0191	0.0469	0.0469	0.0469
MH1	0.0178	0.0470	0.0481	0.0484
LH1	0.0190	0.0517	0.0517	0.0525
LH2	0.0190	0.0537	0.0537	0.0538

Table 4.5
Average Extreme Compression Fiber Strains

Specimen	ϵ_{cy} ($\mu\epsilon$)	ϵ_{cMu} ($\mu\epsilon$)	$\epsilon_{c\theta u}$ ($\mu\epsilon$)	ϵ_{cf} ($\mu\epsilon$)
SL1	1965	3191	3962	3967
SL2	1936	4647	4818	4885
ML1	2046	3901	4097	4213
ML2	1974	5217	5217	5303
LL1	2011	4830	4830	4916
LL2	2204	3979	4081	4088
MH2	2987	4003	4142	4175
SH1	2581	4771	4906	4906
SH2	2690	4886	4886	4886
MH1	2587	4936	5012	5033
LH1	2578	5003	5003	5062
LH2	2589	5089	5089	5097
		Average all Min-Max	4665 3972-5217	
		Std Dev all Variance	466 0.100	
		Average LSC Min-Max	4501 3962-5217	
		Std Dev LSC Variance	520 0.116	
		Average HSC Min-Max	4979 4886-5089	(Excluding MH2)
		Std Dev HSC Variance	83 0.017	

Table 4.6
Neutral Axis Depths

Specimen	c_y (mm)	c_{Mu} (mm)	$c_{\theta u}$ (mm)	c_f (mm)
SL1	103.6	81.0	75.1	74.7
SL2	104.1	68.9	67.9	67.0
ML1	175.6	125.0	122.9	122.3
ML2	169.9	98.1	98.1	97.4
LL1	241.3	178.2	178.2	177.9
LL2	253.8	203.3	202.2	202.2
MH2	198.9	186.5	184.6	184.1
SH1	115.2	82.6	80.5	80.5
SH2	121.2	88.5	88.5	88.5
MH1	194.7	139.6	138.6	138.4
LH1	260.5	184.4	184.4	183.5
LH2	261.7	180.6	180.6	180.4

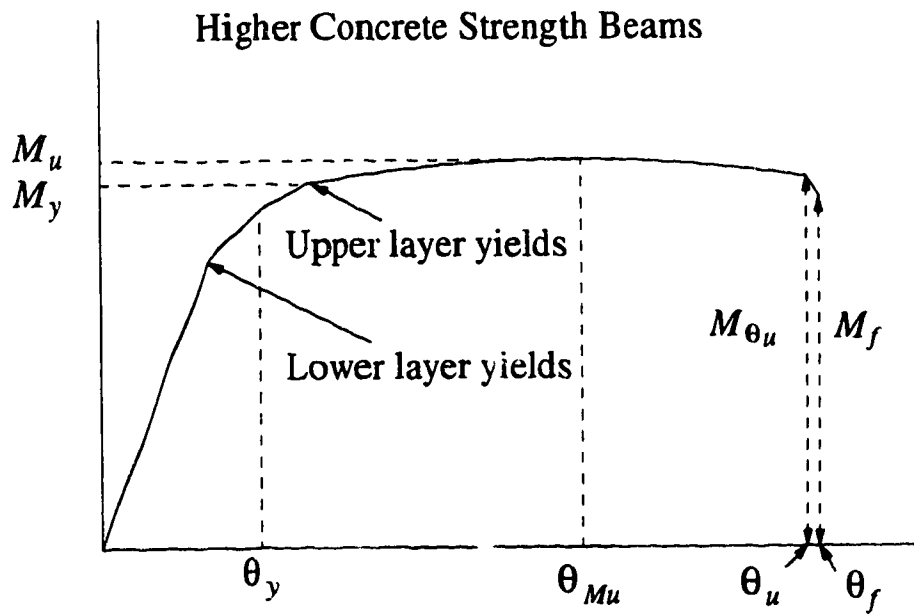
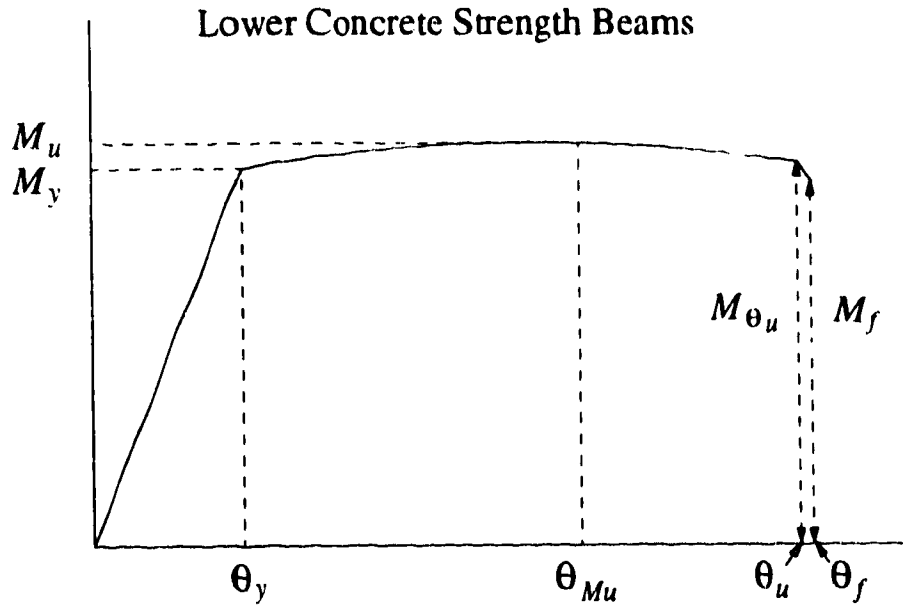


Figure 4.1 Definitions

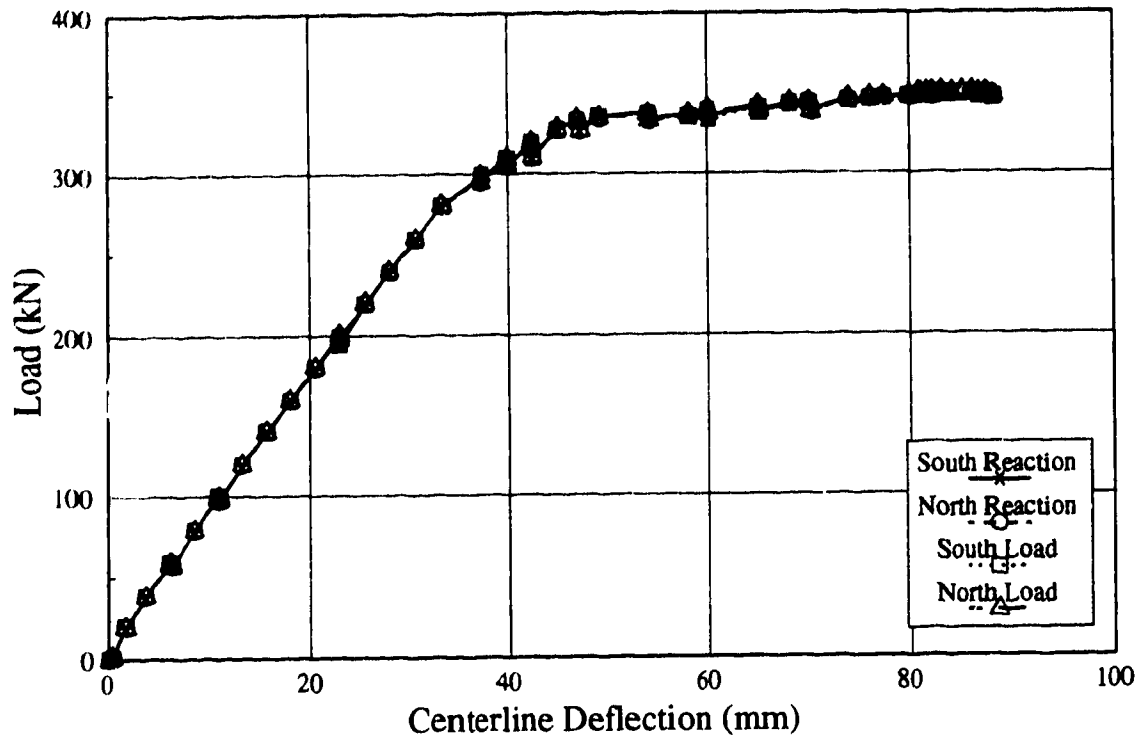


Figure 4.2 Load vs Centerline Deflection, Beam MH1

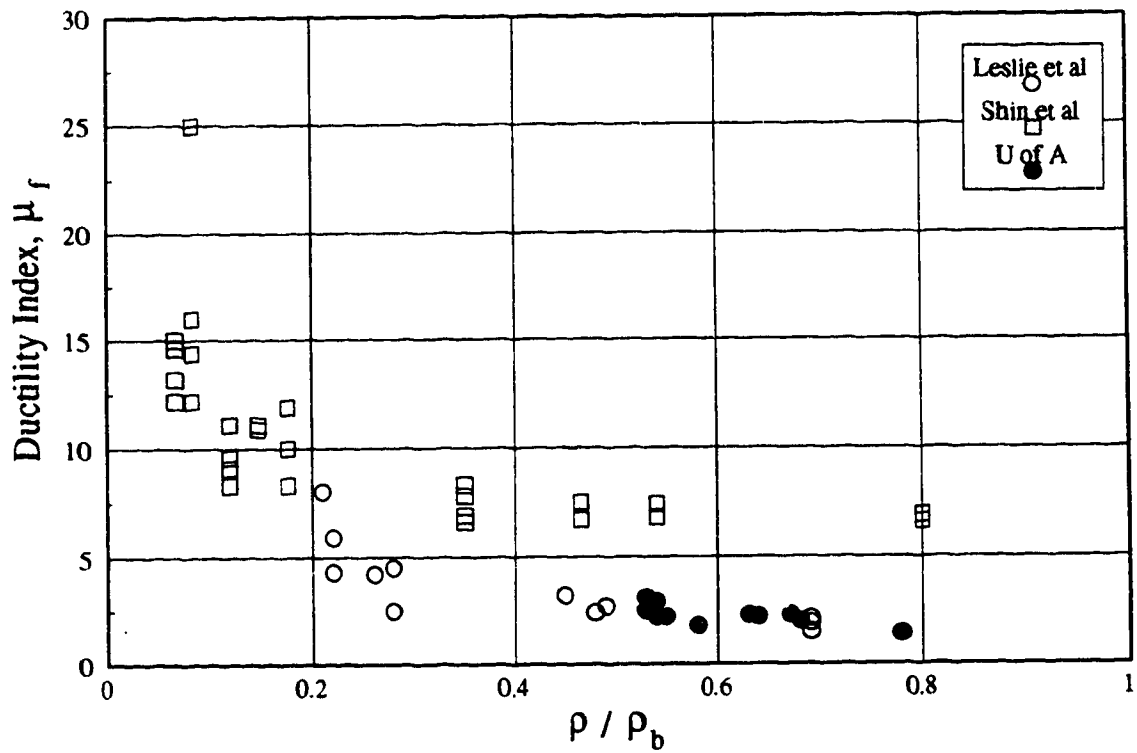


Figure 4.3 Ductility Index vs ρ / ρ_b

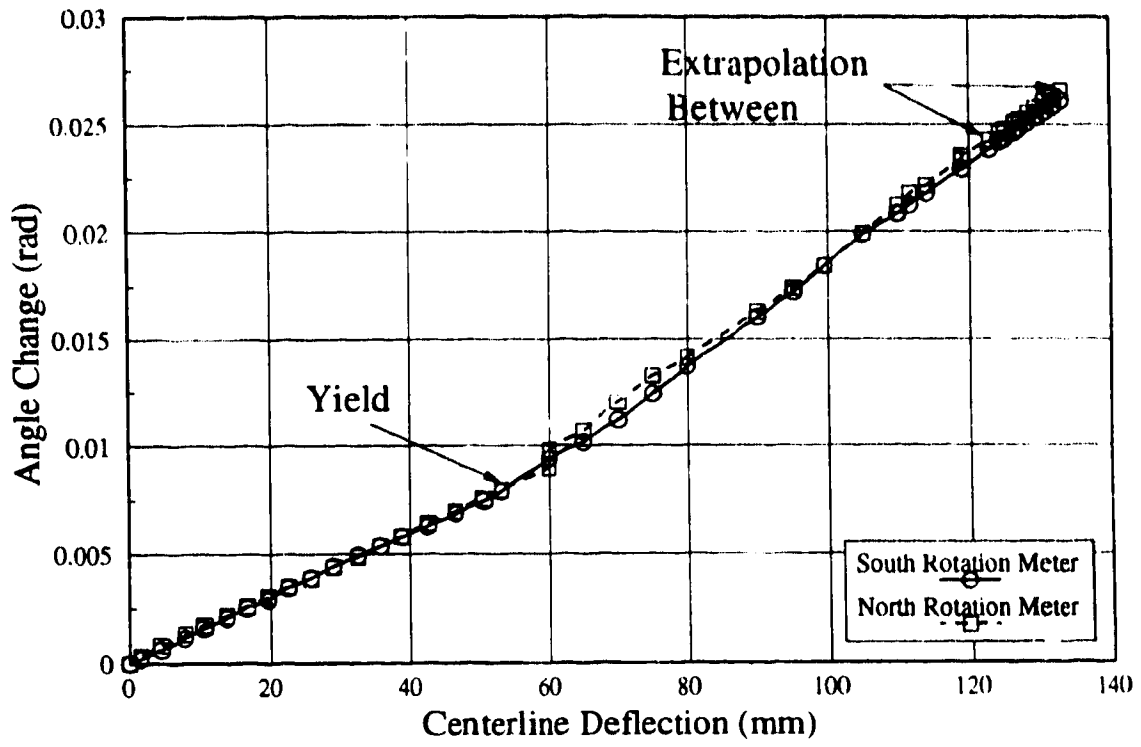


Figure 4.3 Comparison of Rotation Meters, Beam LL1

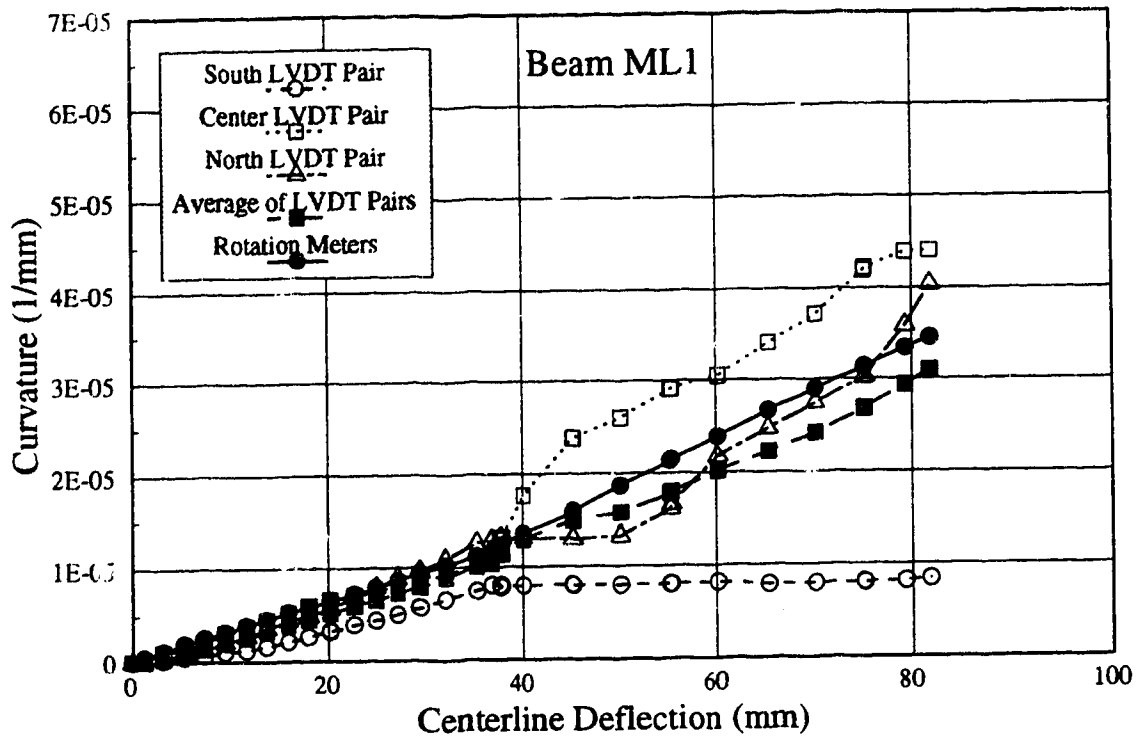


Figure 4.5 Comparison of Curvature Measurements, Worst Case

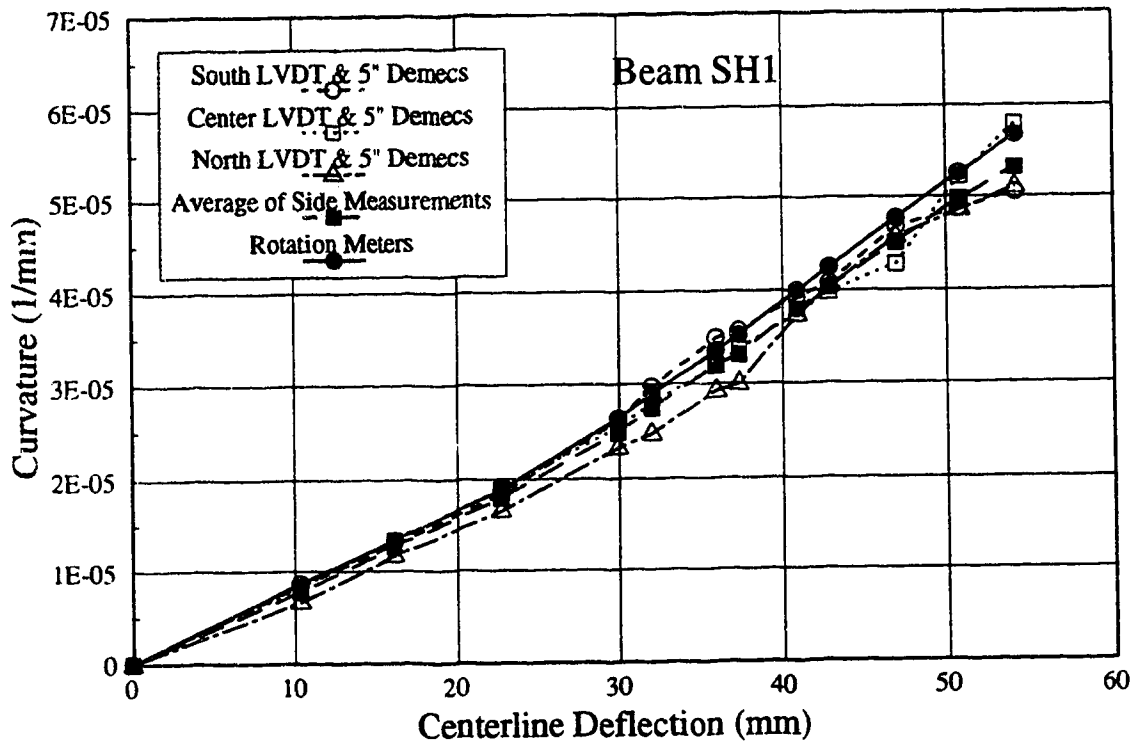


Figure 4.6 Comparison of Curvature Measurements, Best Case

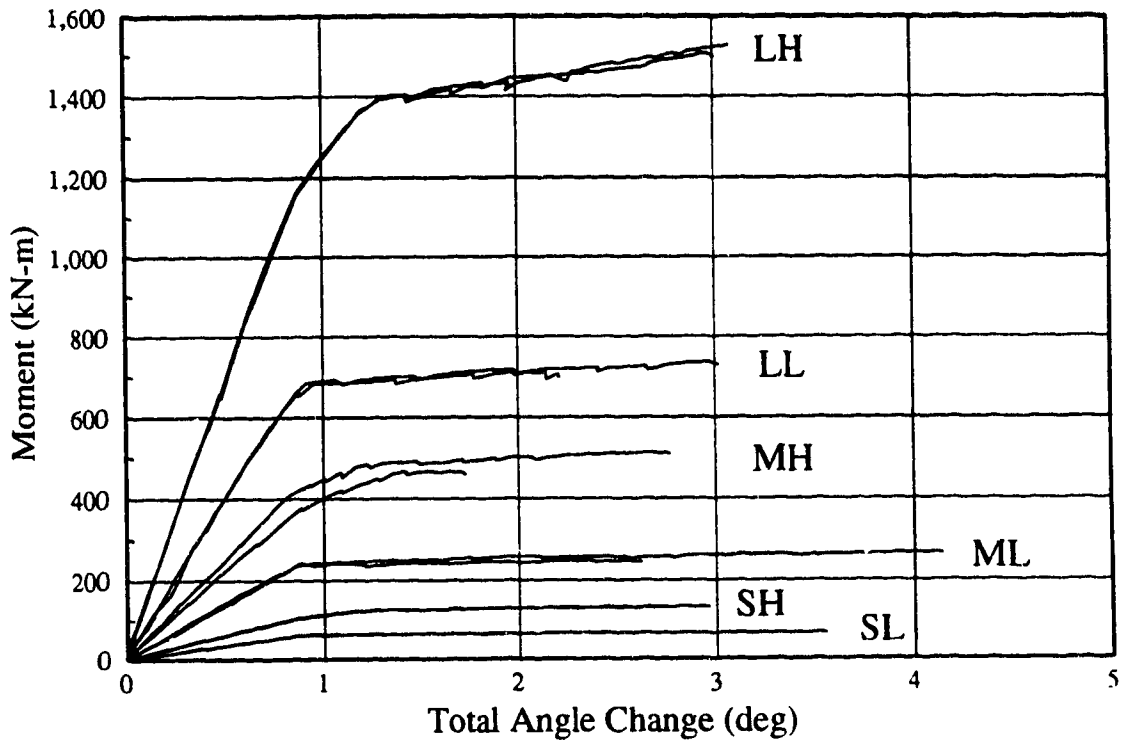


Figure 4.7 Moment vs Total Angle Change

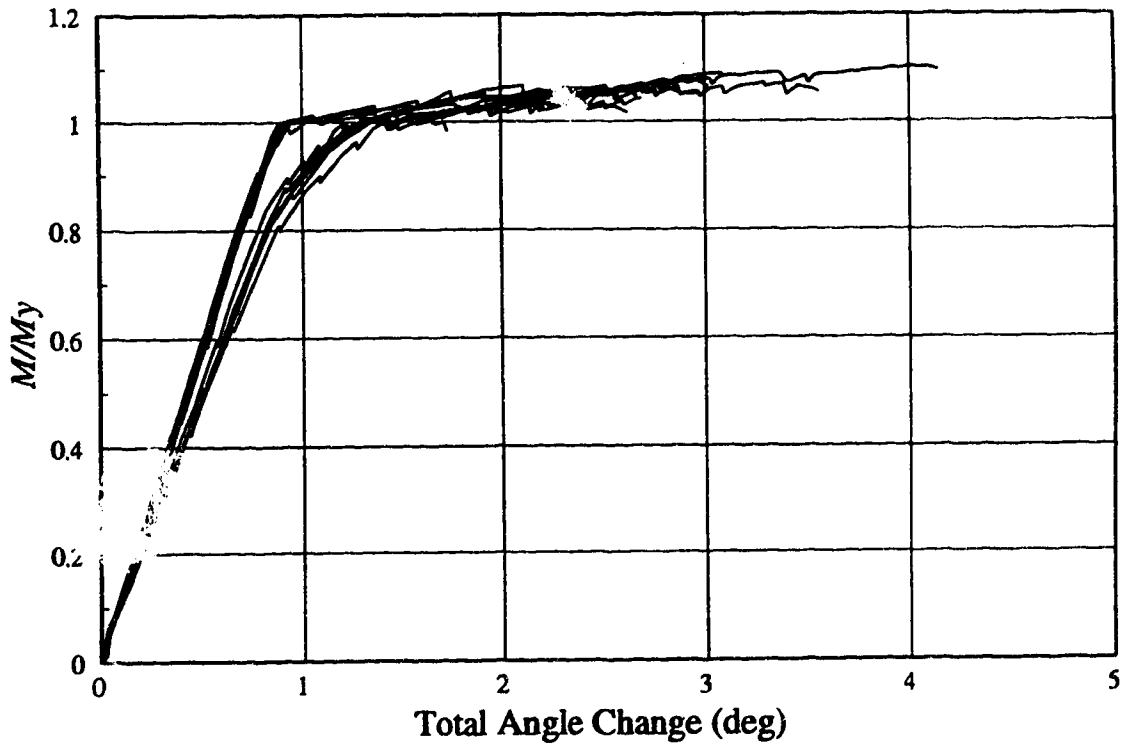


Figure 4.8 Normalized Moment vs Total Angle Change

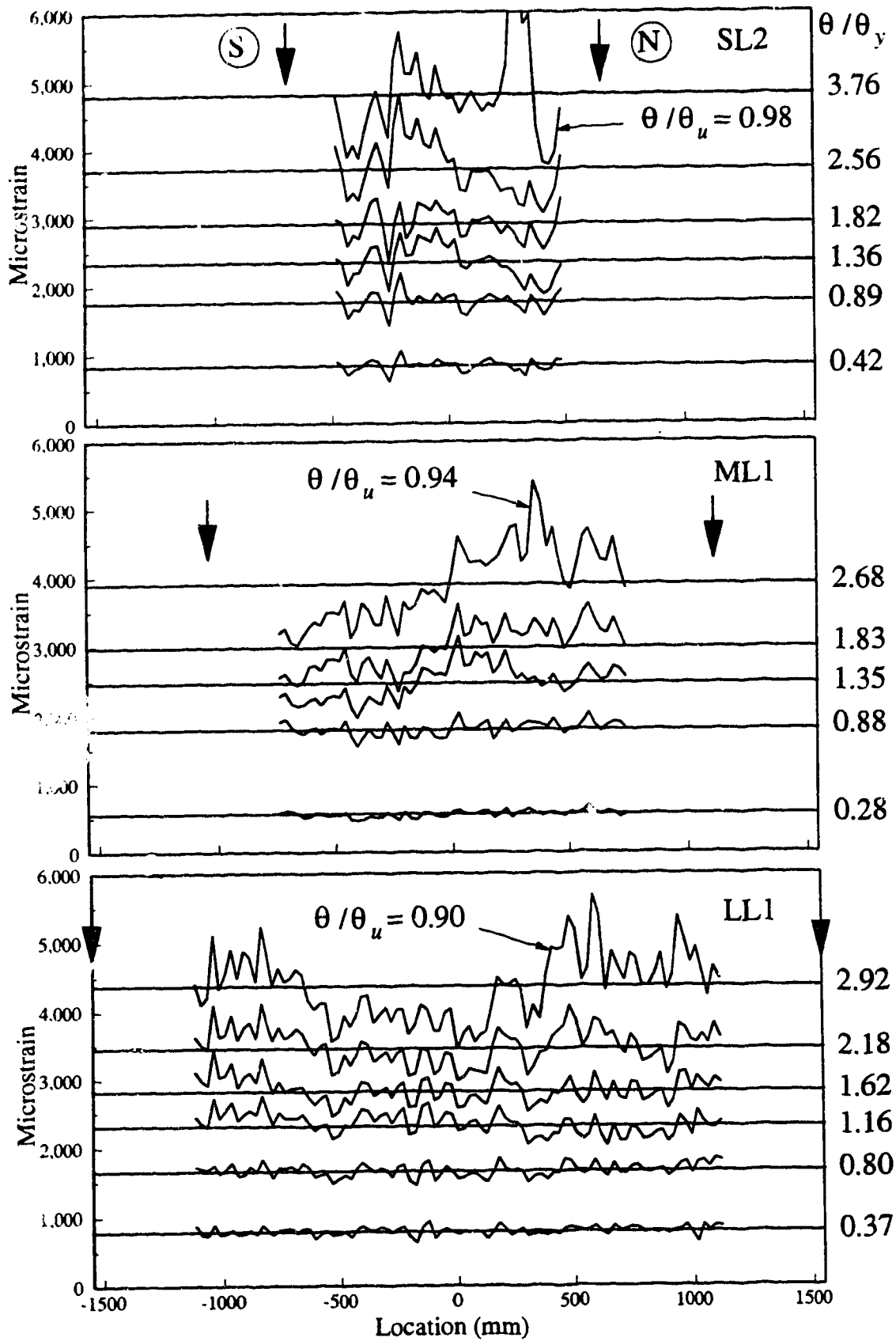


Figure 4.9 Demec Gauge Strains, Lower Concrete Strength Beams

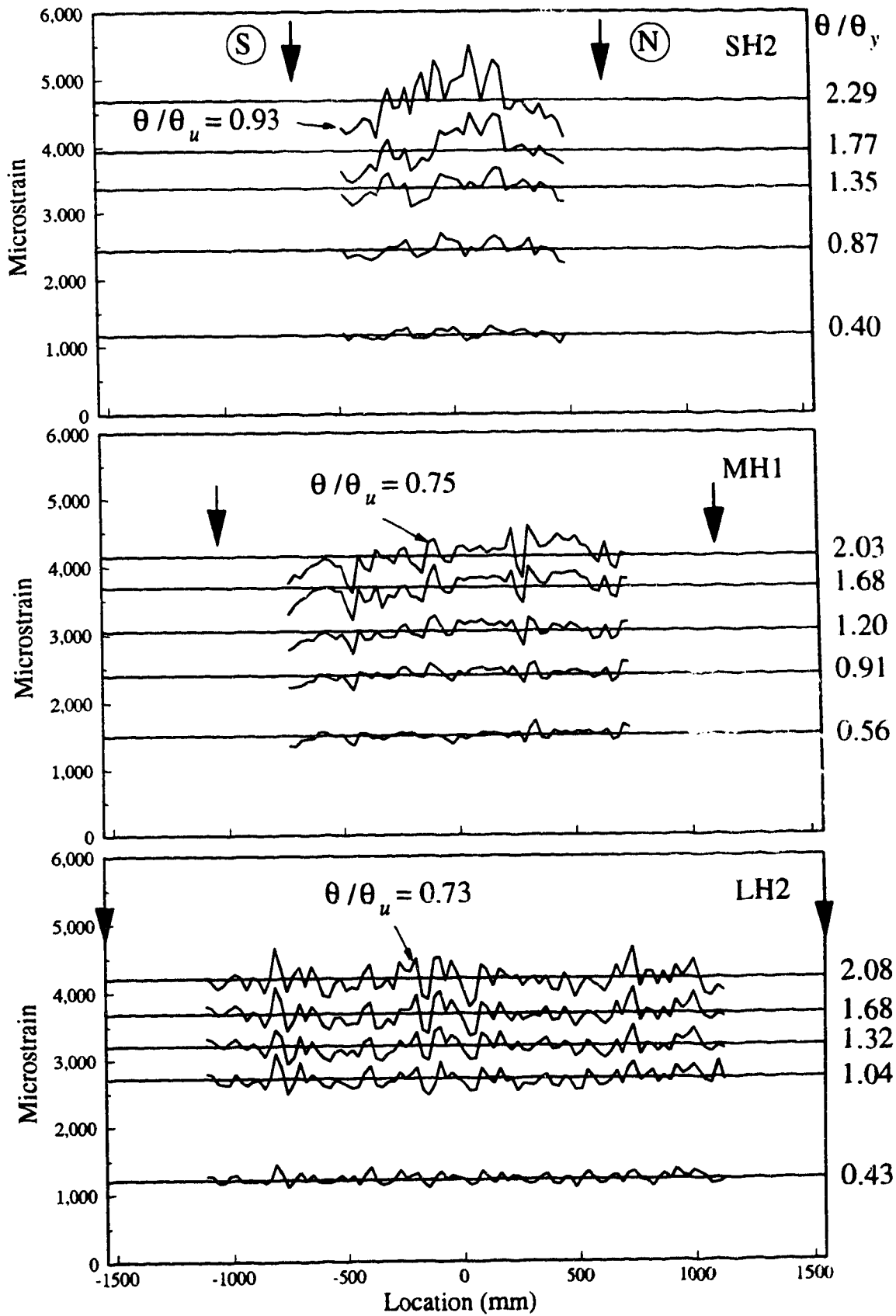


Figure 4.10 Demec Gauge Strains, Higher Concrete Strength Beams

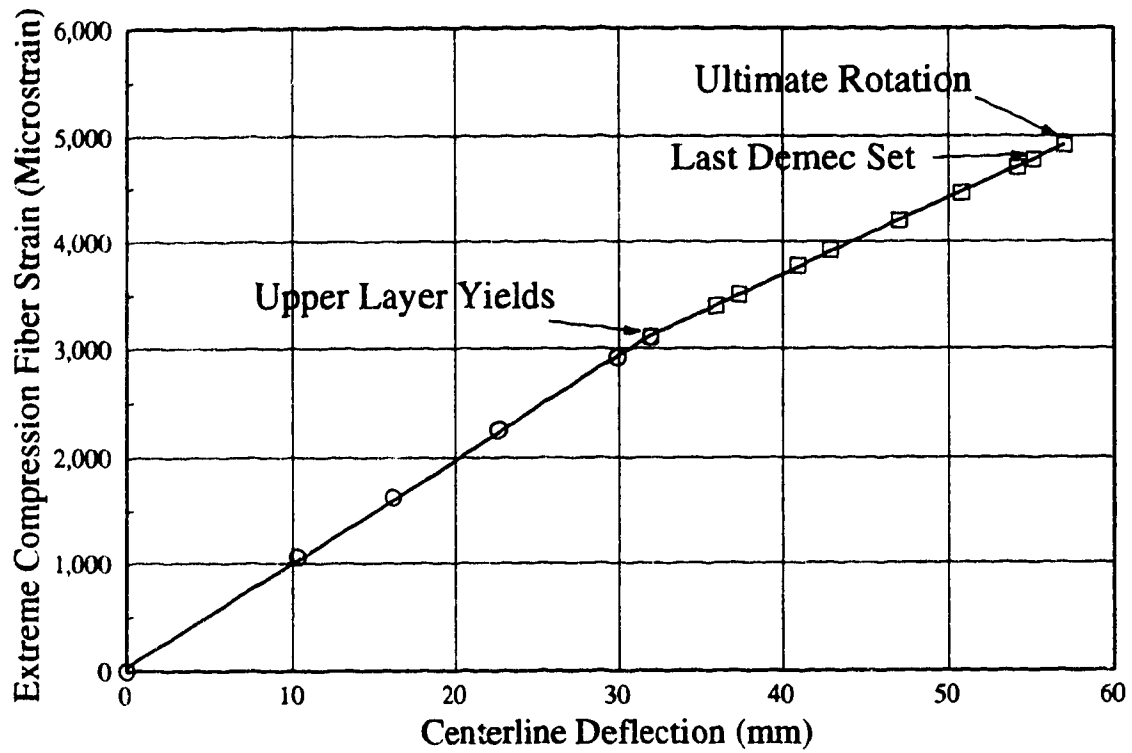


Figure 4.11 Regression of Average 2" Demec Gauge Strains, Beam SH1

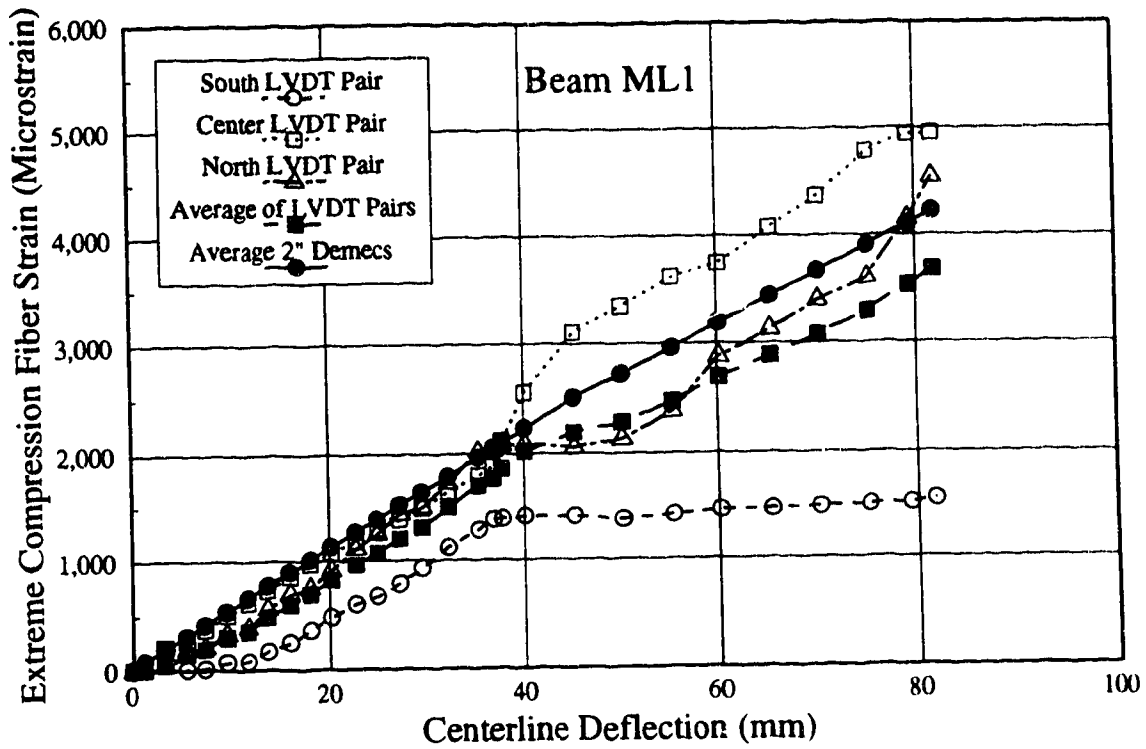


Figure 4.12 Comparison of Strain Measurements, Worst Case

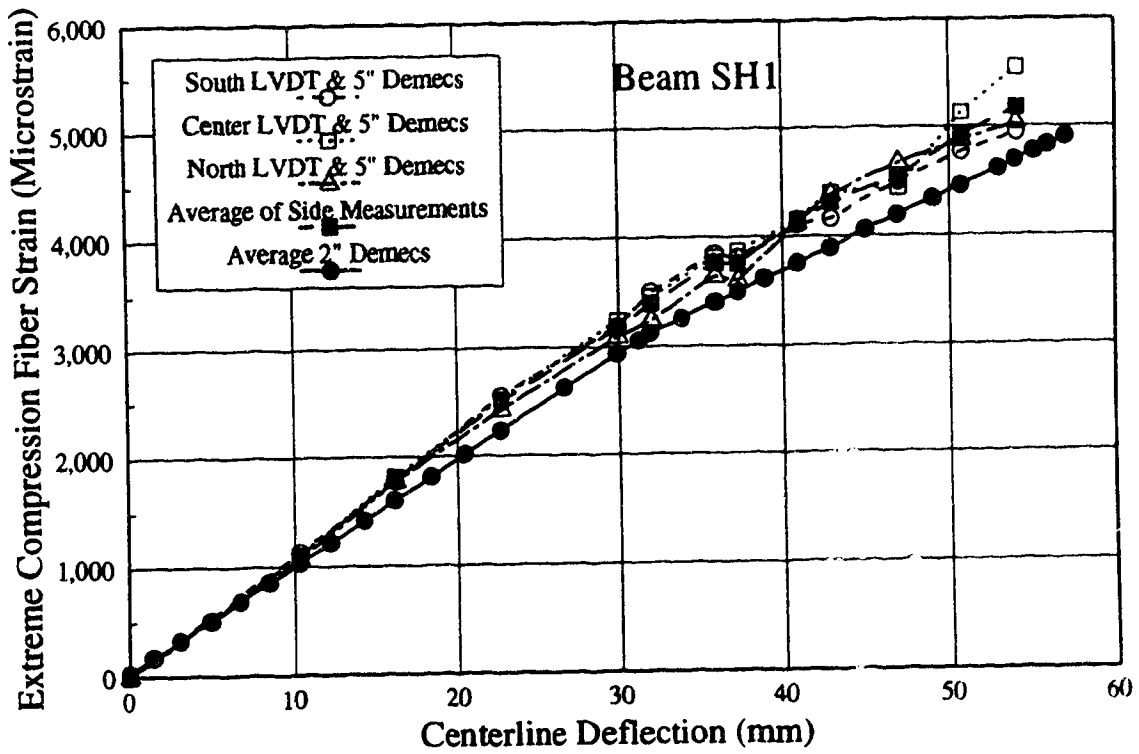


Figure 4.13 Comparison of Strain Measurements, Best Case

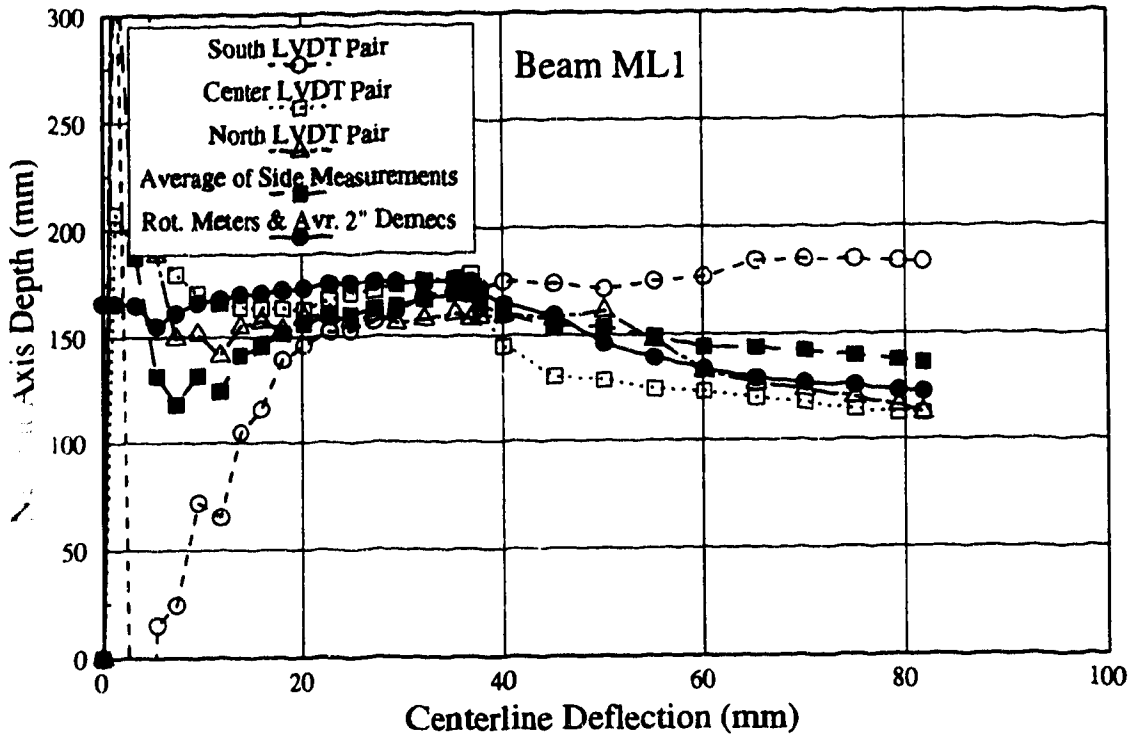


Figure 4.14 Comparison of Neutral Axis Depth Measurements, Worst Case

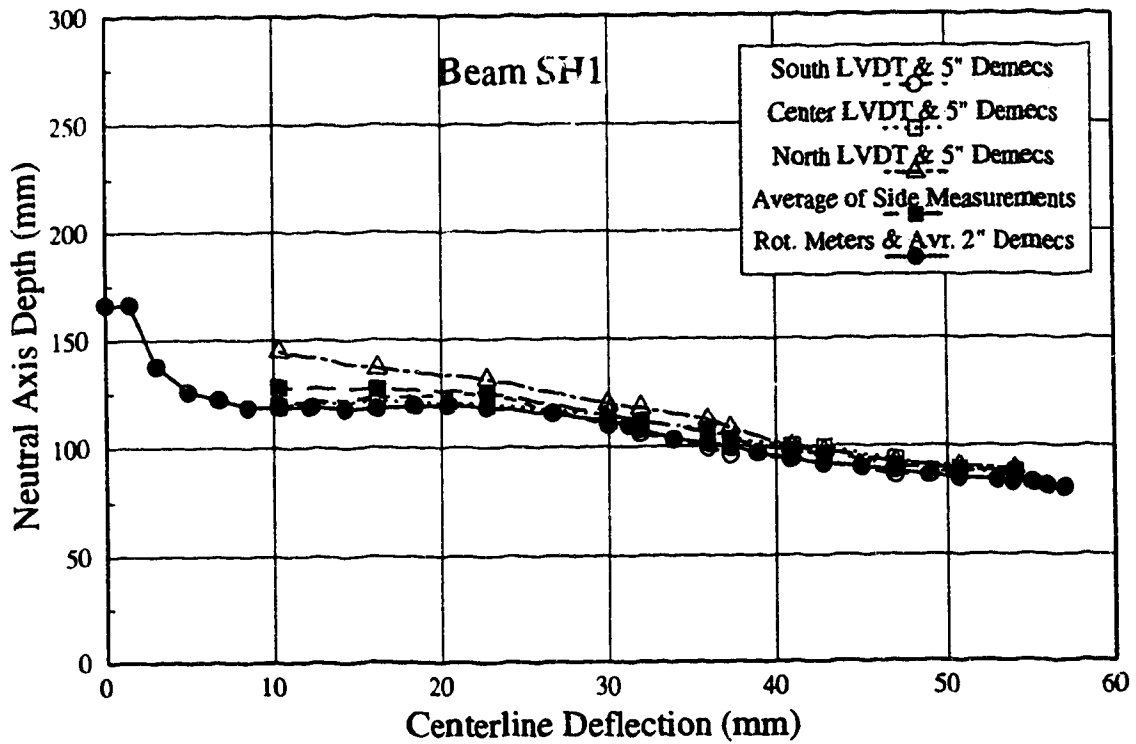


Figure 4.15 Comparison of Neutral Axis Depth Measurements, Best Case

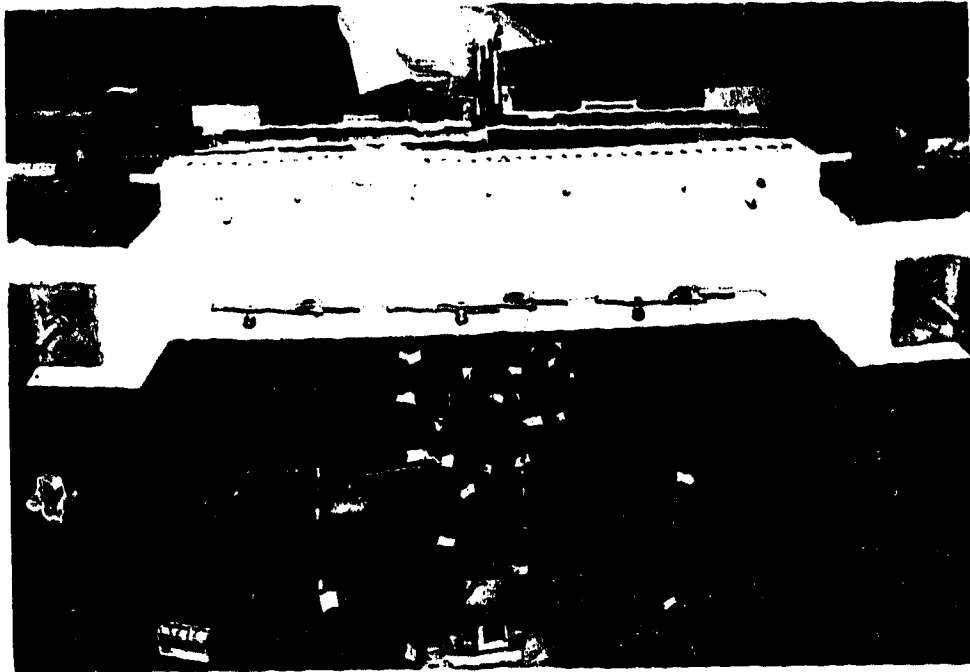


Figure 4.16 Typical Small Lower Concrete Strength Beam After Failure



Figure 4.17 Typical Medium Lower Concrete Strength Beam After Failure

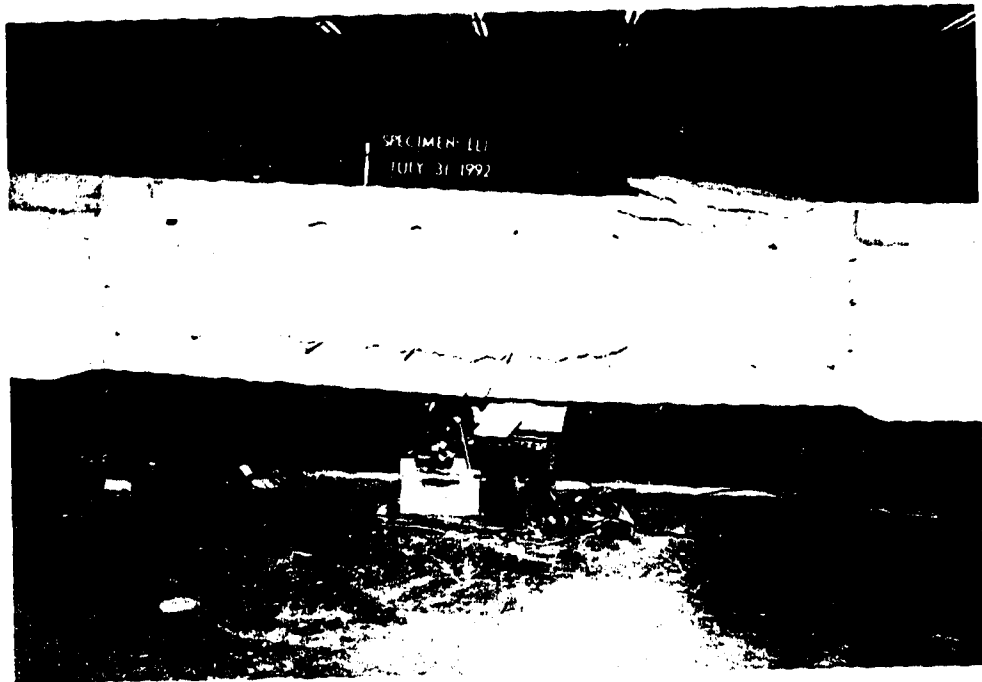


Figure 4.18 Typical Large Lower Concrete Strength Beam After Failure



Figure 4.19 Typical Small Higher Concrete Strength Beam After Failure



Figure 4.20 Typical Medium Higher Concrete Strength Beam After Failure



Figure 4.21 Typical Large Higher Concrete Strength Beam After Failure

5 Effect of Size on Deformation Capacity of Beams

5.1 Introduction

The material presented in this chapter questions the Hillerborg size effect theory in light of the beams tested. The effect of size on the extreme compression fiber strain and on the rotational capacity are viewed separately, followed by a combined discussion.

5.2 Effect of Size on Extreme Compression Fiber Strain

As explained in Section 2.4, the starting point of the Hillerborg theory on size effect on the rotational capacity is the assumption that the extreme compression fiber strain is inversely proportional to the depth of the compression block at ultimate. The ultimate condition referred to here corresponds to the ultimate rotation as defined in Section 4.2 and Figure 4.1. The extreme compression fiber strain at ultimate rotation, $\epsilon_{c\theta_u}$, is plotted in Figure 5.1 against one over neutral axis depth at ultimate rotation, $1/c_{\theta_u}$, for the beams tested. The corresponding values for $\epsilon_{c\theta_u}$ and c_{θ_u} are those reported in Table 4.5 and Table 4.6, respectively. The ACI code limit for the usable extreme compression fiber strain, 3,000 microstrain, is also plotted in Figure 5.1.

The $\epsilon_{c\theta_u}$ vs $1/c_{\theta_u}$ relationship for the tests reported by Mattock (1965) and Corley (1966), and for the beams tested in this series are plotted together in Figure 5.2. Note that, Figure 5.2 was obtained by superimposing the data from the beams tested, on top of Figure 2.7. Both Mattock and Corley had the following definition;

"... the ultimate strains, curvatures, and rotations reported are those corresponding to the instant at which the maximum load on the beam was reached under increasing load; or to the instant at which the beam failed after some time at constant load. Further increase in deformations while the load was decreasing after reaching its maximum value was not considered in this investigation."

This definition implies that the points on the load-deformation curve corresponding to ultimate rotation and ultimate load are the same for the data reported by Mattock and Corley. Thus, it is valid to compare the three series beam tests at the point of ultimate rotation.

5.3 Effect of Size on Rotational Capacity

The Hillerborg size effect theory concludes that the rotational capacity of a hinging region is inversely proportional to its effective depth, d . To prove his theory, Hillerborg (1988a, 1988b, 1989, 1990) plots normalized rotation vs $1/d$ for the beams tested by Corley (1966), as discussed in Section 2.4. The normalized rotation, $\theta_u \omega$, vs $1/d$ relationship for the beams tested is shown in Figure 5.3. The corresponding values for θ_u , ω and d are those reported in Table 4.4, Table 3.6 and Table 3.1, respectively. The ω values were calculated using the average bar force per bar at ultimate moment reported in Table 3.6. The calculated bar force at ultimate moment and at ultimate rotation were the same for every beam. The reason is, in some of the beams both the ultimate moment and ultimate rotation occurred while steel was at its yield plateau, and in the others the ultimate moment and ultimate rotation points corresponded to the same deformation.

In the conventional approach, the normalized rotation is predicted by Equation (2.8).

$$\theta_u \omega = 0.85 \beta_1 \epsilon_{cu} k \quad (2.8)$$

In Equation (2.8), β_1 is the ratio of depth of the rectangular stress block to the neutral axis depth, and ϵ_{cu} is the extreme compression fiber strain at ultimate, k is a constant equal to multiples of d where kd is the gauge length of the rotation measurements. The ACI code assumes $\epsilon_{cu} = 0.003$ regardless of the concrete strength. In the ACI code, $\beta_1 = 0.85$ for concrete strengths lower than 27.6 MPa and $\beta_1 = 0.65$ for concrete strengths higher than 55 MPa. Substituting $k = 3.7$ for the beams tested, Equation (2.8) predicts the normalized rotation, $\theta_u \omega$, as 0.0063 and 0.0081 for β_1 equal to 0.65 and 0.85, respectively. These predictions are plotted in Figure 5.3.

The normalized rotation vs $1/d$ relationship for the tests reported by Mattock (1965) and Corley (1966) and for the beams tested is plotted together in Figure 5.4. In Figure 5.4, the normalized rotation is defined as $\theta_u(\omega - \omega')$ to account for the compression reinforcement in Mattock and Corley beams. For the beams tested in this series ω' is equal to zero. Similar to the extreme compression fiber strains, the tests are comparable at the point of ultimate rotation. The curvatures in the beams reported by Mattock and Corley were measured at the middle of the beams in a gauge length equal to d . In the beams tested, the rotations were measured in a gauge length of $3.7d$. To make proper comparison, the normalized rotations plotted in Figure 5.3 were divided by 3.7 to provide data for Figure 5.4. For more information on how the data from Mattock and Corley beams were analyzed, refer to Section 2.4. The ACI predictions corresponding to $k = 1$ are also plotted in Figure 5.4.

5.4 Discussion

Almost all the extreme compression fiber strains and normalized rotations from Mattock and Corley tests are higher than those from the beams tested. One reason is the Mattock and Corley beams were tested under single point loading and the beams tested here were subjected to two point loading. This was observed by Mattock also. When the shear span alone was increased, lower ultimate curvatures were observed. Mattock tested beams under two point loading as well. These beams gave the lowest curvatures. As discussed in Section 2.4, another reason for the much larger deformations in the Mattock and Corley beams is the confinement of the compression zone due to the compression reinforcement, the stirrups and the loading plate.

High-strength concrete is considered by some to be more brittle than normal strength concrete. Figure 5.1 and Figure 5.3 suggest that the higher concrete strength beams are as deformable as the lower concrete strength beams. Note that, the lowest concrete strength was 44 MPa for the beams tested. This is considered to be approaching high-strength concrete in today's construction world.

The ACI predictions for extreme fiber strains and normalized rotations are lower than those observed from the beams tested. Beams subjected to midpoint loading simulate the plastic hinge occurring in a beam next to the face of a column or at an inner support of a continuous beam. As discussed above, beams subjected to two point loading deform less than those subjected to midpoint loading. The code gives extreme compression fiber strains and normalized rotations even lower than those observed here from beams subjected to two point loading. This suggests that the ACI code is conservative in predicting the ductility of hinging regions in a beam.

The measured extreme compression fiber strains do not suggest any size effect on the strain capacity of concrete in the compression zone of a section under flexure. Similarly, the beams tested do not support the theory that the rotational capacity of reinforced concrete hinging sections is size dependent.

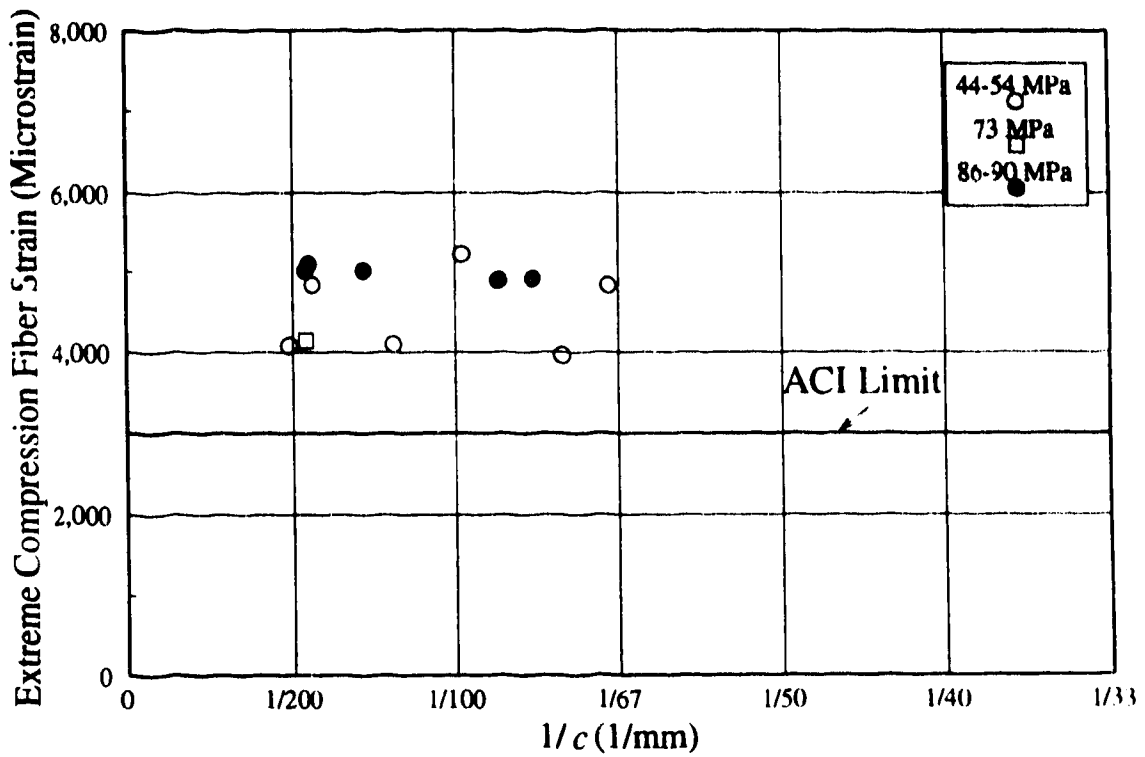


Figure 5.1 Extreme Compression Fiber Strain vs $1/c$, U of A Tests

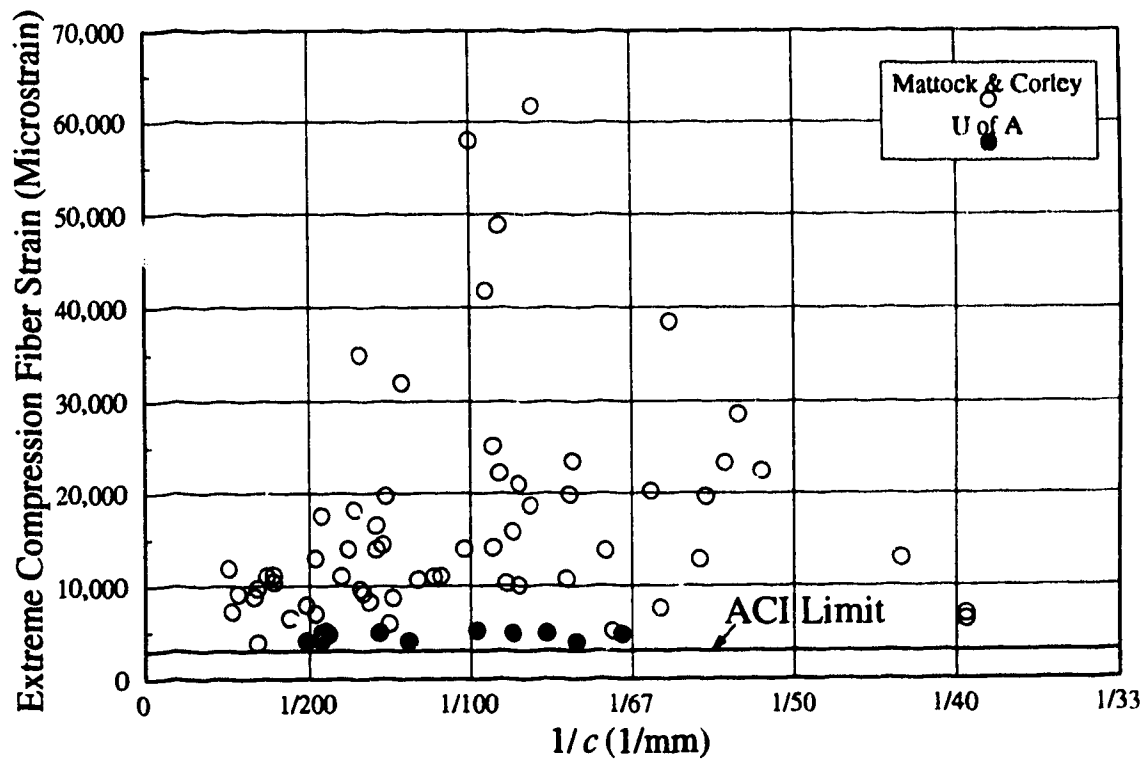


Figure 5.2 Extreme Compression Fiber Strain vs $1/c$

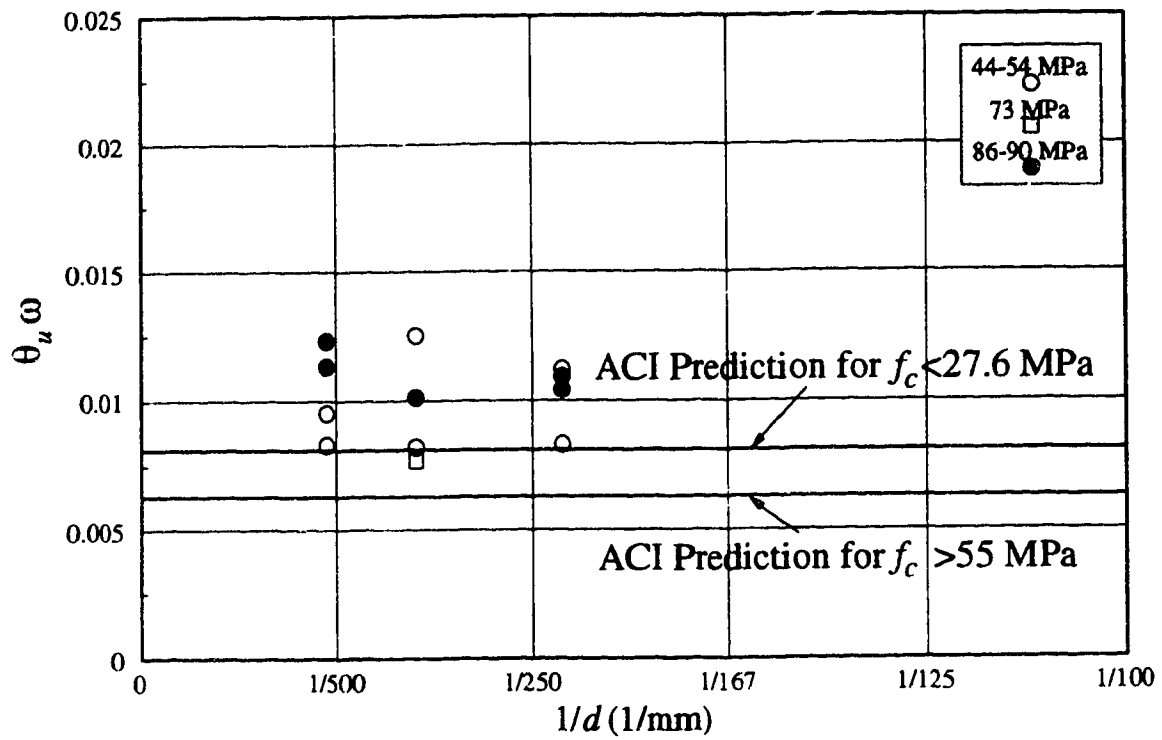


Figure 5.3 Normalized Rotation vs $1/d$, U of A Tests

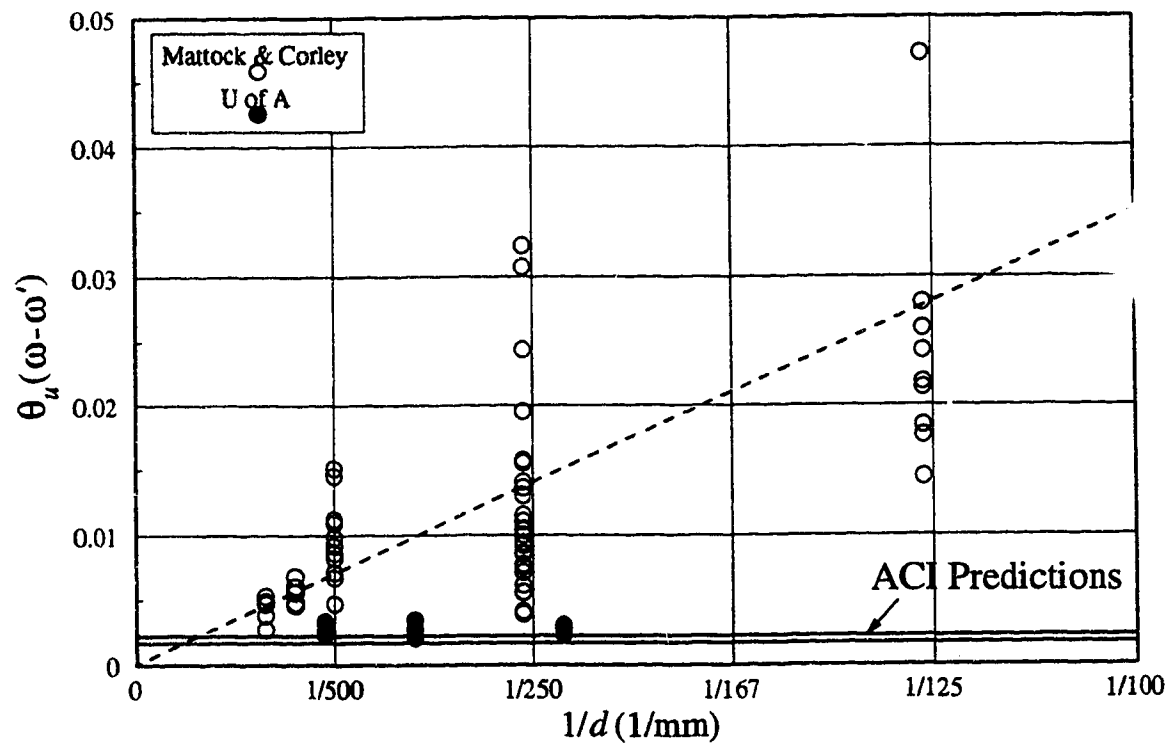


Figure 5.4 Normalized Rotation vs $1/d$

6 Concrete Stress Block Behaviour in Beams

6.1 Introduction

One of the goals of the test project was to investigate the stress block behaviour of high-strength concrete in flexure. Although beams are not the best specimens for this purpose, an attempt is made to obtain the concrete stress-strain curves and stress block parameters.

6.2 Obtaining Concrete Stress-strain Curves

6.2.1 Methods of Analysis

A number of methods to obtain the compressive stress-strain curve of concrete in flexure have been suggested over the years. Early methods were based on assumed shape of stress-strain curves and various coefficients to give the ultimate load carrying capacity of beams. One of these methods is the one developed by Whitney (1940). Whitney assumed that stress-strain curve in a cylinder is the same as in a section subjected to flexure. Later, Prentis (1957), suggested a finite difference method of analysis which involves performing graphical differentiation on some of the plotted parameters from beam tests. Further numerical differentiation methods for beams by Hamann (1952) and by Lee (1953) led to the approach used by Hognestad et al. (1955). Hognestad et al. tested specimens which, in principle, isolated the concrete stress block in flexure. After Hognestad et al., attempts to obtain concrete stress-strain curves from beams were downplayed and most of the later studies were based on tests of specimens similar to those tested by Hognestad et al.. However, Smith and Orangun (1969) developed a method based on using a least squares fit of a polynomial expression to experimental data from reinforced concrete beams.

Two methods were selected from those listed above to analyze the data from the beams tested. These are the methods developed by Hognestad et al. (1955) and by Smith and Orangun (1969). These two methods will be explained briefly in the following paragraphs.

Both of the methods have the same principal assumptions;

1. Linear distribution of strain across the test section.
2. Concrete does not carry any tension
3. All concrete compression fibers follow one and the same stress-strain curve. That is, concrete stress is a function of strain only, $f_c = F(\epsilon_c)$.

The numerical differentiation method developed by Hognestad et al. for eccentrically loaded columns is also applicable to singly reinforced beams with some modification. The method obtains the concrete stress-strain curves from two equations, one related to the axial load equilibrium and the other related to the moment equilibrium in the section. The derivation of the equations will not be presented here as it is given in the paper by the researchers. For a beam, similar equations could be obtained. The equation related to loads is

$$f_c = \epsilon_c \frac{df_o}{d\epsilon_c} + f_o \quad \text{where} \quad f_o = \frac{T}{bc} \quad (6.1)$$

In Equation (6.1), f_c is the stress at the extreme compression fiber, ϵ_c is the extreme compression fiber strain, f_o is the average compressive stress in concrete compression zone, T is the tension in the reinforcement, b is the width of the beam, c is the depth of the compression block.

The equation related to moments is

$$f_c = \epsilon_c \frac{dm_o}{d\epsilon_c} + 2m_o \quad \text{where} \quad m_o = \frac{M'}{bc^2} \quad \text{and} \quad M' = M - T(d - c) \quad (6.2)$$

In Equation (6.2), m_o is a modified moment term, M' is the moment due to the compression force in the concrete alone about neutral axis, M is the moment carried by the section. Note that, from equilibrium of internal forces, the compression in concrete is equal to the tension in the steel.

The method developed by Smith and Orangun uses measured values of: moment M , extreme compression fiber strain ϵ_c , and the neutral axis depth nd . The moment is related to ϵ_c and nd by Equation (6.3) which is obtained from moment equilibrium.

$$\frac{M}{bd^2} = \frac{n(1-n)}{\epsilon_c} \int_0^{\epsilon_c} F(\epsilon)d\epsilon + \frac{n^2}{\epsilon_c^2} \int_0^{\epsilon_c} \epsilon F(\epsilon)d\epsilon \quad (6.3)$$

The objective of the method is to find the best expression for $F(\epsilon)$ which will satisfy Equation (6.3). In order to do that, the method assumes a polynomial in the form given in Equation (6.4):

$$f_c = F(\epsilon) = a_1\epsilon + a_2\epsilon^2 + a_3\epsilon^3 + \dots + a_m\epsilon^m \quad (6.4)$$

where the polynomial coefficients a_1 , a_2 , etc. are yet to be determined.

Substituting Equation (6.4) into Equation (6.3) gives an expression relating the moment to the unknown coefficients. Using the method of least squares to give the closest fit to the measured values of the bending moment leads to a set of simultaneous equations for the coefficients. This method requires selection of the degree of polynomial by the user. The derivation and other details of the method could be found in Smith and Orangun (1969).

6.2.2 Comparison of Methods and Results

Stress-strain curves obtained by the two methods explained in Section 6.2.1 are compared in Figure 6.1 for a lower concrete strength beam and a higher concrete strength beam. The load and moment related curves derived using the Hognestad et al method have considerable noise due to the numerical differentiation of the average compressive force, f_o , and the modified moment term, m_o . This noise could be eliminated by curve fitting to the terms f_o and m_o . The true stress strain curve is somewhere between the two curves. Both of the curves are strongly affected from the tension force, T . The tension force was calculated using the steel coupon tests and measured average compressive strains together with the measured rotations. The method developed by Smith and Orangun was preferred over the Hognestad et al. method mainly because it does not require the value of the tension force. Besides, the Smith and Orangun method seems to be easier for analyzing beams. It was believed that if smoothing was done for the curves from Hognestad et al method, similar curves would be obtained. The stress-strain curves obtained using the Smith and Orangun method will be discussed in detail in the rest of this chapter.

In the Smith and Orangun method, the main decision is the selection of the degree of polynomial to be used in the least squares solution. It was suggested by the researchers that 4th degree polynomial gave the best results. The degree of polynomial has considerable effect on the shape of the stress-strain curve but negligible effect on the area under the curve and on the centroid of this area. In other words, C , the total compression force carried by concrete and, M , moment carried by the section are not affected strongly from the selection of the degree of polynomial. This is expected as the basics of the method are related to moment equilibrium. As a result, the selection of degree of polynomial was rather qualitative.

When a polynomial is fit to the data using the least squares method, there is error in the calculated polynomial coefficients a_1 , a_2 , etc. As a result, the moments predicted by the stress-strain curves may be different than the measured test moments. In their paper, Smith and Orangun used the standard error and the index of correlation to check the goodness of fit between the experimental and predicted moments. The important criteria for goodness

of fit in the investigation presented here was to make sure that the ultimate moment, M_u , was predicted with good precision. Figure 6.2 illustrates the goodness of fit for all the points on the normalized moment, $M/f_c b d^2$, vs extreme compression fiber strain curves for beams MH1 and SL2, the best and the worst cases, respectively. A 4th degree polynomial for SL2 and a 5th degree polynomial for MH1 were used. In most of the cases, test and predicted moments were as close as those shown for MH1. In lower concrete strength beams, the definite yield point acted as the point of discontinuity. As a result, although moments were predicted well in the elastic and plastic region, at yield point predicted moments were lower than test moments as the method tends to smoothen the curve. This can be observed from Table 6.1. The test to predicted moment ratios, M_t/M_{pr} and compression to tension ratios, C/T , at yield and at ultimate moment, obtained by curve fitting to all the points, are given in Table 6.1. The C/T and M_t/M_{pr} values, obtained using the same degree of polynomial to fit the data up to yield only, are given in Table 6.1. The tension force, T , used to calculate the ratios in Table 6.1 is calculated using the average bar forces at yield and at the ultimate moment given in Table 3.6. In Table 6.1, M_t/M_{pr} values at yield obtained by curve fitting to all the data are higher for the lower concrete strength beams than those for higher concrete strength beams.

The effect of the degree of polynomial on the shape of stress-strain curve is illustrated in Figure 6.3. Usually, the curves were close to each other as in the case for MH1. The resulting curve was strongly affected from the degree of polynomial for some of the beams. For example, for beam SL2 which was the worst case, using 5th degree polynomial, $C/T = 1.036$ and $M_t/M_{pr} = 1.01$ were obtained instead of $C/T = 1.020$ and $M_t/M_{pr} = 1.027$ computed using 3rd degree polynomial at ultimate moment. The 3rd degree curve was preferred for beam SL2 qualitatively.

The stress-strain curves obtained from the lower concrete strength beams and from higher concrete strength beams (excluding Beam MH2), are plotted together with a typical stress-strain curve from cylinder test in Figure 6.4 and Figure 6.5, respectively. All the stress-strain curves from beam tests are plotted in Figure 6.6. Smith and Orangun method was used to obtain all of these stress-strain curves.

6.2.3 Discussion

The method developed by Smith and Orangun is reliable for analyzing the data from beam tests. The main reason is that this method uses only the data measured directly from the beam tests. The confidence on measured values of moment, M , average extreme compression fiber strain, ϵ_c , and average neutral axis depth, c , is high.

The stress-strain curves explained in Section 6.2.2 seemed to divide into two groups, one for higher concrete strength and one for lower concrete strength. The stress-strain curves for lower concrete strength beams showed considerable descending branch behaviour before failure. In the higher concrete strength beams, failure took place without much of a descending branch in the stress-strain curves. Especially for higher concrete strengths, the stress-strain curves from beams were significantly different from those obtained from cylinders. The peak in the stress-strain curves from the beam tests occurred at a higher strain than in the cylinder test. This may be due in part to creep. The cylinder tests took about 7 days to reach failure, a beam test took 8 to 12 hours to reach failure.

6.3 Concrete Stress Block Parameters

6.3.1 Methods of Analysis

The stress and strain conditions at ultimate load capacity for a rectangular section subjected to pure flexure are shown in Figure 6.7. The equilibrium of internal forces and moments is expressed by

$$T = C = k_1 k_3 f_c b c \quad \text{where} \quad T = A_s f_s \quad (6.5)$$

$$M_u = k_1 k_3 f_c b c (d - k_2 c) \quad (6.6)$$

From Equations (6.5) and (6.6)

$$\frac{M_u}{b d^2 f_c} = \omega \left(1 - \frac{k_2}{k_1 k_3} \omega \right) \quad (6.7)$$

In Figure 6.7 and Equations (6.5), (6.6) and (6.7), T is the total tension force in reinforcement, C is the total compression force in concrete, M_u is the ultimate moment carried by the section, k_1 is the ratio of the average stress to the maximum stress, k_2 is the ratio of the distance between the extreme compression fiber and the resultant of the compressive

force to the depth of the neutral axis, c , k_3 is the ratio of the maximum stress in the compression zone to the cylinder strength, f_c , ω is the mechanical reinforcement index, A_s is the area of steel, f_s is the stress in the steel, b is the width, d is the effective depth.

Knowing the ratio k_2/k_1k_3 alone is adequate to predict the load carrying capacity of a beam. If the properties of the stress block is known in terms of the parameters, k_1 , k_2 , k_3 , any shape of section and nonsymmetrical bending of rectangular sections can be analyzed. These parameters for the beams tested were obtained using two different methods. These methods will be explained in the following paragraphs.

A way of obtaining the stress block parameters is by the use of Equations (6.5) to (6.7). Rather than the individual values of k_1 and k_3 , the product of the two is obtained from Equation (6.5). The value of k_2 can be expressed in a number of ways, one of them is given in Equation (6.9). From Equation (6.7) k_2/k_1k_3 is defined as in Equation (6.10). The parameters required for this method are M_u , T , b , c , d , ω and f_c . The stress block parameters which could be calculated from this method are k_1k_3 , k_2 and k_2/k_1k_3 . Note that, c is equal to c_{Mu} , neutral axis depth at ultimate moment in Equations (6.5) to (6.10) and Figure 6.7.

$$k_1k_3 = \frac{T}{f_c b c} \quad (6.8)$$

$$k_2 = 1 - \frac{M_u - T(d - c)}{Tc} \quad (6.9)$$

$$\frac{k_2}{k_1k_3} = \frac{1}{\omega} \left(1 - \frac{M_u}{\omega b d^2 f_c} \right) \quad (6.10)$$

The second method of obtaining stress block parameters was using the stress-strain curves given in Sections 6.2.2. The area under the curve up to the extreme compression fiber strain at ultimate moment, ϵ_{cMu} , gave the total compressive force in concrete, C , and using Equation (6.5) the value of k_1k_3 was obtained. The value of k_3 was obtained dividing the peak stress of the stress-strain curve by the cylinder strength. Knowing k_3 , an individual value of k_1 was calculated. Finding the centroid of the area under the curve defined above, and knowing the value of C and the neutral axis depth at ultimate, c_{Mu} , k_2 was calculated. As the stress-strain curves were known in the form of polynomials, the area and the centroid of the area under the curve were calculated easily. The parameters required for this method are moment M , extreme compression fiber strain, ϵ_c , b , c , d and f_c . The stress block parameters which could be calculated from this method are k_1 , k_2 , k_3 , k_1k_3 and k_2/k_1k_3 .

6.3.2 Comparison of Methods and Results

The concrete stress block parameters obtained using the methods explained in Section 6.3.1 are given in Table 6.2.

The k_1 values obtained from stress-strain curves are plotted in Figure 6.8 against the concrete cylinder strength together with the ACI code predictions. A k_1 value of 0.5 corresponds to a triangular stress block.

The k_2 values obtained from both methods are plotted in Figure 6.9 against the concrete cylinder strength together with the ACI code predictions. The k_2 values obtained from Equation (6.9) are unreasonably low. A triangular stress block gives 0.33 for k_2 . As the triangular stress block corresponds to linear elastic case, a k_2 value smaller than 0.33 is not possible. Note that, Equation (6.9) is very sensitive to both neutral axis depth at ultimate moment, c_{Mu} , and total tension force, T . When T was kept constant and c_{Mu} was decreased by 8%, a 10% increase in k_2 was observed. Keeping c_{Mu} constant and increasing T by 2% caused 20% increase in k_2 . In Table 6.1, C/T ratios from 1.008 to 1.055 are reported for ultimate moment and curves fit to all the data. When the total compression force, C , was used in Equation (6.9) instead of T in Equation (6.9), k_2 values close to those obtained from stress-strain curves are obtained.

The k_3 values obtained from stress-strain curves are plotted in Figure 6.10 against the concrete cylinder strength together with the ACI code predictions. For lower concrete strength beams the k_3 values seem to be lower than those would be expected.

The k_1k_3 values obtained from both methods are plotted in Figure 6.11 against the concrete cylinder strength together with the ACI code predictions. The k_1k_3 values for lower concrete strength beams seem to be lower than would be expected. Note that, k_1k_3 is very sensitive to c_{tu} . The difference between the two methods are directly related to the difference in forces, C , and T .

The k_2/k_1k_3 values obtained from both methods are plotted in Figure 6.12 against the concrete cylinder strength together with the ACI code predictions.

6.3.3 Discussion

All the stress block parameters are sensitive to both tension force carried by the reinforcement and the neutral axis depth when they are obtained from Equations (6.8) to (6.10).

Although confidence in the measured values of the average neutral axis depth is high because they are average values, this might have considerable effect on the compression force and its location. As discussed in Chapter 4, the neutral axis depths were quite different from one section to another in the lower concrete strength beams. Failure in those beams were localized at a section. Reducing the neutral axis depth values by 10% for beam LL2 and using the Smith and Orangun approach gave 2% lower compression force and shifted the centroid of the area by 10%. This trial showed that the same k_1 and k_2 but higher k_3 values were obtained with a reduction in the neutral axis depth. As a result, the stress-strain curves for lower concrete strength beams might have the same shape of stress-strain curve with higher peak stresses than that are given in Section 6.2.2. To obtain a C/T ratio equal to 1.0 very small neutral axis depths were required. It was interesting to note that the total compression force, its location and the parameters were not affected by changing the extreme compression fiber strains. The beam tests reported here were not designed for the purpose of obtaining stress-strain curves. It was not always possible to measure the required parameters at the specific failure sections.

Based on studies of this sort, the k_2 values obtained from the stress-strain curves are believed to be quite reliable. The k_3 values for lower concrete strength beams would be higher than the calculated values as peak stresses are expected to be higher for these beams. Similarly, the $k_1 k_3$ values from both methods are expected to be higher for lower concrete strength beams as the total compression force will be divided by a smaller value of neutral axis depth, c_{Mu} .

The ACI code tends to predict a smaller value for k_2 and hence a longer moment arm than calculated from the beam tests. This makes little difference in a beam but could be serious in a column. When the compression force, C , is used instead of the tension force, T , to calculate M_u code, test/code values became unconservative.

6.4 Overall Discussion and Recommendations

The method developed by Smith and Orangun is quite powerful in obtaining concrete stress-strain curves and stress block parameters from beam tests. More dependable results might be obtained by testing beams particularly designed for the purpose.

The size of the specimens did not seem to effect the stress-strain curves. For each concrete strength group, similar stress-strain curves were obtained regardless of the size of the specimen.

Although the ACI code assumes a longer moment arm, due to the involvement of other parameters it predicts the moment capacity of a beam conservatively given the tensile force.

The reason for the difference between the tension force and the compression force was not found. At ultimate load, the contribution of the concrete in tension is very small. A simple calculation revealed that the tension carried by concrete was not big enough to compensate for compression to tension ratios as high as 1.055.

The k_2 values obtained from the stress-strain curves were not sensitive to the measured neutral axis depth values. It is believed that these k_2 values are dependable. The k_1k_3 and k_2/k_1k_3 values are strongly affected from the neutral axis depth used in the calculations. Due to the reasons discussed in Section 6.3.3, it is believed that the k_1k_3 and k_2/k_1k_3 obtained from the stress-strain curves are dependable for higher concrete strength beams.

Table 6.1
Concrete Stress-strain Curve Fitting Data

Specimen	Curve Fit to All				Curve Fit Up To Yield		Deg of poly	M_u test/code ¹
	At Yield		At Ultimate Moment		At Yield			
	C/T	M_i/M_{pr}	C/T	M_i/M_{pr}	C/T	M_i/M_{pr}		
SL1	0.997	1.032	1.055	0.997	1.022	1.003	3	1.025
SL2	0.975	1.054	1.020	1.027	1.016	1.001	4	1.034
ML1	1.007	1.016	1.008	0.999	1.017	1.004	4	0.974
ML2	1.007	1.027	1.053	1.003	1.030	1.000	5	1.055
LL1	0.998	1.024	1.020	1.005	1.019	1.000	5	0.984
LL2	1.028	1.015	1.050	1.007	1.037	1.006	4	1.016
MH2	1.028	1.001	1.024	1.004	1.025	1.005	4	0.971
SH1	1.030	1.000	1.043	1.002	1.031	1.001	5	1.033
SH2	1.043	0.996	1.038	1.001	1.033	1.008	3	1.023
MH1	1.063	0.992	1.055	1.003	1.057	0.999	5	1.030
LH1	1.060	0.982	1.015	1.003	1.045	0.994	5	1.011
LH2	1.040	0.991	1.009	1.001	1.034	1.000	5	1.016

$$^1 M_u = A_s f_s \left(d - \frac{A_s f_s}{1.7 f_c b} \right)$$

Table 6.2
Concrete Stress Block Parameters

Specimen	f_c (MPa)	From Equations (6.8) to (6.10)			From Stress-strain Curves					M_u test/code
		k_2	k_1k_3	k_2/k_1k_3	k_1	k_2	k_3	k_1k_3	k_2/k_1k_3	
SL1	51.1	0.25	0.53	0.47	0.69	0.38	0.81	0.56	0.68	1.025
SL2	51.1	0.27	0.62	0.43	0.74	0.41	0.86	0.63	0.64	1.034
ML1	52.7	0.38	0.53	0.71	0.73	0.40	0.73	0.53	0.74	0.974
ML2	54.1	0.20	0.65	0.31	0.61	0.38	1.03	0.68	0.56	1.055
LL1	54.2	0.35	0.53	0.67	0.78	0.42	0.69	0.54	0.77	0.984
LL2	43.8	0.29	0.55	0.53	0.76	0.41	0.76	0.58	0.71	1.016
MH2	73.4	0.34	0.50	0.68	0.69	0.39	0.74	0.51	0.75	0.971
SH1	90.1	0.27	0.59	0.45	0.65	0.38	0.94	0.61	0.61	1.033
SH2	85.6	0.29	0.58	0.50	0.67	0.37	0.89	0.60	0.63	1.023
MH1	90.3	0.25	0.54	0.46	0.67	0.38	0.85	0.57	0.66	1.030
LH1	90.3	0.33	0.61	0.54	0.65	0.38	0.96	0.62	0.61	1.011
LH2	87.7	0.35	0.65	0.53	0.63	0.37	1.05	0.66	0.56	1.016
Average all		0.30	0.57	0.52	0.69	0.39	0.86	0.59	0.66	1.014
Std Dev all		0.05	0.05	0.12	0.05	0.02	0.12	0.05	0.07	0.026
Average LSC		0.29	0.57	0.47	0.72	0.40	0.81	0.59	0.68	1.015
Std Dev LSC		0.07	0.05	0.15	0.06	0.02	0.12	0.06	0.08	0.031
Average HSC (Excl. MH2)		0.30	0.59	0.50	0.65	0.38	0.94	0.61	0.63	1.022
Std Dev HSC (Excl. MH2)		0.04	0.04	0.04	0.02	0.01	0.07	0.03	0.03	0.008

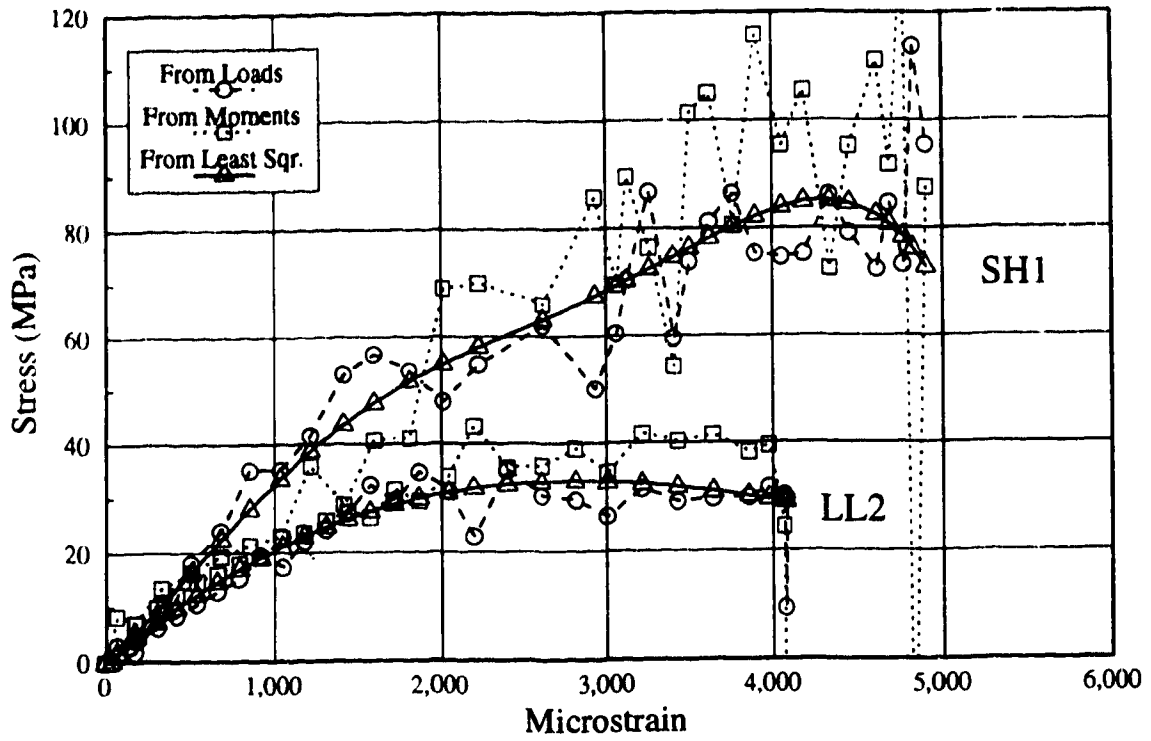


Figure 6.1 Comparison of Methods of Obtaining Stress-strain Curves

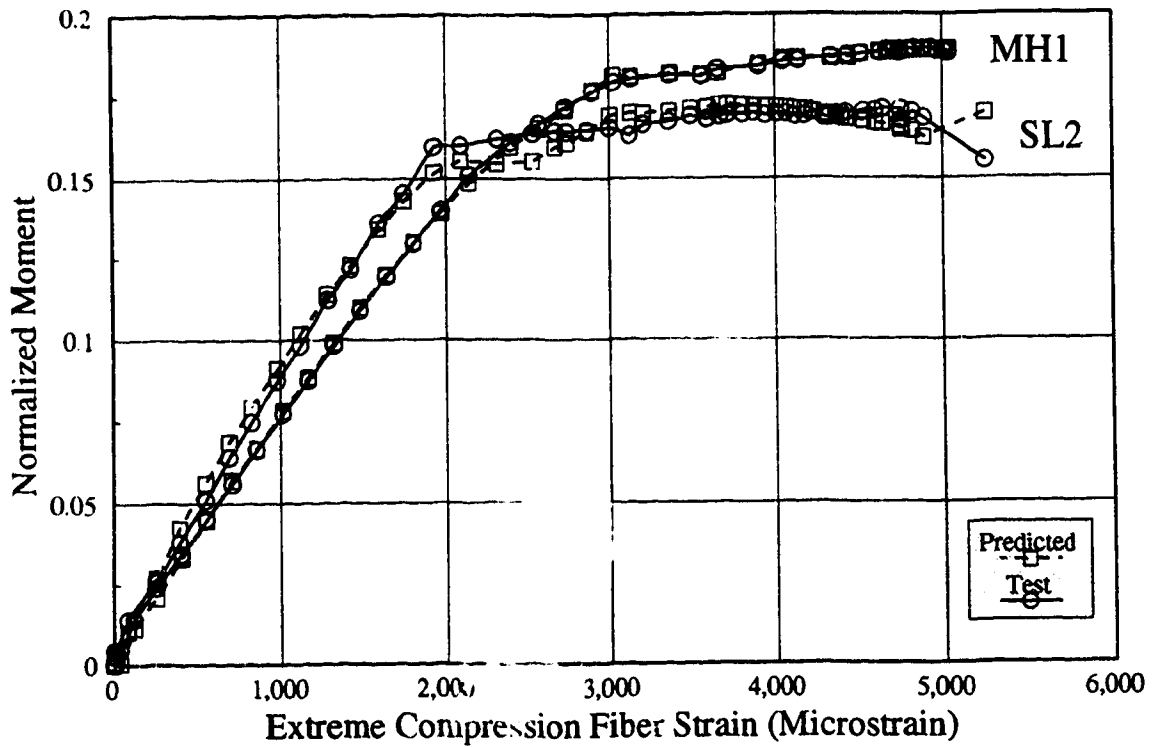


Figure 6.2 Normalized Moment vs Extreme Compression Fiber Strain

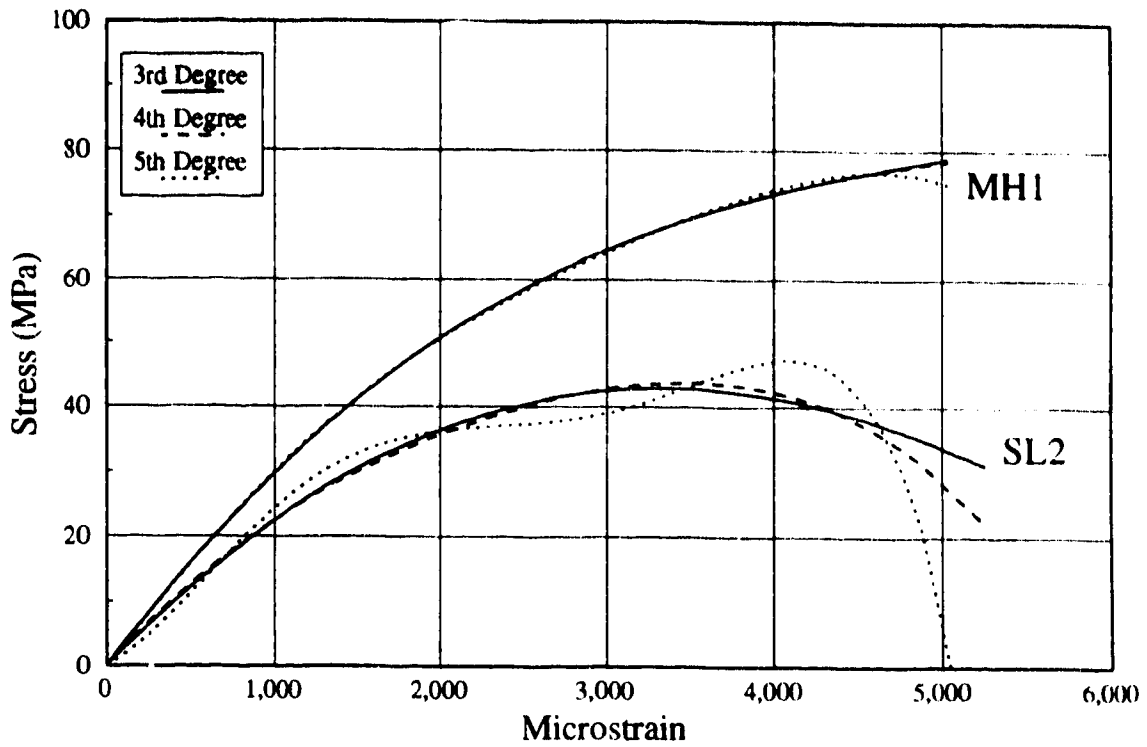


Figure 6.3 Effect of Degree of Polynomial on Stress-strain Curves

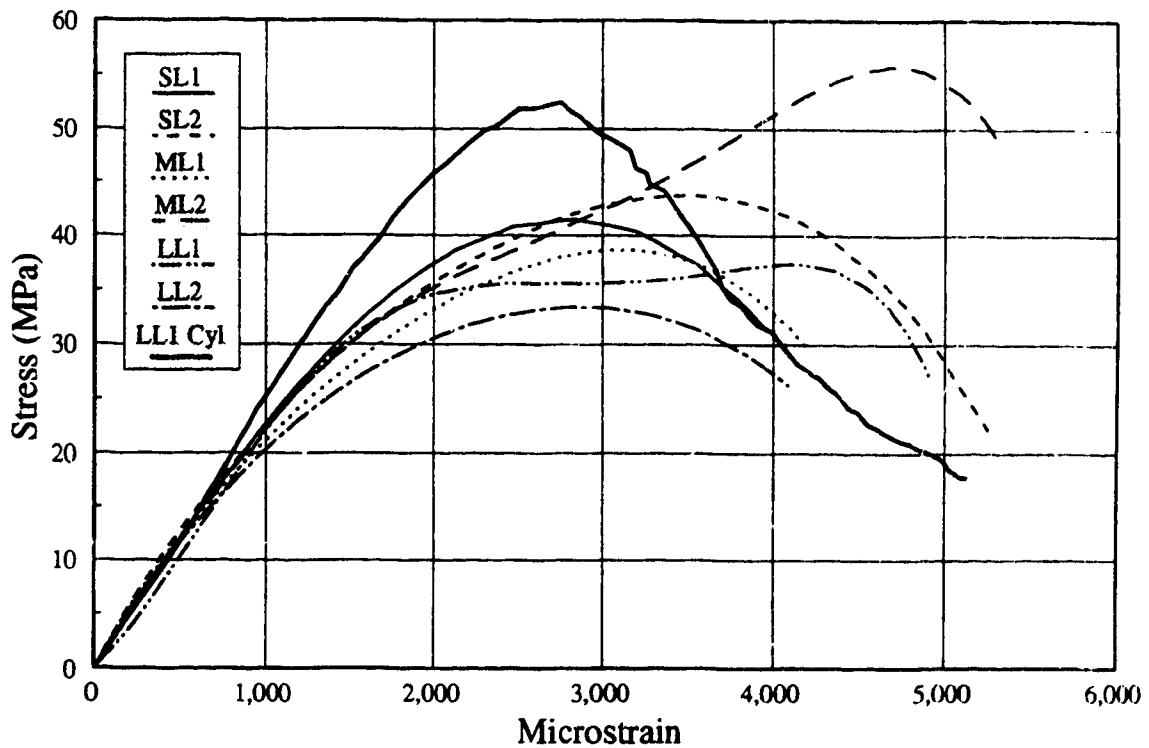


Figure 6.4 Concrete Stress-strain Curves, LSC Beams

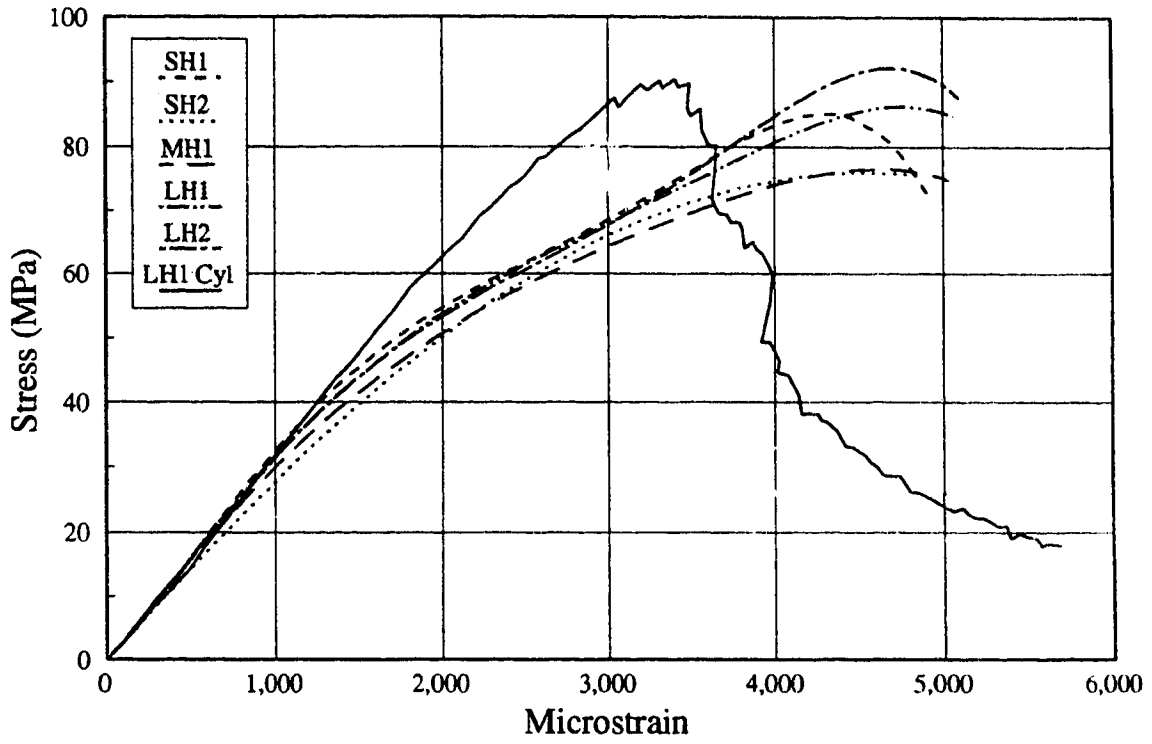


Figure 6.5 Concrete Stress-strain Curves, HSC Beams

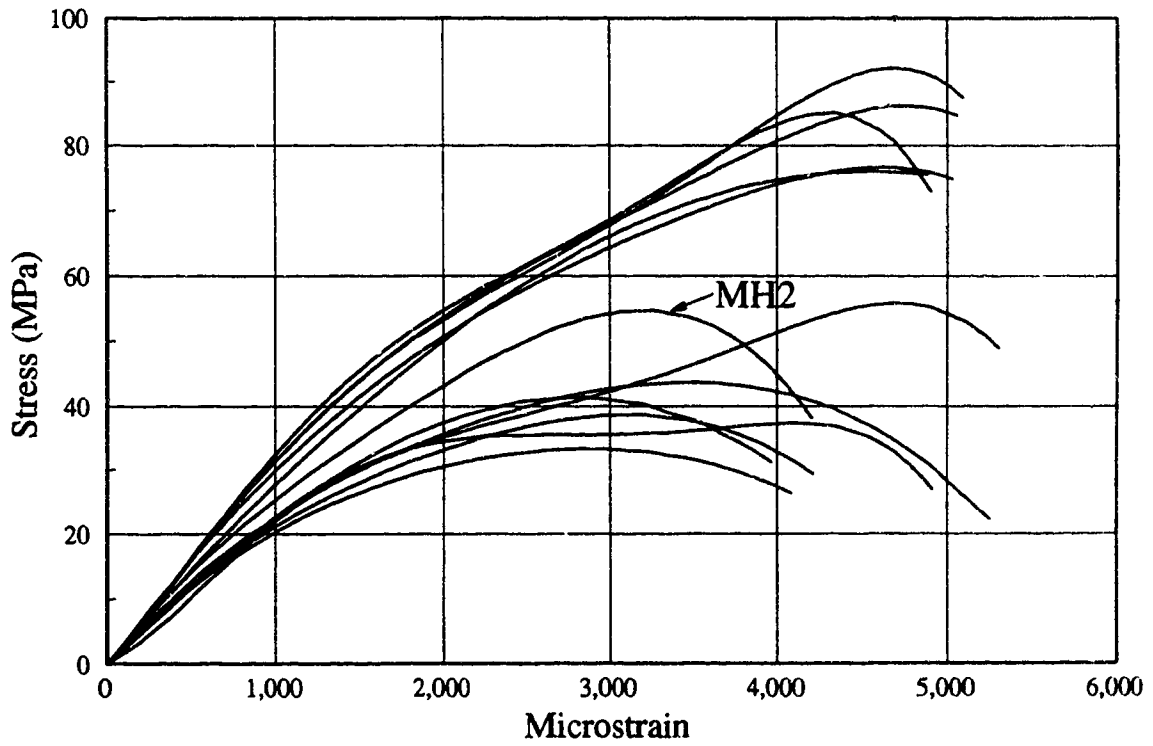


Figure 6.6 Concrete Stress-strain Curves, All Beams

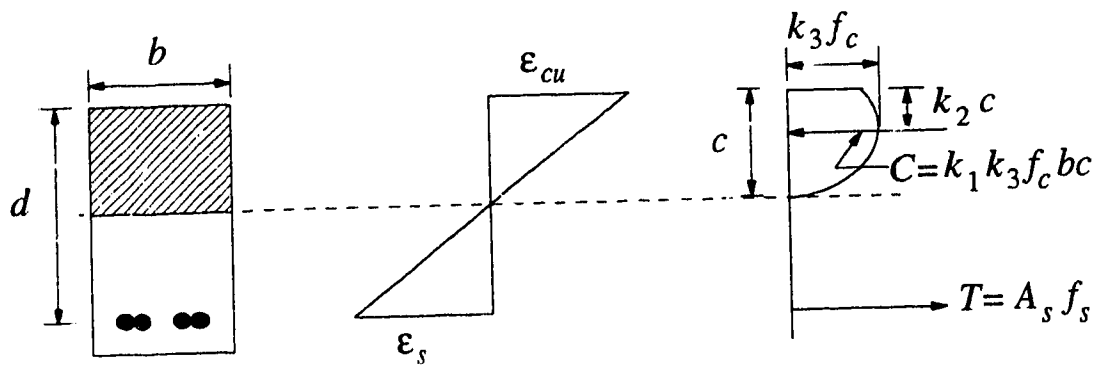


Figure 6.7 Conditions at Ultimate Load

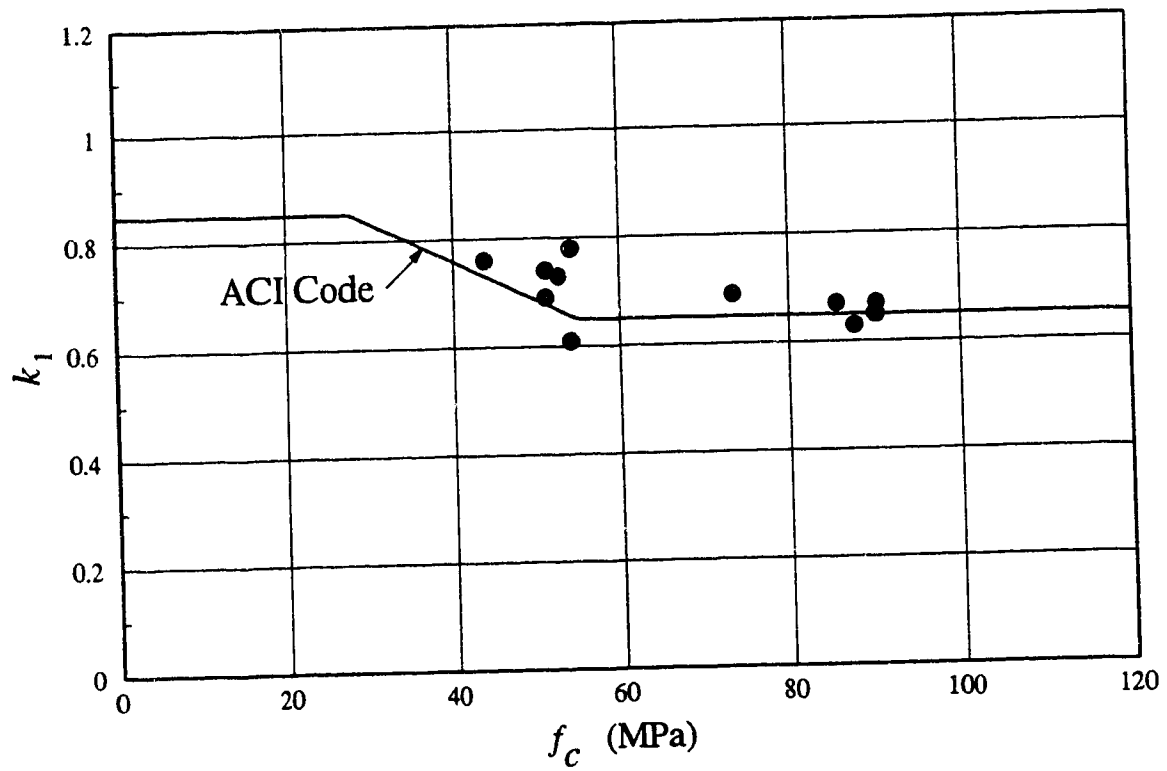


Figure 6.8 k_1 from Stress-strain Curves vs Concrete Cylinder Strength

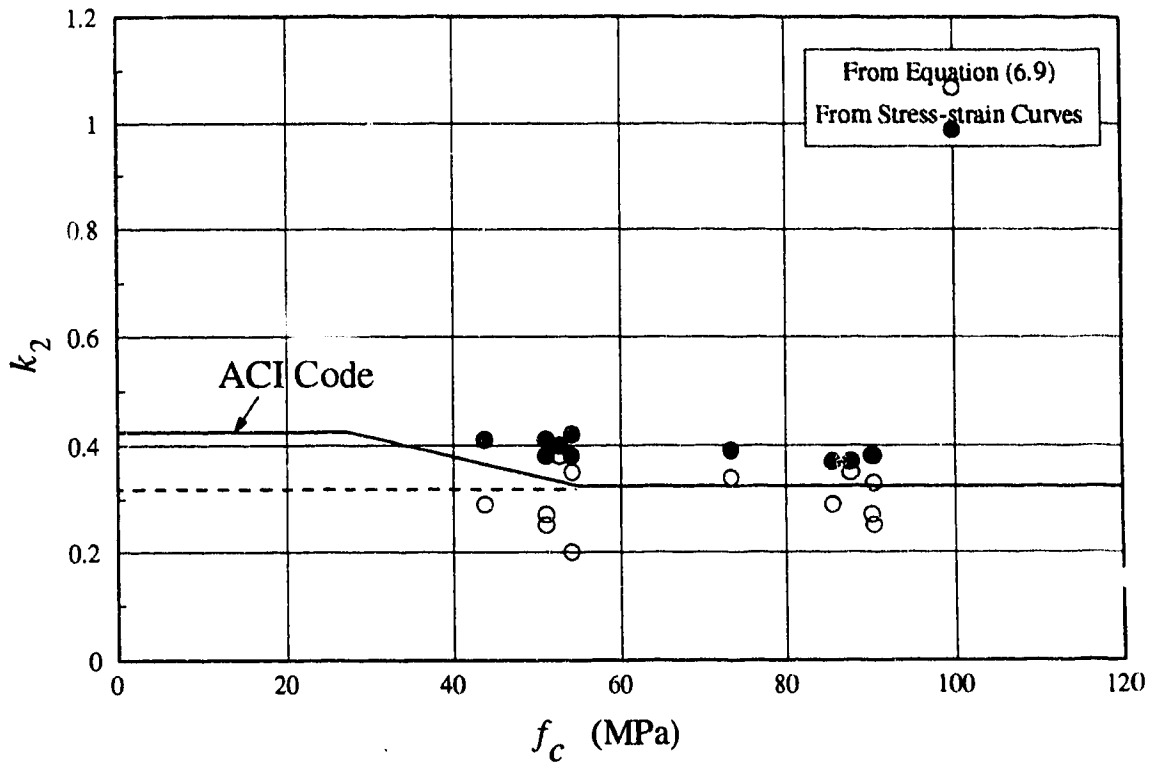


Figure 6.9 k_2 vs Concrete Cylinder Strength

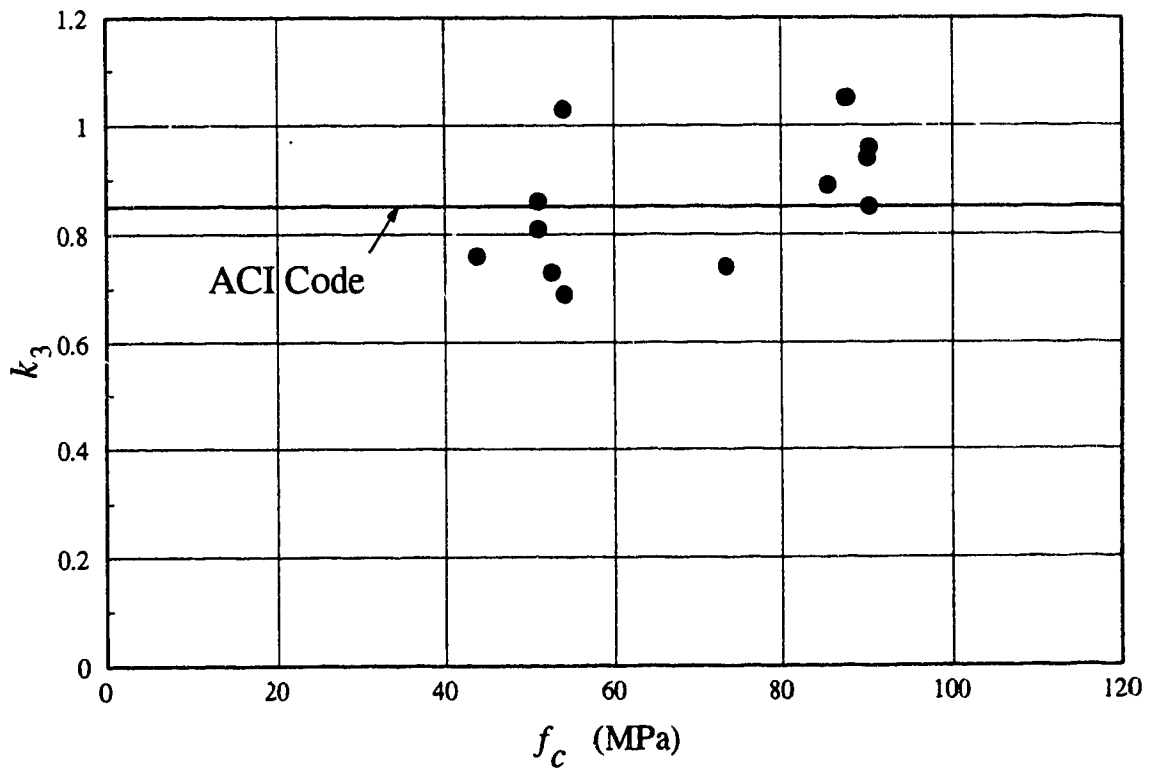


Figure 6.10 k_3 from Stress-strain Curves vs Concrete Cylinder Strength

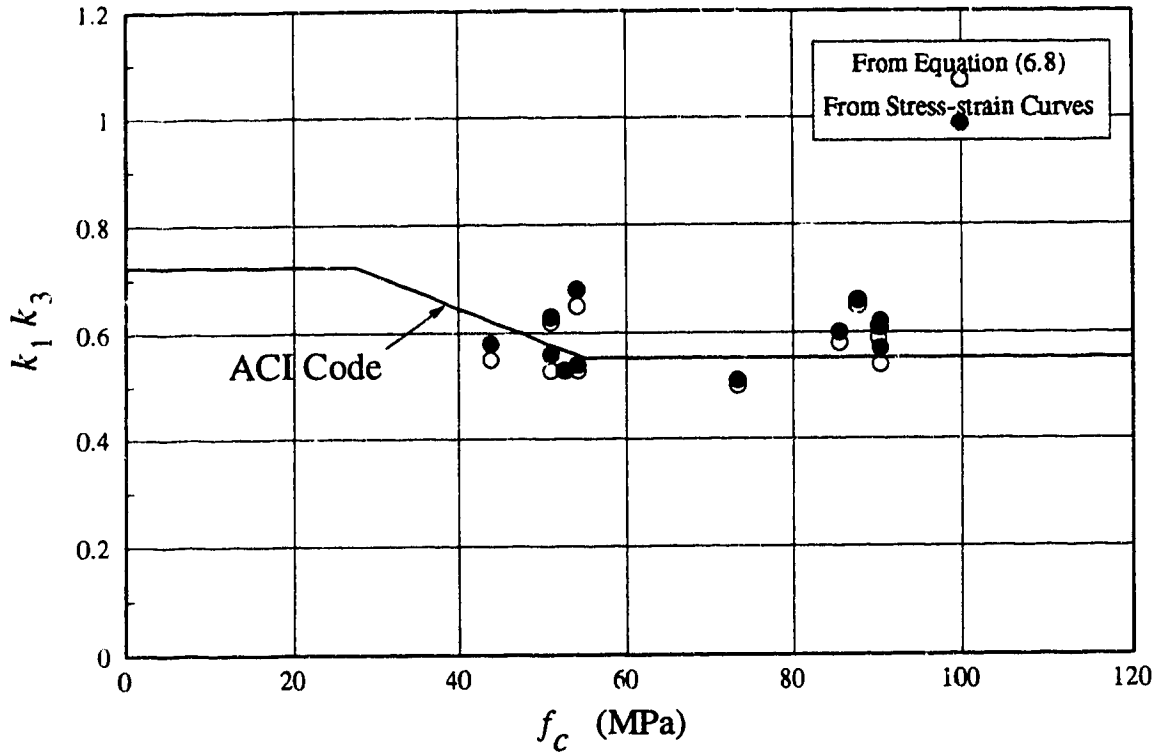


Figure 6.11 $k_1 k_3$ vs Concrete Cylinder Strength

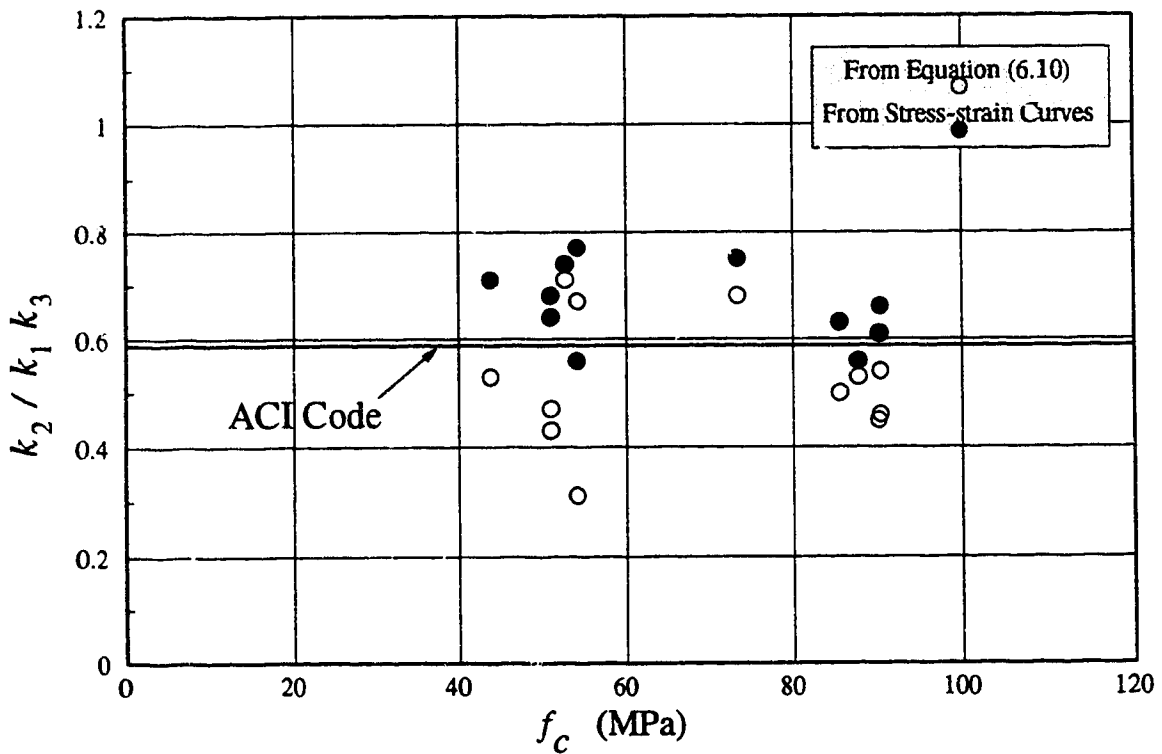


Figure 6.12 $k_2 / k_1 k_3$ vs Concrete Cylinder Strength

7 Summary and Conclusions

7.1 Summary

The rotational capacity of a hinging section is important for the overall behaviour of a structure. One of the factors affecting the rotational capacity of a hinging section may be its size. A literature review showed that the effect of size on the rotational capacity of reinforced concrete hinging beam sections was not clear. This led to the experimental program presented in this thesis.

A total of 12 under-reinforced high-strength concrete beams were tested. The beams were subjected to two point loading. The design of the tests was based on three different sizes and two different concrete strengths. The beams were geometrically scaled relative to the bar diameter. Longitudinal bars 16.0, 25.2 and 35.7 mm in diameter were used. The smallest beams were 150 by 300 mm and the largest beams were 335 by 680 mm. Six of the beams had concrete strengths around 50 MPa, one of the beams had a concrete strength of 74 MPa and five of the beams had concrete strength around 90 MPa.

Total angle change inside the test regions and centerline deflections were measured. The distribution of longitudinal strains along the test region of the beams was studied. The failure types and surfaces were examined for the beams and the material test specimens.

A method based on a least squares fit of a polynomial expression to the experimental data from the beam tests was used to obtain the stress-strain curves for the concrete in the compression zone of the beams. Two different methods were used to calculate the concrete stress block parameters.

7.2 Conclusions

The behaviour of the beams tested was not affected by the size. No effect of size on the strain capacity of concrete in the compression zone of the beams was observed. Similarly, no effect of size on the rotational capacity of hinging reinforced medium or high-strength concrete beam sections was found. No effect of size on the stress-strain curves for the concrete in the compression zone of the beams was observed.

Measured extreme compression fiber strains and rotations indicated that beams having concrete strengths around 90 MPa are as deformable as the beams having concrete strengths around 50 MPa. All the beams deformed more than predicted by the ACI code.

Depending on the concrete strength of the beams, different crack propagation and failure patterns, and different extreme compression fiber strain distributions along the test region were observed. Failure surfaces in the higher concrete strength beams and material test specimens passed through the aggregates. Bond failures between the mortar and aggregates were observed in the lower concrete strength specimens. Explosive failures destroying almost all of the test region were observed in the higher concrete strength beams. More uniform extreme compression fiber strains measured in the higher concrete strength beams indicate that strain energy was stored more uniformly in those beams. This may be the reason for explosive failures.

The analyses of the beam test data suggest that, stress-strain curves for concrete in flexure may be different from that in a uniaxially loaded cylinder.

Calculated concrete stress block parameters vary from those used in the ACI code. The code tends to overestimate the moment arm in a beam although the predicted ultimate moments are very close to test values.

References

ACI Committee 211.4, "Guide for Selecting Proportions for High Strength Concrete," ACI 211.4R-XX report, Submitted to the Technical Activities Committee of the American Concrete Institute in June 1990.

ACI Committee 318 (1989), "Building Code Requirements for Reinforced Concrete," American Concrete Institute, Detroit.

Baker, A.L.L. (1956), "The Ultimate-Load Theory Applied to the Design of Reinforced & Prestressed Concrete Frames," Concrete Publications, London, England.

Baker, A.L.L., and Amarakone, A.M.N. (1964), "Inelastic Hyperstatic Frames Analysis," Proceedings of the International Symposium on the Flexural Mechanics of Reinforced Concrete, Miami, Fla., November, pp. 85-136.

Bartlett, F.M., and MacGregor, J.G. (1993a), "Cores from High Performance Concrete Beams," submitted to ACI Materials Journal for possible publication.

Bartlett, F.M., and MacGregor, J.G. (1993b), "Effect of Moisture Condition on Concrete Core Strengths," submitted to ACI Materials Journal for possible publication.

Bazant, Z.P., and Cedolin, L. (1991), "Stability of Structures," Oxford University Press, New York.

Bosco, C., Carpinteri, A., and Debernardi, P.G. (1990a), "Fracture of Reinforced Concrete: Scale Effects and Snap-back Instability," Engineering Fracture Mechanics, Vol. 35, No. 4/5, pp. 665-677.

Bosco, C., Carpinteri, A., and Debernardi, P.G. (1990b), "Minimum Reinforcement in High-Strength Concrete," J. of Str. Eng., ASCE, V. 116, n. 2, Feb., pp. 427-437.

Chan, W.W.L. (1962), "The Rotational Capacity of Reinforced Concrete Plastic Hinges at Ultimate Load," Magazine of Concrete Research, Vol. 14, No. 41, July, pp. 63-72.

Corley, G.W. (1966), "Rotational Capacity of Reinforced Concrete Beams," Proceedings, ASCE, Vol. 92, ST 5, October, pp. 121-146. (paper also available as Portland Cement Association, Development Dept., Bulletin D108). Discussion by Mattock, A.H., Proceedings, ASCE, ST2, October 1967, pp. 519-522.

Ernst, G.C. (1956), "A Brief for Limit Design," Transactions, ASCE, Vol. 121, p.605.

Hamann, H. (1952), "Berechnung der Druckspannungs-Kurve in Stahlbeton-Biegequerschnitt," Schweizerische Bauzeitung, Zurich, V. 70, No. 44, Nov., pp.629-630.

Hillerborg, A. (1988a), "Fracture Mechanics Concepts Applied to Moment Capacity and Rotational Capacity of Reinforced Concrete Beams," paper presented at the International Conference on FRACTURE OF CONCRETE AND ROCK, Vienna, July 4-6.

Hillerborg, A. (1988b), "Rotational Capacity of Reinforced Concrete Beams," Norwegian Concrete Research, Publication No. 7, pp. 121-134.

Hillerborg, A. (1989), "The Compression Stress-Strain Curve for Design of Reinforced Concrete Beams," SP-118, American Concrete Institute, Detroit, pp. 281-294.

Hillerborg, A. (1990), "Fracture Mechanics Concepts Applied to Moment Capacity and Rotational Capacity of Reinforced Concrete Beams," Engineering Fracture Mechanics, Vol. 53, No. 1/2/3, pp. 233-240.

Hognestad, E., Hanson, N.W., and McHenry, D. (1955), "Concrete Stress Distribution in Ultimate Strength Design," ACI JOURNAL, Proceedings V. 52, Dec., pp. 455-479.

Kani, G.N.J. (1967), "How Safe Are Our Large Concrete Beams?," ACI JOURNAL, Vol. 64, Mar., pp. 128-141.

Koike, S., Okufuji, K., and Okuya, N. (1987), "Size Effect on Expression for Stress-Strain Curves of Concrete under Compression and its Application for Moment-Curvature Relationship of Reinforced Concrete Beams," Transactions of the Japan Concrete Institute, Vol. 9, pp. 249-256.

Koike, S., Hatanaka, S., and Okuya, N. (1989), "Size Effect on Plastic Deformation Capacity of Reinforced Concrete Beams," Transactions of the Japan Concrete Institute, Vol. 11, pp. 363-370.

Kotsovos, M.D. (1982), "A Fundamental Explanation of the Behaviour of Reinforced Concrete Beams in Flexure Based on the Properties of Concrete under Multiaxial Stress," Materials and Structures, RILEM, Vol. 15, No. 90, Nov./Dec., pp. 529-537.

Lee, L.H.N. (1953), "Inelastic Behaviour of Reinforced Concrete Members Subjected to Short Time Static Loading," Proceedings, ASCE, V. 79, No. 286, Sept., 26 pp.

Leahy, K.H., Rajagopalakrishnan, S., and Everard, N.J. (1976), "Flexural Behaviour of High-Strength Concrete Beams," ACI JOURNAL, Proceedings V. 73, No. 9, Sept., pp. 517-521. Discussion, ACI JOURNAL, Proceedings V. 74, No. 3, Mar. 1977, pp. 140-145.

Macchi, G. (1960). "Proposition de Calcul Basee sur la Theorie des Rotations Imposees," Bulletin d'Information, Comite Europeen du Beton, No. 21, Paris, January, pp. 121-158.

Mattock, A.H. (1965). "Rotational Capacity of Hinging Regions in Reinforced Concrete Beams," Portland Cement Association, Development Dept., Bulletin D101 (reprinted from; Proceedings of the International Symposium on the Flexural Mechanics of Concrete, Miami, Fla., November 1964, pp. 143-180).

Hognestad, E. (1962), "High-Strength Bars as Concrete Reinforcement, Part 2: Control of Flexural Cracking," Portland Cement Association, Development Dept., Bulletin D53. (Also see, Park, R., and Pauley, T., "Reinforced Concrete Structures," Wiley, New York, 1975, pp. 479-486).

Prentis, J.M. (1951), "The Distribution of Concrete Stress in Reinforced and Prestressed Concrete Beams When Tested to Destruction by a Pure Bending Moment," Magazine of Concrete Research, London, No. 5, Jan., pp. 73-77.

RILEM Draft Recommendation (1986), "Determination of the Fracture Energy of Mortar and Concrete by Means of Three-Point Bend Tests on Notched Beams," Submitted by 50FMC Committee, Fracture Mechanics of Concrete.

Roy, H.E., and Sozen, M.A. (1964), "Ductility of Concrete," Proceedings of the International Symposium on the Flexural Mechanics of Reinforced Concrete, Miami, Fla., November, pp. 213-224.

Sawyer, H.A. (1955), "Elastic-Plastic Design of Single-Span Beams and Frames," Proceedings, ASCE, Vol. 81, December, pp. 1-29.

Shin, S., Ghosh, S.K., and Moreno J. (1989), "Flexural Ductility of Ultra-High-Strength Concrete," ACI Structural Journal, V. 86, No. 4, July-August, pp. 394-400.

Smith, R.G., and Orangun, C.O. (1969), "Evaluation of the Stress-Strain Curve of Concrete in Flexure Using Method of Least Squares," ACI JOURNAL, July, pp. 553-559. Discussion by Ghosh, S.K., and Sargin, M., ACI JOURNAL, Jan. 1970, pp. 70-72.

van Mier, J.G.M. (1986), "Multiaxial Strain-Softening of Concrete, Part 1: Fracture," Materials and Structures, RILEM, Vol. 19, No. 111, May/June.

Whitney, C.S. (1940), "Plastic Theory of Reinforced Concrete Design," Proceedings, ASCE, December.